

The local radio-galaxy population at 20 GHz

Elaine M. Sadler^{1*}, Ronald D. Ekers², Elizabeth K. Mahony³, Tom Mauch^{4,5}, Tara Murphy^{1,6}

¹*Sydney Institute for Astronomy, School of Physics, The University of Sydney, NSW 2006, Australia*

²*Australia Telescope National Facility, CSIRO, PO Box 76, Epping, NSW 1710, Australia*

³*ASTRON, the Netherlands Institute for Radio Astronomy, Postbus 2, 7990 AA, Dwingeloo, The Netherlands*

⁴*Oxford Astrophysics, Department of Physics, Keble Road, Oxford OX1 3RH*

⁵*SKA Africa, 3rd Floor, The Park, Park Road, Pinelands, 7405, South Africa*

⁶*School of Information Technologies, The University of Sydney, NSW 2006, Australia*

Accepted 0000 December 08. Received 0000 December 08; in original form 0000 December 08

ABSTRACT

We have made the first detailed study of the high-frequency radio-source population in the local universe, using a sample of 202 radio sources from the Australia Telescope 20 GHz (AT20G) survey identified with galaxies from the 6dF Galaxy Survey (6dFGS). The AT20G-6dFGS galaxies have a median redshift of $z=0.058$ and span a wide range in radio luminosity, allowing us to make the first measurement of the local radio luminosity function at 20 GHz.

Our sample includes some classical FR-1 and FR-2 radio galaxies, but most of the AT20G-6dFGS galaxies host compact (FR-0) radio AGN which appear lack extended radio emission even at lower frequencies. Most of these FR-0 sources show no evidence for relativistic beaming, and the FR-0 class appears to be a mixed population which includes young Compact Steep-Spectrum (CSS) and Gigahertz-Peaked Spectrum (GPS) radio galaxies.

We see a strong dichotomy in the Wide-field Infrared Survey Explorer (WISE) mid-infrared colours of the host galaxies of FR-1 and FR-2 radio sources, with the FR-1 systems found almost exclusively in WISE ‘early-type’ galaxies and the FR-2 radio sources in WISE ‘late-type’ galaxies.

The host galaxies of the flat- and steep-spectrum radio sources have a similar distribution in both K-band luminosity and WISE colours, though galaxies with flat-spectrum sources are more likely to show weak emission lines in their optical spectra. We conclude that these flat-spectrum and steep-spectrum radio sources mainly represent different stages in radio-galaxy evolution, rather than beamed and unbeamed radio-source populations.

Key words: radio continuum: general – catalogues – surveys – galaxies: active

1 INTRODUCTION

Measurements of the radio-source population in the local universe provide an essential benchmark for studying the co-evolution of galaxies and their central black holes over cosmic time. The local radio-source population has now been mapped out in detail at 1.4 GHz through the combination of large-area radio continuum and optical redshift surveys (Condon et al. 2002; Sadler et al. 2002; Best et al. 2005a; Mauch & Sadler 2007; see also De Zotti et al. 2010 for a recent review), and the radio luminosity functions of both star-forming galaxies and active galactic nuclei (AGN) have been accurately measured. Members of the two classes overlap in

radio luminosity, but can usually be distinguished using optical spectra (Sadler et al. 1999; Best et al. 2005b).

Much less is known about the local radio-source population at other frequencies, and the recent completion of a sensitive, large-area radio continuum survey at 20 GHz, the AT20G survey (Murphy et al. 2010) provides a first opportunity to study the high-frequency radio properties of nearby galaxies in a systematic way.

The radio emission from active galaxies at 20 GHz arises mainly from the galaxy core, rather than from extended radio lobes (e.g. Sadler et al. 2006, De Zotti et al. 2010, Massardi et al. 2011a, Mahony et al. 2011). The AT20G survey therefore allows us to identify some of the youngest radio galaxies in the local universe, with radio spectra peaking above 5 GHz, which can provide new insights into the earliest stages of radio-galaxy evolution (Snellen et al. 2000; Hancock et al. 2009).

* E-mail: ems@physics.usyd.edu.au

Our aim in this paper is to map out the overall properties of the local radio-source population at 20 GHz, compare this with earlier studies of local radio sources selected at 1.4 GHz (Best et al. 2005a; Mauch & Sadler 2007; Best & Heckman 2012) and use the radio spectral-index information available from the AT20G sample to test whether the host galaxies of flat-spectrum and steep-spectrum radio sources are drawn from the same population.

Section 2 describes the construction of the first 20 GHz-selected sample of nearby galaxies, and provides a data table for the 202 southern (dec $< 0^\circ$) galaxies in this sample. The radio properties of the sample are discussed in §3, and the local radio luminosity function at 20 GHz derived in §4. §5 discusses the optical and infrared properties of our galaxy sample. §6 compares the local radio-source population at 20 GHz with that seen in earlier studies at 1.4 GHz, and §7 presents our conclusions and some suggestions for further work. Some notes on individual sources are added in Appendix A.

Throughout this paper, we assume $H_0 = 71 \text{ km s}^{-1} \text{ Mpc}^{-1}$, $\Omega_M = 0.27$ and $\Omega_\Lambda = 0.73$.

2 THE AT20G–6DFGS GALAXY SAMPLE

We assembled the galaxy sample studied in this paper by matching radio sources from the Australia Telescope 20 GHz Survey catalogue (AT20G; Murphy et al. 2010) with nearby galaxies from the Third Data Release of the 6dF Galaxy Survey (6dFGS DR3; Jones et al. 2009). The 6dFGS was chosen because it is a large-area survey well-matched to the area covered by AT20G, and shallow enough in redshift that the effects of cosmic evolution within the sample volume can be neglected.

In assembling the AT20G–6dFGS sample we used a similar methodology to that of Mauch & Sadler (2007), who assembled and studied a sample of several thousand nearby radio sources selected at 1.4 GHz from the 6dFGS DR2 (Jones et al. 2004) and NVSS (Condon et al. 1998) catalogues. By doing this, we can make direct comparisons between two galaxy samples selected from the same optical survey but at very different radio frequencies.

The AT20G source catalogue covers the whole southern sky¹ (declination $< 0^\circ$ and Galactic latitude $|b| > 1.5^\circ$) and includes 5890 sources above a 20 GHz flux density limit of 40 mJy. The 6dFGS catalogue contains infrared JHK photometry and optical redshifts for a sample of about 125,000 southern (declination $< 0^\circ$ and Galactic latitude $|b| > 10^\circ$) galaxies brighter than $K = 12.75$ mag. The median redshift of the 6dFGS galaxies is $z = 0.053$.

2.1 Source selection

We matched the AT20G catalogue (Murphy et al. 2010) against the 6dFGS DR3 spectroscopic catalogue for galaxies in the main K-band sample (progID=1 in the 6dFGS catalogue), taking into account the following points:

(i) Most AT20G sources are unresolved on scales of 10–15 arcsec, and are associated with the radio cores of galaxies and QSOs (Sadler et al. 2006). For these objects, making an optical identification is generally straightforward.

(ii) Around 5–6% of AT20G sources show extended structure within the 2.4 arcmin ATCA primary beam at 20 GHz, and are flagged as extended in the catalogue (Murphy et al. 2010). The AT20G catalogue position for these sources corresponds to the peak flux in the image. This is usually the flat-spectrum core, and for these sources the optical identification will again be straightforward. In a small number of the strongest peak is a hotspot in the lobes or jet, rather than the core, and extra effort is needed to make the correct optical identification.

(iii) Previous work on the AT20G sources generally used a 2.5 arcsec cutoff radius in making optical identifications (e.g. Sadler et al. 2006; Massardi et al. 2008). While this is appropriate for the AT20G sample as a whole (where distant QSOs are the dominant source population), a larger matching radius should be used for the 6dFGS galaxies because of their large angular size and the relatively low surface density of these bright galaxies.

We began by setting a cutoff radius of 60 arcsec for candidate AT20G/6dFGS matches. This produced a total of 425 candidates, 218 of which were galaxies in the main 6dFGS sample (progID=1) with the remainder belonging to one of the “additional target” samples carried out in parallel with the 6dFGS (Jones et al. 2009). These additional target objects (which include samples of QSOs, radio and infrared-selected AGN as well as other galaxies which are fainter than the $K=12.75$ mag cutoff) are not discussed here, but are analysed in a separate paper (Mahony et al. 2011).

We then visually inspected all the candidate matches, looking at the 20 GHz AT20G images, optical overlay plots and (lower-resolution) low-frequency radio images from the 843 MHz SUMSS and 1.4 GHz NVSS images (Bock et al. 1999; Condon et al. 1998). We also cross-matched the full AT20G catalogue with the lower-frequency southern 2Jy (Morganti et al. 1993) and MS4 (Burgess & Hunstead 2006) bright radio-source samples to check whether any AT20G sources were identified with hotspots of nearby radio galaxies with very large angular sizes (which would have been missed by our 1 arcmin cutoff radius).

In most cases there was good agreement between the AT20G and 6dFGS positions. About 20% of the candidate matches showed extended or double structure in the AT20G image, and in a few cases there was more than one catalogued AT20G source near the same 6dFGS galaxy, suggesting that the AT20G catalogue may be listing several discrete components of a single radio source (see §2.2).

Our next step was to accept as genuine IDs the 183 candidate matches with a position difference of less than 10 arcsec. Monte Carlo tests imply that all matches out to this radius are likely to be genuine, with less than one match expected to occur by chance. Of these 183 sources, 24 (13%) were flagged as extended in the AT20G catalogue and the remainder were unresolved on scales of 10–15 arcsec at 20 GHz.

2.2 Sources with large radio-optical offsets

On the basis of our visual inspection (and cross-comparison with low-frequency radio images where necessary), we accepted a further 19 galaxies with AT20G–6dFGS position offsets > 10 arcsec as genuine IDs. These are listed in Table 1.

All but one of the 19 galaxies in Table 1 are associated with

¹ As noted by Massardi et al. (2011a), the AT20G catalogue has low completeness in a strip of sky at 16–18 hours RA at declination north of -15° because of bad weather during the final observing run. The 6dFGS also has a small number of fields which could not be observed during the survey, mainly in the RA range 6–12 hours with declination south of -40° . Diagrams showing the survey completeness as a function of position on the sky can be found in Figure 1 of Massardi et al. (2011a) for AT20G and Figure 1(c) of Jones et al. (2009) for 6dFGS.

Table 1. AT20G-6dFGS radio galaxies with a large (>10 arcsec) offset between the optical and 20 GHz positions. The AT20G positions and flux densities of each component are listed, along with the offset Δ between the radio and optical positions, the fractional linear polarization at 20 GHz (m20) and a classification of the radio structure.

Source	comp	AT20G name	AT20G position (J2000)		Δ arcsec	S_{20} (mJy)	\pm	m20 %	Notes
(a) Galaxies associated with two or more catalogued AT20G sources									
PKS 0043-42	1	J004613-420700	00 46 13.32	-42 07 00.1	71	363	15	7.4	Hotspot
	2	J004622-420842	00 46 22.30	-42 08 42.6	72	139	14	17.9	Hotspot
Pictor A	1	J051926-454554	05 19 26.34	-45 45 54.5	245	1464	55	38.0	Hotspot
	2	J051949-454643	05 19 49.70	-45 46 43.7	0	1107	54	<1.0	Core
	3	J052006-454745	05 20 06.47	-45 47 45.4	186	426	10	8.6	Hotspot
PKS 0634-20	1	J063631-202857	06 36 31.24	-20 28 57.6	356	55	3	<14.7	Hotspot
	2	J063633-204239	06 36 33.00	-20 42 39.3	466	183	6	12.1	Hotspot
PKS 1717-00	1	J172019-005851	17 20 19.74	-00 58 51.2	126	313	7	<11.0	Hotspot
	2	J172034-005824	17 20 34.24	-00 58 24.6	94	122	6	<8.1	Hotspot
PKS 1733-56	1	J173722-563630	17 37 22.24	-56 36 30.0	185	208	8	<9.2	Hotspot
	2	J173742-563246	17 37 42.95	-56 32 46.4	97	488	19	5.9	Hotspot
(b) Galaxies associated with a single catalogued AT20G source which is offset by more than 10 arcsec from the nucleus									
PKS 0000-550		J000311-544516	00 03 11.04	-54 45 16.8	19	95	3	<17.0	Resolved double
PKS 0349-27		J035145-274311	03 51 45.09	-27 43 11.4	149	122	8	24.8	Hotspot
PKS 0625-53		J062620-534151	06 26 20.58	-53 41 51.4	16	253	4	<7.8	Resolved double
PKS 0625-545		J062648-543214	06 26 48.91	-54 32 14.0	21	106	3	<12.9	Resolved triple
PKS 0651-60		J065153-602158	06 51 53.67	-60 21 58.4	21	44	2	23.0	Resolved double
PKS 0806-10		J080852-102831	08 08 52.49	-10 28 31.9	55	131	5	<7.9	Hotspot
Hydra A		J091805-120532	09 18 05.82	-12 05 32.5	12	1056	52	13.6	Resolved double
MRC 0938-118		J094110-120450	09 41 10.74	-12 04 50.6	47	44	2	<18.6	Resolved triple
PKS 1251-12		J125438-123255	12 54 38.55	-12 32 55.7	68	83	2	23.4	Resolved double
PKS 1801-702		J180712-701234	18 07 12.55	-70 12 34.5	12	62	3	<13.5	Resolved double
PKS 1954-55		J195817-550923	19 58 17.08	-55 09 23.3	14	581	12	43.5	Resolved double
PKS 2053-20		J205603-195646	20 56 03.52	-19 56 46.8	16	159	3	<14.4	Resolved double
PKS 2135-147		J213741-143241	21 37 41.17	-14 32 41.9	60	256	7	4.5	Hotspot
PKS 2158-380		J220113-374654	22 01 13.79	-37 46 54.3	50	174	5	<18.3	Hotspot

sources flagged as extended in the AT20G catalogue (the exception is J031545-274311, which is an unresolved hotspot in one lobe of the radio galaxy PKS 0349-27). Five of the 6dFGS galaxies in Table 1 are associated with two or more sources which are listed separately in the AT20G catalogue.

Most of the objects in Table 1 (11/19) are nearby FR-2 radio galaxies, where the catalogued AT20G source corresponds to one of the hotspots and so is offset from the optical position of the host galaxy. The remaining sources have extended radio emission in which the brightest region at 20 GHz is slightly offset from the galaxy nucleus. Adding the 19 galaxies from Table 1 to the 183 galaxies identified the matching process described in §2.1 gives a total of 202 galaxies in our final AT20G-6dFGS sample.

2.3 Optical spectroscopy and spectral classification

Of the 202 galaxies in our final sample, 139 have a good-quality 6dFGS optical spectrum. The remaining 62 galaxies were not observed in the 6dFGS survey because a published redshift was already available in the literature and so they were given lower priority when scheduling optical spectroscopy for the 6dFGS.

For each galaxy where a 6dFGS spectrum was available, we visually classified the optical spectrum in the same way as Mauch & Sadler (2007) to determine the dominant physical process responsible for the radio emission.

Each object is first classified as either a star-forming galaxy (if the spectrum shows emission lines with ratios characteristic of

Table 2. Spectral classes visually assigned to the 6dFGS-AT20G objects, as described in §2.2. As discussed later in this paper (§5.3), objects classified as AGN with strong emission lines (classes ‘Ae’ and ‘AeB’) will generally have an [OIII] emission-line equivalent width of at least 5 Å.

Class	Type of spectrum	6dF only	6dF +2Jy
Aa	AGN, pure absorption-line spectrum	67	72
Aae	AGN, weak narrow emission lines	40	51
Ae	AGN, strong narrow emission lines	25	27
AeB	AGN, strong emission with broad Balmer lines	7	9
SF	HII region-like emission spectrum	0	1
..	No spectral class, redshift from literature	63	42
Total		202	202

star-formation regions) or an active galactic nucleus (AGN) if no evidence of star formation is seen. The AGN class is then further sub-classified into objects which have strong, weak or no emission lines in their spectra. Table 2 lists the different classifications used and the number of objects in each class.

As noted by Mauch & Sadler (2007), the 6dFGS spectra are obtained through 6 arcsec fibres which correspond to a projected diameter of about 6.8 kpc at the median redshift of the survey ($z \sim 0.05$). As a result, the 6dF fibres include an increasing fraction of the total galaxy light for higher-redshift galaxies and so galaxies

with weak emission lines in their nuclei may be harder to recognize at higher redshift.

Less information is available for the 63 galaxies without 6dFGS spectra, but 21 of these galaxies are members of the 2 Jy radio galaxy sample (Morganti et al. 1993) for which optical spectra at 3500–5500 Å have been published by Tadhunter et al. (1993; see their Figure 1) along with detailed notes on the spectral features. For these 21 objects, we made a spectral classification using the Tadhunter et al. (1993) spectra. These spectral classifications are marked with quality flag ‘J’ in Table 3. For objects with spectra from both 6dFGS and Tadhunter et al. (1993), the two classifications agree well. For the remaining objects where no 6dFGS spectrum was available, no spectral classification was generally made. In these cases, the catalogued 6dFGS redshift is included in Table 3 (see below) but the quality flag and spectral class are left blank.

2.4 Origin of the radio emission

As can be seen from Table 2, 159 of the 160 20 GHz-selected galaxies with good-quality optical spectra are classified as AGN and only one (NGC 253) as a star-forming galaxy.

This is quite different from the 1.4 GHz-selected NVSS-6dFGS sample (Mauch & Sadler 2007), which contains roughly 60% star-forming galaxies and 40% AGN. The difference is not simply due to the higher flux limit of the AT20G sample (40 mJy, compared to 2.4 mJy for NVSS), since at least 15% of the Mauch & Sadler (2007) sources stronger than 40 mJy at 1.4 GHz are star-forming galaxies, but also reflects differences in the radio spectral index distribution of AGN and star-forming galaxies over the frequency range 1–20 GHz.

Murphy et al. (2010) note that the AT20G survey is insensitive to extended 20 GHz emission on angular scales larger than about 45 arcsec, making it difficult to detect diffuse synchrotron emission from the disks of nearby spiral galaxies. In practice, however, the relatively low radio luminosity and steeply-falling radio spectrum of the disk emission from ‘normal’ galaxies means that we would expect to detect very few such objects above the 40 mJy AT20G survey limit even if the brightness sensitivity was not an issue.

NGC 253, the lowest-redshift galaxy in our sample, is the only galaxy in which the 20 GHz radio emission appears to arise from a central starburst rather than an AGN. The main supporting evidence for this is the lack of a parsec-scale central radio source with the high brightness temperature characteristic of AGN cores (Sadler et al. 1995; Lenc & Tingay 2006). NGC 253 is also one of only two starburst galaxies so far detected as high-energy gamma-ray sources by the Fermi satellite (Abdo et al. 2010).

2.5 The main data table

Table 3 lists radio and optical measurements for the 202 galaxies in the final AT20G-6dFGS sample. Galaxies with unresolved 20 GHz sources are listed first, followed by galaxies where the 20 GHz radio source is flagged as extended in the AT20G catalogue and/or has multiple components.

The column headings are as follows:

- (1) Source name from the AT20G catalogue. For galaxies which are identified with two or more AT20G sources (see Table 1), we list a commonly-used source name instead.
- (2) The 20 GHz radio position (J2000) as catalogued by Murphy et al. (2010).
- (3,4) The catalogued 20 GHz flux density, and its error (Murphy et

al. 2010). For sources with multiple AT20G components, we list the sum of the component flux densities.

(5,6) Where available, the catalogued 8.4 GHz flux density and its error (Murphy et al. 2010).

(7,8) Where available, the catalogued 5 GHz flux density and its error (Murphy et al. 2010).

(9) For sources north of declination -40° , the total 1.4 GHz flux density measured from the NVSS catalogue (Condon et al. 1998). For sources with more than one NVSS component the listed flux is the sum of the components, as described by Mauch & Sadler (2007).

(10) For sources south of declination -30° , the total 843 MHz flux density measured from the SUMSS catalogue (Mauch et al. 2003). For sources with more than one SUMSS component the listed flux is the sum of the components.

(11) 6dFGS name.

(12) Offset between the AT20G and 6dFGS positions, in arcsec.

(13) Total infrared K-band magnitude K_{tot} from the 2MASS extended source catalogue (Jarrett et al. 2000), as listed in the 6dFGS database.

(14) Optical redshift, as listed in the 6dFGS catalogue (Jones et al. 2009).

(15) 6dFGS redshift quality, q , where $q=4$ represents a reliable redshift and $q=3$ a probable redshift (Jones et al. 2004).

(16) Spectral classification for galaxies with a good-quality 6dFGS spectrum. Aa = absorption-line spectrum, Aae = absorption lines plus weak emission lines, Ae = strong emission lines (see Sadler et al. 1999, 2002).

(17) Notes on individual sources.

The final AT20G-6dFGS sample contains 202 galaxies, 42 of which are flagged in the AT20G catalogue as extended radio sources at 20 GHz.

3 RADIO PROPERTIES OF THE AT20G-6DFGS SAMPLE

We now consider the radio morphology and spectral-index distribution of the AT20G-6dFGS galaxies.

The available radio data allow us to probe a range of size scales, as summarized in Figure 1. At frequencies near 1 GHz, the NVSS and SUMSS images can resolve extended radio structure on scales larger than about 30 arcsec. In the redshift range covered by our sample, this corresponds to radio emission on scales of tens to hundreds of kpc, typical of classical FR-1 and FR-2 radio galaxies (Fanaroff & Riley 1974). Around 25% of the galaxies in Table 3 have extended low-frequency radio emission in the NVSS/SUMSS images, as discussed below in §3.1.

At high frequency, the AT20G snapshot images have an angular resolution of 10–15 arcsec (Murphy et al. 2010), corresponding to a projected linear size of 10–15 kpc for galaxies at $z \sim 0.06$ (the median redshift of galaxies in our sample). In most cases, therefore, a source which is unresolved in the 20 GHz images is confined within its host galaxy. This size scale is characteristic of Compact Steep Spectrum (CSS) radio sources, which are usually smaller than 15 kpc in extent (Fanti et al. 1990).

Measurements of the visibilities on the longest (~ 6 km) ATCA baselines at 20 GHz allow us to identify sources which are smaller than ~ 0.2 arcsec in size (Massardi et al. 2011a; Chhetri et al. 2012) and so confined to the central kiloparsec of their host galaxy. This size scale is characteristic of Gigahertz Peaked Spectrum (GPS) galaxies, which are generally smaller than a few hun-

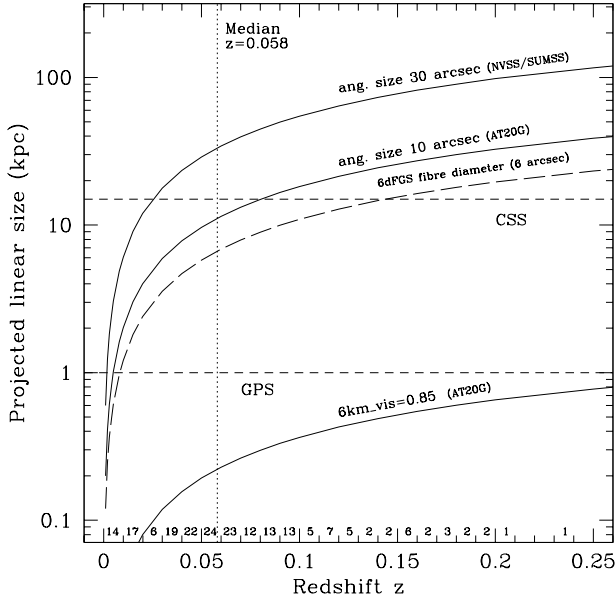


Figure 1. Summary of the angular and linear scales probed by the radio data available for the AT20G-6dFGS galaxies. Solid lines show the approximate resolution limits of the low-frequency NVSS/SUMSS images, the 20 GHz AT20G snapshot images and the ATCA 6 km baseline at 20 GHz (see Chhetri et al. 2012). The angular size of the 6dFGS fibres used for optical spectroscopy is also shown for comparison. Horizontal lines show indicative sizes for the two main classes of ‘young’ radio galaxies, the Compact Steep Spectrum (CSS) sources, and Gigahertz Peaked Spectrum (GPS) objects (O’Dea 1998). The vertical dotted line marks the median redshift of galaxies in our sample, and the number of galaxies in each individual $\Delta z = 0.01$ redshift bin is shown at the bottom of the plot.

dred parsecs in size (Stanghellini et al. 1997). The high-frequency radio structure of the AT20G-6dFGS galaxies is discussed further in §3.2.

Finally, we note that the 6dFGS spectra are taken with 6-arcsec diameter optical fibres (Jones et al. 2009), and so sample a large fraction of the galaxy light for all but the closest AT20G-6dFGS objects. In particular, optical emission lines seen in the 6dFGS spectra could arise either from the nucleus or from ionized gas distributed more widely within the galaxy.

3.1 Radio morphology at frequencies near 1 GHz

All the galaxies in AT20G-6dFGS sample have low-frequency radio images available from the NVSS (1.4 GHz) or SUMSS (843 MHz) surveys. NVSS and SUMSS are well-matched in sensitivity, and both surveys have similar angular resolution of around 45 arcsec (i.e. about a factor of three lower than the AT20G 20 GHz images). NVSS covers the sky north of declination -40° , and SUMSS the region south of declination -30° , so there is a 10-degree band at declination $-30 < \delta < -40$ where images are available from both these surveys. The main motivation for studying these low-frequency images was to link the high-frequency core properties of nearby radio galaxies to the FR-1 and FR-2 classifications traditionally used in lower-frequency studies (Fanaroff & Riley 1974).

Of the 201 radio galaxies in our sample², 65 (32%) have extended radio emission (on scales larger than about 30 arcsec) in the 1.4 GHz NVSS or 843 MHz SUMSS images. These 65 galaxies are listed in Table 3 along with a classification as either FR-1 or FR-2. For 36 of the 65 objects we used existing FR classifications from the literature, mainly from the southern 2-Jy sample (Morganti, Killeen & Tadhunter 1993) and the Molonglo Southern 4-Jy sample (Burgess & Hunstead 2006). The other 29 extended sources had no published FR classification, and were classified by the authors as either FR-1 or FR-2 using the NVSS and SUMSS images. The final column of Table 3 indicates whether the galaxy is known to be a member of an Abell cluster, and in some cases gives additional information about the low-frequency radio structure.

We classify the remaining 136 galaxies in our sample, for which the 1 GHz emission is unresolved in the NVSS and SUMSS images as ‘FR-0’ radio galaxies. The FR-0 classification was introduced by Ghisellini et al. (2011) as the name of a class of weak, compact radio sources described by Baldi & Capetti (2009) but dating back to Slee et al. (1994) and possibly even earlier. In this paper, we adopt the FR-0 designation as a convenient way of linking the compact radio sources seen in nearby galaxies into the canonical Fanaroff-Riley classification scheme.

Our final set of low-frequency classifications contains 49 FR-1, 16 FR-2 and 136 FR-0 radio galaxies. Thus only about one-third of the nearby radio AGN in our 20 GHz-selected sample are classical FR-1/FR-2 radio galaxies at frequencies near 1 GHz.

3.2 Radio morphology at 20 GHz

The AT20G data provide a range of information on the radio morphology at 20 GHz, as discussed by Murphy et al. (2010) and Mascardi et al. (2011a). The angular resolution of the 20 GHz AT20G snapshot images made with the ATCA is typically ~ 10 arcsec (Murphy et al. 2010), corresponding to a linear size of ~ 10 kpc at the median redshift ($z = 0.058$) of the AT20G-6dFGS galaxies. The 20 GHz snapshot images therefore provide information on the high-frequency radio morphology of the AT20G-6dFGS galaxies on kiloparsec scales.

We can recover some extra information on the smaller-scale structure of most AT20G sources by examining the 20 GHz visibilities on baselines to the fixed ATCA ‘6 km’ antenna, which were not used for imaging (Murphy et al. 2010). These ‘6 km visibility’ measurements are available for 186 of the AT20G-6dFGS galaxies (92%), and provide information about the source compactness on sub-kpc scales as discussed in §3.2.2.

3.2.1 20 GHz morphology on kpc scales, from the AT20G snapshot images

Murphy et al. (2010) flagged 337 of the 5890 sources in the AT20G catalogue (5.7%) as extended (i.e. generally larger than about 10 arcsec in size) at 20 GHz. If we remove the 82 objects flagged by Murphy et al. (2010) as Galactic or LMC sources, then the fraction of extended sources falls slightly, to 308 out of 5806 or 5.3%.

The fraction of AT20G-6dFGS galaxies with extended 20 GHz emission (42/202 or 20.8%) is significantly higher than the 5% fraction seen for all extragalactic sources in the AT20G survey (Mascardi et al. 2011a). This is not too surprising, since the AT20G-

² Excluding the star-forming galaxy NGC 253

Table 3. Galaxies with extended (FR-1 or FR-2) radio emission at 1 GHz. The listed 408 MHz flux density is from the Molonglo Reference Catalogue (MRC; Large et al. 1981).

Source	AT20G name	2 Jy name	MS4 name	z	Spec. class	S_{20} (Jy)	$S_{0.4}$ (Jy)	FR class	Ref.	Notes
PKS 0001-531	J000413-525458	0.0328	..	0.065	1.25	1	v	
3C 015	J003704-010907	0034-01	...	0.0734	Aa	0.404	9.74	2	a	
PKS 0043-42	(Two sources)	0043-42	B0043-424	0.1160	Aae	0.438	21.0	2	a, b	
3C 029	J005734-012328	0055-01	...	0.0450	Aa	0.055	10.88	1	a	
NGC 547	J012600-012041	0123-01	...	0.0184	Aa	0.147	16.4	1	a	In cluster Abell 194
NGC 612	J013357-362935	0131-36	B0131-367	0.0305	Ae	0.440	17.1	2	a,b	
ESO 198-G01	J021645-474908	...	B0214-480	0.0643	Aa	0.093	9.5	1	b	In cluster Abell 239S
PKS 0229-208	J023137-204021	0.0898	Aa	0.160	1.87	1	v	
PMN J0315-1906	J031552-190644	0.0671	Ae?	0.108	..	1	c	In cluster Abell 428
PKS 0344-34	J034630-342246	...	B0344-345	0.0535	..	0.102	9.3	2	b	Complex source, in cluster
PKS 0349-27	J035145-274311	0349-27	...	0.0657	Ae	(0.122)	8.75	2	a	Lower limit at 20 GHz
IC 2082	J042908-534940	0427-53	B0427-539	0.0380	Aa	0.145	14.6	1	a,b	In cluster Abell 463S
PKS 0429-61	J043022-613201	...	B0429-616	0.0555	Aa	0.148	6.5	1	b	In cluster Abell 3266
Pictor A	(Three sources)	0518-45	B0518-458	0.0351	AeB	6.320	166.0	2	a, b	
PKS 0545-199	J054754-195805	0.0551	Aa	0.042	1.81	1	d	
PKS 0620-52	J062143-524132	0620-52	B0620-52	0.0511	Aae	0.266	9.3	1	a, b	
ESO 161-IG07	J062620-534151	0625-53	B0625-536	0.0551	Aa	0.253	26.0	1	a, b	In cluster Abell 3391
PKS 0625-545	J062648-543214	...	B0625-545	0.0517	..	0.106	7.86	1	b	In cluster Abell 3395
PKS 0625-35	J062706-352916	0625-35	B0625-354	0.0549	Aa	0.688	9.23	1	a, b	In cluster Abell 3392
PKS 0634-20	(Two sources)	0.0551	Ae	0.238	210.0	2	e	
PKS 0651-60	J065153-602158	0.1339	Aa	0.044	3.06	1	v	
PKS 0652-417	J065359-415144	0.0908	Aa	0.056	1.02	1	v	
ESO 207-G19	J070459-490459	0.0419	..	0.084	..	1	v	In cluster Abell 3407
PKS 0707-35	J070914-360121	...	B0707-35	0.1108	..	0.094	4.60	2	b	
PKS 0803-00	J080537-005819	0.0902	Aa	0.081	3.39	1	v	Wide-angle tail, in cluster Abell 623
PKS 0806-10	J080852-102832	0806-10	...	0.1090	Ae	0.131	10.2	2	a	
ESO 060-IG02	J081611-703944	0.0332	Aa	0.062	2.56	1	v	Complex source
PMN J0844-1001	J084452-100059	0.0429	Aa	0.046	..	1	v	
PMN J0908-1000	J090802-095937	0.0535	Aa	0.060	..	1	v	Narrow-angle tail
PMN J0908-0933	J090825-093332	0.1590	Aa	0.046	..	1	v	In cluster Abell 0754
Hydra A	J091805-120532	0915-11	...	0.0548	Aae	1.056	132.0	1	a	In cluster Abell 780
PMN J0941-1205	J094110-120450	0.1500	Aa	0.044	1.77	2	v	Compact triple
NGC 3557	J110957-373220	0.0101	Aa	0.052	0.96	1	f	
PKS 1118-000	J112119-001316	0.0993	..	0.108	1.50	1	v	Wide-angle tail
PKS 1130-037	J113305-040046	0.0520	Aa	0.108	1.18	1	v	In cluster Abell 1308
NGC 4783	J125438-123255	1251-12	...	0.0150	Aae	0.083	14.7	1	a	
ESO 443-G24	J130100-322628	0.0170	..	0.176	2.99	1	g	In cluster Abell 3537
PKS 1308-441	J131124-442240	0.0506	Aae	0.044	1.07	1	v	Giant radio galaxy
NGC 5090	J132112-434216	1318-43	B1318-434	0.0112	Aae	0.705	10.0	1	a, b	
NGC 5128	J132527-430104	1322-42	B1322-427	0.0018	Aae	28.35	2740.	1	a, b	
IC 4296	J133639-335756	1333-33	B1333-33	0.0125	Aae	0.323	30.8	1	a, b	In cluster Abell 3565
ESO 325-G16	J134624-375816	0.0376	Aa	0.071	1.44	1	v	Complex structure, in cluster Abell 3570
PKS 1452-367	J145509-365508	0.0946	Aae	0.198	2.90	1	v	
PKS 1637-77	J164416-771548	1637-77	B1637-771	0.0430	Aae	0.399	13.5	2	a, b	
PKS 1717-00	(Two sources)	1717-00	...	0.0304	Aae	0.435	61.28	2	a	
PKS 1733-56	(Two sources)	1733-56	B1733-565	0.0985	Ae	0.696	20.3	2	a, b	
MRC 1758-473	J180207-471930	0.1227	Aa	0.114	1.06	1	v	
PMN J1818-5508	J181857-550815	0.0726	Aa	0.075	..	1	v	
PKS 1839-48	J184314-483622	1839-48	B1839-487	0.1108	Aa	0.305	9.08	1	a, b	
PMN J1914-2552	J191457-255202	0.0631	Aa	0.147	1.06	1	v	Head-tail source
MRC 1925-296	J192817-293145	0.0244	Aa	0.078	3.18	1	v	Wide-angle tail, in cluster?
PKS 1954-55	J195817-550923	1954-55	B1954-552	0.0581	Aae	0.581	14.8	1	a, b	
ESO 234-G68	J204552-510627	0.0485	Aa	0.054	0.96	1	v	
IC 1335	J205306-162007	0.0427	Aa	0.056	..	1	v	
ESO 106-IG15	J205754-662919	0.0754	Aa	0.049	..	1	v	In cluster Abell 2597?
PMN J2122-5600	J212222-560014	0.0518	Aae	0.058	..	1	v	Head-tail source?
NGC 7075	J213133-383703	0.0182	Aa	0.046	1.79	1	v	
PKS 2135-147	J213741-143241	2135-14	B2135-147	0.1999	AeB	0.256	8.78	2	a, b	
PMN J2148-5714	J214824-571351	0.0806	..	0.048	1.67	1	v	Head-tail source, in cluster?
PKS 2148-555	J215129-552013	...	B2148-555	0.0388	..	0.088	..	1	b	In cluster Abell 3816
ESO 075-G041	J215706-694123	2152-69	B2152-699	0.0285	AeB	3.400	61.6	2	a, b	
PKS 2158-30	J220113-374654	...	B2158-380	0.0334	Ae	0.174	4.12	2	b	
PKS 2316-423	J231905-420648	0.0543	Aae	0.150	..	1	v	Complex structure, in cluster Abell 1111S
PKS 2316-538	J231915-533159	0.0958	Aa	0.075	..	1	v	
PKS 2339-164	J234205-160840	0.0649	Aa	0.043	0.95	1	v	Complex structure, in cluster?

References for FR 1/2 classification: (a) 2Jy, Morganti et al. 1993; (b) MS4, Burgess & Hunstead 2006; (c) Ledlow & Owen 1996; (d) Zirbel & Baum 1995; (e) Baum et al. 1988; (f) Birkinshaw & Davies 1985; (g) Marshall et al. 2005; (v) visual classification by the authors, based on NVSS/SUMSS images.

Table 4. 20 GHz radio morphology of the AT20G-6dFGS galaxy sample.

Description	Class	Number
Single source, centred on galaxy nucleus (compact at 20 GHz)	Core	178
(extended at 20 GHz)		(159)
Single source, offset from nucleus	Hotspot	4
Two sources within a single ATCA beam	Compact double	11
Two separate AT20G detections	Wide double	4
Three sources within a single ATCA beam	Compact triple	3
Three separate AT20G detections	Wide triple	2
Total		202

6dFGS galaxies are generally the lowest-redshift objects in the AT20G catalogue. The extended AT20G-6dFGS sources show a variety of radio morphologies, as summarized in Table 4. The classifications in this table are based on visual inspection of the AT20G snapshot images. The radio galaxy NGC 612 (J013357-010907), which has very extended 20 GHz radio emission imaged by Burke-Spolaor et al. (2009), is classified here as a ‘wide triple’.

Sources which are unresolved in the AT20G images will generally be smaller in extent than the galaxies which host them, but may still be several kpc in size. Classical GPS and CSS radio sources, with typical sizes of < 1 kpc and < 15 kpc respectively (O’Dea 1998), are expected to be unresolved or marginally resolved sources in the AT20G images.

For the great majority of AT20G-6dFGS galaxies (77%), the high-frequency radio emission arises from an unresolved point source centred on the galaxy nucleus (i.e. a ‘radio core’). A further 11% have an extended AT20G source centred on the galaxy nucleus. Only 12% of the detected galaxies have 20 GHz emission which is significantly offset from the galaxy nucleus or resolved into two or more components.

3.2.2 20 GHz morphology on sub-kpc scales, from ATCA 6 km visibilities

Chhetri et al. (2012) introduced a second measure of compactness for the AT20G sources, based on a visibility determined by the ratio of the average scalar amplitude of the five long (~ 4.5 km) ATCA baselines to the ten short (30–214 m) baselines in the H214 configuration. Sources with a flux density ratio > 0.85 were considered to be unresolved, and therefore have angular sizes smaller than about 0.2 arcsec. Measurements of the compactness parameter are available for 92% of the AT20G-6dFGS galaxies (Chhetri et al., in preparation).

Figure 2 shows the 20 GHz compactness parameter versus the 1–20 GHz spectral index for the AT20G-6dFGS galaxies. The clean separation between steep-spectrum extended sources and flat-spectrum compact sources seen by Massardi et al. (2011a; their Figure 4) is also visible here, and the fraction of sub-kpc scale 6dFGS-AT20G sources (i.e. those with compactness parameter > 0.85) is 87% (81/93) for flat spectrum sources, but only 35% (32/92) for steep-spectrum sources. We find no significant correlation between the compactness parameter and either redshift or 20 GHz radio luminosity.

3.3 20 GHz flux density measurements for extended sources

The AT20G survey images are insensitive to extended 20 GHz emission on scales larger than about 45 arcsec (Murphy et al. 2010).

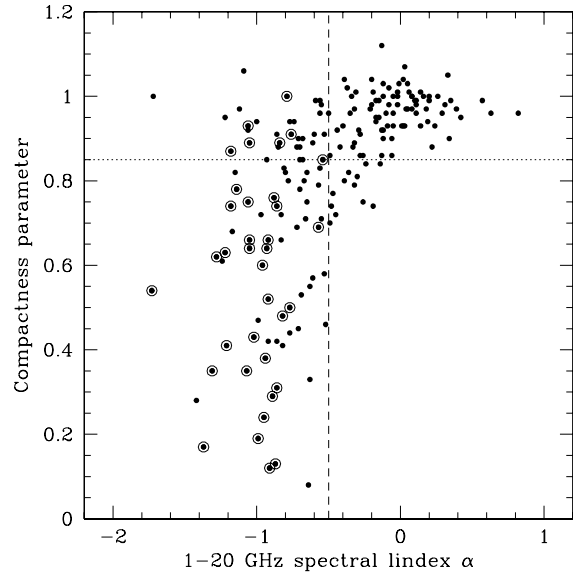


Figure 2. Plots of the compactness parameter R (defined as the ratio of the 20 GHz flux densities measured on long and short baselines, as discussed in §3.2.2) versus the 1–20 GHz spectral index for AT20G-6dFGS galaxies. The vertical dashed line at $\alpha = -0.5$ shows the division between ‘steep-spectrum’ and ‘flat-spectrum’ radio sources, and sources above the horizontal dotted line at $R = 0.85$ are expected to have angular sizes smaller than about 0.2 arcsec (i.e. smaller than about 220 pc at the median redshift of $z = 0.058$ for this galaxy sample). Open circles show sources which are flagged as extended (on scales larger than 10–15 arcsec) in the AT20G catalogue.

As can be seen from Figure 1, this may affect the measured 20 GHz flux densities of sources which are either at very low redshift ($z < 0.01$) or extend well beyond their host galaxy.

Figure 3 allows us to estimate the importance of this effect, by comparing the AT20G catalogue measurements at 5 GHz with the Parkes-MIT-NRAO (PMN) catalogue (Gregory et al. 1994) which used the single-dish Parkes telescope (with a 4 arcmin beam at 5 GHz). The observations were taken more than a decade apart, so the flux density of individual sources may have varied, but the average value of the ratio $S_{\text{AT20G}}/S_{\text{PMN}}$ is 0.93 ± 0.04 for the AT20G sources which are unresolved in both the 20 GHz and NVSS/SUMSS images. In this case, it seems plausible that the small departure from unity could be due to confusing sources within the Parkes beam, or small differences in the flux-density scale, rather than missing flux in the AT20G images.

We therefore conclude that for the 70% of AT20G-6dFGS sources which fall into the FR-0 class, the catalogued AT20G flux densities at 5, 8 and 20 GHz represent an accurate measurement of the total radio flux density at these frequencies.

For AT20G-6dFGS galaxies with extended low-frequency radio emission (i.e. the FR-1 and FR-2 radio galaxies listed in Table 3, which represent around 30% of the AT20G-6dFGS sample), the ratio $S_{\text{AT20G}}/S_{\text{PMN}}$ is 0.47 ± 0.05 . We therefore need to keep in mind that the listed AT20G flux densities for the FR-1 and FR-2 radio galaxies often reflect the high-frequency radio emission from the central core alone, rather than the core plus extended jets and lobes.

Burke-Spolaor et al. (2009) made new 20 GHz images of nine of the most extended sources in the AT20G sample, and their flux-density measurements were incorporated into

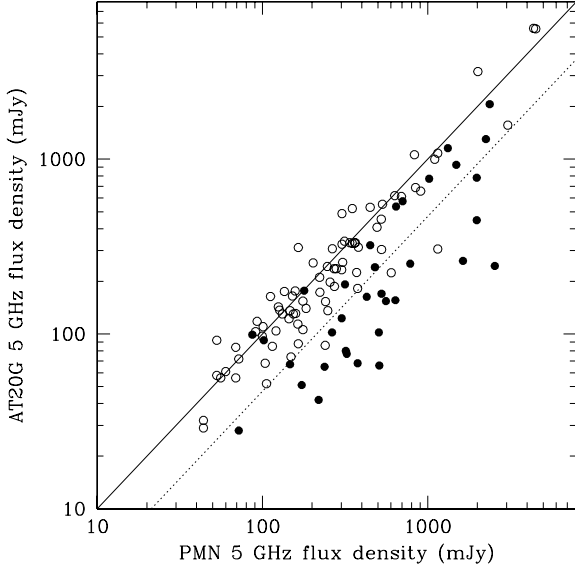


Figure 3. Comparison of 5 GHz flux density measurements from the AT20G catalogue (Murphy et al. 2010) and the PMN catalogue (Gregory et al. 1994). Filled circles show the FR-1 and FR-2 sources listed in Table 3, which have extended (angular size > 30 arcsec) low-frequency radio emission. Open circles represent galaxies which are unresolved in the low-frequency NVSS and SUMSS images. The solid diagonal line shows the relation $S_{\text{AT20G}} = S_{\text{PMN}}$, and the dashed line $S_{\text{AT20G}} = 0.47 S_{\text{PMN}}$ as discussed in the text.

the final AT20G catalogue (Murphy et al. 2010). Five of these sources (J013357-362935 (=NGC 612), J133639-335756 (=IC 4296), J215706-694123 (=ESO 075-G41), Pictor A and Centaurus A) are also members of the AT20G-6dFGS sample. Additional radio observations, with better sensitivity to extended emission, would be valuable to measure the total high-frequency flux density accurately for the other AT20G-6dFGS sources which have extended 20 GHz radio emission.

3.4 Radio spectral-index distribution

The spectral-energy distribution of radio sources is commonly expressed in terms of a two-point spectral index α_a^b (where $S_\nu \propto \nu^\alpha$) between frequencies ν_a and ν_b . Since many radio sources have curved rather than power-law continuum spectra, particularly at higher frequencies (Taylor et al. 2004; Sadler et al. 2006; Chhetri et al. 2012), it is important to keep in mind that the measured value of α may shift with observing frequency and/or redshift.

Most radio-loud AGN have both a compact, flat-spectrum core and extended, steep-spectrum radio lobes, so the observed value of α reflects the relative dominance of compact (recent) versus extended (longer-term) radio emission. While most core-dominated radio sources have flat radio spectra, compact steep-spectrum (CSS) radio sources are also seen (Fanti et al. 1990; O’Dea 1998).

At low frequencies, the radio AGN population is commonly divided into ‘steep-spectrum’ ($\alpha \leq -0.5$) and ‘flat-spectrum’ ($\alpha > -0.5$) sources (De Zotti et al. 2010; Chhetri et al. 2012). Steep-spectrum radio sources dominate in samples selected at frequencies near 1 GHz. For example, Mauch et al. (2003) measured a median 843–1400 MHz spectral index of -0.89 for sources brighter than

50 mJy at 843 MHz. About 25% of these sources were classified as flat-spectrum and 75% as steep-spectrum.

Samples selected at higher radio frequencies are known to contain more flat-spectrum sources (e.g De Zotti et al. 2010). Sources brighter than 40 mJy in the 20 GHz–selected AT20G survey (Murphy et al. 2010) have a median 5–20 GHz spectral index of -0.28 , with 69% classified as flat-spectrum objects (Massardi et al. 2011a).

3.4.1 Near-simultaneous spectral indices at 5–20 GHz

124 of the 202 galaxies in Table 3 (61%) have near-simultaneous radio flux density measurements at 5, 8 and 20 GHz available from the AT20G catalogue (Murphy et al. 2010). These multi-frequency data allow us to calculate high-frequency spectral indices between 5, 8 and 20 GHz, α_5^{20} , in the same way as Massardi et al. (2011a) have done for the full AT20G sample.

As can be seen from Table 5, the distribution of spectral behaviour for the AT20G-6dFGS galaxies is similar to that found by Massardi et al. (2011a) for the weaker ($S_{20} < 100$ mJy) sources in the full AT20G sample, with a roughly equal mix of flat and steep-spectrum objects and a much smaller fraction of peaked or upturning radio spectra.

The main difference is that the local AT20G-6dFGS galaxies contain almost no ‘inverted-spectrum’ sources with both $\alpha_5^8 > 0$ and $\alpha_8^{20} > 0$. This is consistent with a picture in which the inverted-spectrum AT20G population (with a spectral peak above 20 GHz) is dominated by flares from relativistically-beamed objects (blazars), as discussed by Bonaldi et al. (2013). We would not expect these beamed objects to be present in the AT20G-6dFGS sample of nearby, K-band selected galaxies.

Bonaldi et al. (2013) estimate that the fraction of genuine ‘high-frequency peaker’ (HFP) radio galaxies in the full AT20G sample is < 0.5 per cent, implying that we would expect to see no more than one such object in the 6dFGS-AT20G sample of 201 galaxies. In fact, our sample does contain one galaxy (AT20G J212222-560014) which appears to have a genuine HFP radio spectrum. Hancock et al. (2010) note that J212222-560014 has a radio spectrum peaking above 40 GHz and shows no evidence for variability at 20 GHz, consistent with the behaviour expected for a very young GPS radio galaxy.

The median spectral indices measured for the local AT20G-6dFGS galaxies, $\tilde{\alpha}_5^8 = -0.28 \pm 0.07$ and $\tilde{\alpha}_8^{20} = -0.26 \pm 0.05$ are similar to those measured for the AT20G sample as a whole ($\tilde{\alpha}_5^8 = -0.16$ and $\tilde{\alpha}_8^{20} = -0.28$; Massardi et al. 2011a), though it should be noted that (in contrast to the full AT20G sample) the median radio spectral index for the local AT20G-6dFGS galaxies is no steeper at 8–20 GHz than at 5–8 GHz.

This lack of curvature in the median 5–20 GHz radio spectrum for the AT20G-6dFGS galaxies is almost certainly due to their low redshift. Chhetri et al. (2012) show that the radio spectra of compact AT20G sources start to steepen above a rest frequency of about 30 GHz. For the nearby galaxies in the AT20G-6dFGS sample, unlike the more distant sources in the AT20G catalogue as a whole, this high-frequency curvature has not been shifted into the 8–20 GHz spectral range, so it is not surprising that the median 5–8 and 8–20 GHz spectral indices are similar for the local AT20G-6dFGS sample.

Table 5. High-frequency spectral-index classifications for the 6dFGS-AT20G AGN, compared to the results for the full AT20G sample from Table 2 of Massardi et al. (2011a).

Spectrum	Class	AT20G-6dFGS galaxies No. (per cent)	Full AT20G sample No. (per cent)	Full AT20G, $S_{20} < 100$ mJy No. (per cent)
$-0.5 < \alpha_{1-20}^{20} < +0.5$ and $-0.5 < \alpha_{5-20}^{20} < +0.5$	Flat (F_{high})	55 (44.7)	1766 (53.0)	694 (45.0)
$\alpha_{1-20}^{20} < 0, \alpha_{5-20}^{20} < 0$	Steep (S_{high})	54 (43.9)	1086 (32.6)	619 (40.1)
$\alpha_{1-20}^{20} > 0, \alpha_{5-20}^{20} > 0$	Inverted (I_{high})	1 (0.8)	195 (5.8)	66 (4.3)
$\alpha_{1-20}^{20} > 0, \alpha_{5-20}^{20} < 0$	Peak (P_{high})	6 (4.9)	183 (5.5)	92 (5.9)
$\alpha_{1-20}^{20} < 0, \alpha_{5-20}^{20} > 0$	Upturn (U_{high})	7 (5.7)	102 (3.1)	73 (4.7)
Any		123 (100)	3332 (100)	1544 (100)

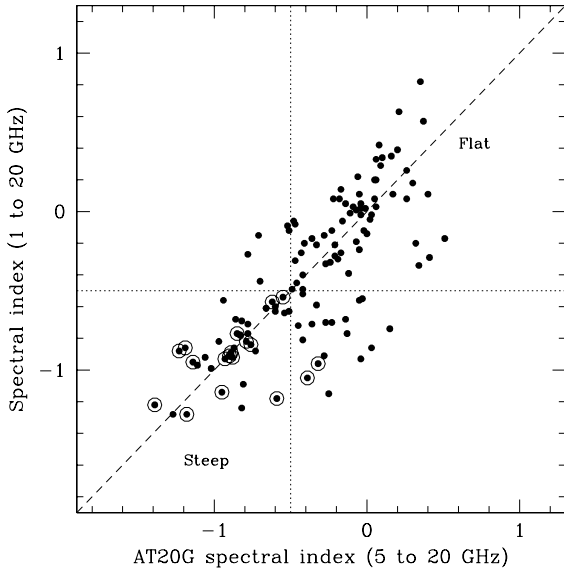


Figure 4. Comparison of radio spectral indices measured at 5–20 GHz from near-simultaneous AT20G data, and at 1–20 GHz by cross-matching the AT20G and NVSS/SUMSS source catalogues. As in Figure 2, the points plotted within larger open circles correspond to galaxies with extended 20 GHz sources.

3.4.2 1–20 GHz spectral indices

All 202 galaxies in the AT20G-6dFGS sample have low-frequency radio data available from the 1.4 GHz NVSS (Condon et al. 1998) or 843 MHz SUMSS (Mauch et al. 2003) surveys, allowing us to calculate a 1–20 GHz spectral index α_{1-20}^{20} for each galaxy. These spectral-index values need to be used with some caution since (i) the radio measurements were made several years apart and some sources may be variable, and (ii) the low- and high-frequency radio measurements have slightly different spatial resolution, which may affect the measured spectral index for extended sources.

Figure 4 compares α_{1-20}^{20} with the near-simultaneous α_{5-20}^{20} values for the 6dFGS galaxies which have multi-frequency AT20G data. The median 1–20 GHz spectral index for the 123 galaxies with 5, 8 and 20 GHz data, -0.39 ± 0.05 , is slightly steeper than the median 5–20 GHz spectral index of -0.27 ± 0.05 for the same group of galaxies. This is mainly because (as we discuss later in §3.5), some of the flat-spectrum objects seen at 5–20 GHz are embedded in more diffuse steep-spectrum lobes which contribute to the total flux density measured at frequencies near 1 GHz.

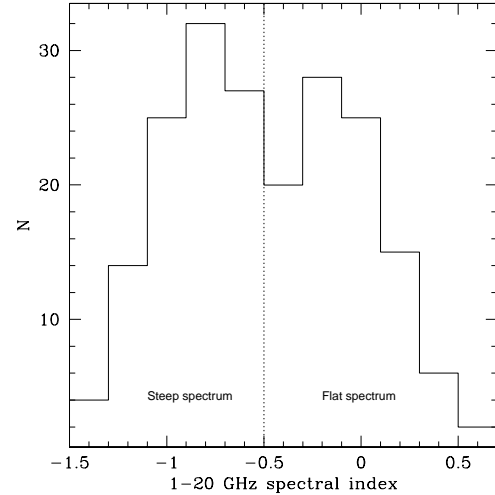


Figure 5. Distribution of 1–20 GHz radio spectral index for galaxies in the AT20G-6dFGS sample.

In the analysis which follows, we will use the values of α_{1-20}^{20} (which are available for the whole AT20G-6dFGS sample) as a guide to separating the ‘flat-spectrum’ and ‘steep-spectrum’ radio-source populations (though it is important to keep in mind that, as can be seen from Figure 4, roughly 15% of the AT20G-6dFGS galaxies will have radio spectra which are ‘steep’ at low frequencies and ‘flat’ at higher frequencies).

Figure 5 shows the distribution of α_{1-20}^{20} for the 202 sources in the AT20G-6dFGS sample. The median 1–20 GHz spectral index for the full AT20G-6dFGS sample is -0.53 ± 0.04 and although this plot suggests that the distribution may be bimodal, the data are statistically consistent with a normal distribution with a mean value of $\alpha_{1-20}^{20} = -0.498$ and a standard deviation of 0.503.

3.5 Candidate GPS and CSS radio sources

In §3.1, we divided the AT20G-6dFGS radio galaxies into three subclasses (FR-0, FR-1 and FR-2) based on their low-frequency radio morphology. We now use the radio morphology and spectral index information presented in §3.2 and §3.4 to identify possible members of the class of Compact Steep Spectrum (CSS) and Gigahertz-Peaked Spectrum (GPS) sources which are generally thought to represent the earliest stages of radio-galaxy evolution (O’Dea 1998).

We have chosen to sub-divide the FR-0 class (i.e. the AT20G-6dFGS galaxies whose radio emission is unresolved in the 1 GHz NVSS/SUMSS images) as follows:

- **Candidate GPS sources (FR-0g).** These are radio sources with a compactness parameter $R \geq 0.85$ and 1-20 GHz spectral index $\alpha_1^{20} > 0$, i.e. likely to be less < 1 kpc in size and have a radio spectrum peaking above 1 GHz (many of these sources peak at or above 5–10 GHz).

- **Candidate CSS sources (FR-0c).** These are radio sources with a steep 1-20 GHz spectral index $\alpha_1^{20} < -0.50$, i.e. less than 10-20 kpc in size and likely to have a radio spectrum peaking below 1-5 GHz.

- **Unclassified compact sources (FR-0u).** These are sources which can't be classified as either CSS or GPS using the currently available data, either because they have no measured compactness parameter or because they have $-0.5 < \alpha_1^{20} < 0$ (making it difficult to locate a radio spectral peak in these objects, which generally have only a few data points available).

These results confirm that the AT20G-6dFGS sample contains a high fraction of possible CSS and GPS galaxies. At least 83 objects (41% of the total sample) are candidate CSS/GPS sources, and the fraction rises to 67% if we include the unclassified FR-0u objects.

Further analysis of the CSS/GPS candidate sources is difficult at this stage, though we discuss the possible effects of relativistic beaming in §6.2. Higher-resolution (VLBI) radio images of these objects, together with improved multi-wavelength radio data to measure their spectral turnover frequency, are needed to estimate the source ages and establish how many of them are genuinely young radio galaxies.

4 THE LOCAL RADIO LUMINOSITY FUNCTION (RLF) AT 20 GHz

The local radio luminosity function (RLF) is the global average space density of radio sources at the present epoch (Auremma et al. 1977; Condon et al. 1989), and provides an important benchmark for studying the cosmic evolution of radio-source populations (De Zotti et al. 2010). The local radio luminosity function of galaxies at 20 GHz provides a particularly useful benchmark for the study of high-redshift radio galaxies (since, for example, 1.4 and 5 GHz measurements of a galaxy at redshift $z \sim 3$ correspond to 8 and 20 GHz in the object's rest frame). High-frequency data also provide important constraints for the 'simulated skies' (Wilman et al. 2008) which are increasingly used in the science planning for future large radio telescopes like the Square Kilometre Array.

4.1 Calculating the local RLF

To calculate the local radio luminosity function of galaxies at 20 GHz, we used the same methodology as Mauch & Sadler (2007).

For the radio data, we set a flux-density limit of 50 mJy at 20 GHz and assumed a differential completeness of 78% above 50 mJy and 93% above 100 mJy (Massardi et al. 2011a).

For the 6dFGS data, we used a magnitude limit of $K=12.75$ mag. and assumed a spectroscopic completeness of 92.5% (Jones et al. 2009). The sky area covered by the AT20G-6dFGS sample was assumed to be the total 6dFGS area of 5.19 sr (16,980 deg²).

We calculated the local radio luminosity function using the

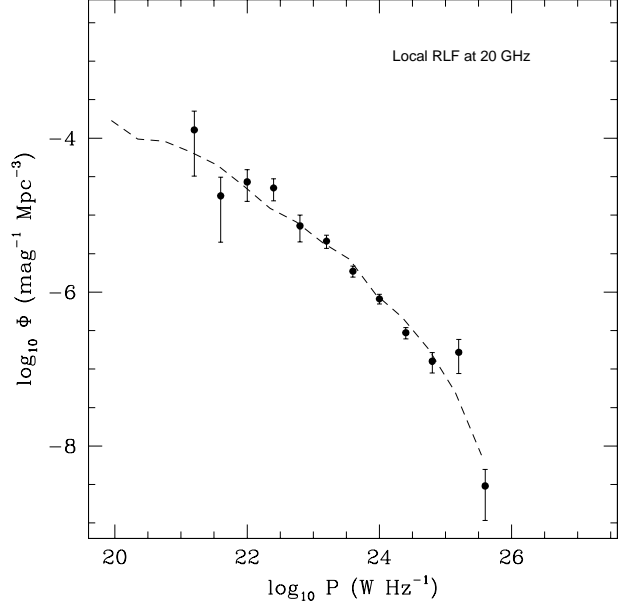


Figure 6. The local radio luminosity function for galaxies at 20 GHz (filled circles). The dashed line shows the 1.4 GHz RLF for AGN from Mauch & Sadler (2007), shifted in radio power by adopting a 1.4–20 GHz spectral index of -0.74 as discussed in the text.

Table 6. Local radio luminosity function (RLF) at 20 GHz for radio AGN.

$\log_{10} P_{20}$ (W Hz ⁻¹)	N	$\log \Phi$ (mag ⁻¹ Mpc ⁻³)
21.2	1	$-3.89^{+0.24}_{-0.60}$
21.6	1	$-4.75^{+0.24}_{-0.60}$
22.0	3	$-4.57^{+0.16}_{-0.25}$
22.4	7	$-4.65^{+0.12}_{-0.17}$
22.8	6	$-5.14^{+0.14}_{-0.21}$
23.2	20	$-5.34^{+0.08}_{-0.09}$
23.6	28	$-5.73^{+0.07}_{-0.08}$
24.0	39	$-6.09^{+0.06}_{-0.07}$
24.4	33	$-6.53^{+0.07}_{-0.08}$
24.8	22	$-6.90^{+0.11}_{-0.15}$
25.2	10	$-6.78^{+0.17}_{-0.27}$
25.6	2	$-8.52^{+0.22}_{-0.45}$

$\langle V/V_{\max} \rangle = 0.45 \pm 0.02$

$1/V_{\max}$ method of Schmidt (1968), where V_{\max} is the maximum volume within which a galaxy can satisfy all the sample selection criteria (for the AT20G-6dFGS sample, $S_{20 \text{ GHz}} \geq 50$ mJy, $K \leq 12.75$ mag. and $0.003 < z < 0.200$).

4.2 Results

The local 20 GHz radio luminosity function measured from the AT20G-6dFGS galaxy sample is listed in Table 6 and plotted in Figure 6.

We derive a mean value of V/V_{\max} (0.45 ± 0.02) for these galaxies, which is slightly lower than the value of 0.50 expected for a complete sample. This is almost certainly because the total

20 GHz flux density for some extended AT20G sources is underestimated, as discussed in §3.3. If these sources have measured flux densities below 50 mJy, they will be excluded from the RLF sample when they should have been included. If we separate the extended 20 GHz sources from those which are unresolved, we find $\langle V/V_{\max} \rangle = 0.47 \pm 0.02$ for unresolved sources and $\langle V/V_{\max} \rangle = 0.37 \pm 0.05$ for the extended sources, confirming that the small incompleteness in our overall sample arises mainly from the extended 20 GHz sources. Because of the relatively small size of the AT20G sample and the likely incompleteness in the extended-source population, we have not attempted to fit a functional form to the 20 GHz RLF. Instead, we used the parameterized form of the 1.4 GHz local RLF from equation (6) of Mauch & Sadler (2007), and fitted this to the 20 GHz data by making a simple shift in radio power set by a single characteristic 1–20 GHz spectral index α_0 for the RLF as a whole. The best-fitting value, $\alpha_0 = -0.74$, is shown by the dashed line in Figure 6.

It is important to note that the shift of $\alpha_0 = -0.74$ which provides the best match for the 1.4 GHz and 20 GHz radio luminosity functions is steeper than the median 1–20 GHz spectral index of $\tilde{\alpha}_{10}^2 = -0.53 \pm 0.04$ which we found for the AT20G-6dFGS galaxies in §3.4.2. The reason for this difference is not yet completely clear, but one plausible explanation is that the value of -0.74 represents a characteristic 1–20 GHz spectral index for the local radio-galaxy population as a whole. Since the individual objects which make up this population have a broad spread in radio spectral index, the flat-spectrum members of this population are more likely to be detected at 20 GHz than the steep-spectrum objects and so this will flatten the observed spectral-index distribution for sources selected at 20 GHz.

5 OPTICAL AND INFRARED PROPERTIES OF THE AT20G-6DFGS SAMPLE

5.1 Redshift and infrared K-band luminosity

Figure 7 shows the distribution of the sample galaxies in K-band apparent magnitude and redshift. Since the infrared K-band light in these nearby galaxies arises mainly from old giant stars, the K-band luminosity is closely related to the stellar mass of the galaxy.

Most of the galaxies in Table 3 lie close to the well-known K– z relation for radio galaxies (Lilly & Longair 1984; Willott et al. 2003; De Breuck et al. 2002). The K– z relation derived by Willott et al. (2003) and plotted in Figure 7,

$$K = 17.37 + 4.53 \log_{10} z - 0.31 (\log_{10} z)^2$$

is very close to the expected K-magnitude evolution of a passively-evolving galaxy which formed at high redshift ($z \sim 10$) and has a present-day ($z \sim 10$) luminosity of around $3 L_*$. We therefore find that the AT20G-6dFGS radio sources are hosted by galaxies which have K-band luminosities matching those of powerful radio galaxies in the distant universe.

5.2 The radio/optical luminosity diagram

Figure 8 shows the distribution of the sample galaxies in radio and K-band luminosity. A radio k -correction of the form $k_{\text{radio}}(z) = (1+z)^\alpha$ has been applied, where α is the radio spectral index ($S_\nu \propto \nu^\alpha$). Different symbols show galaxies classified as FR-1, FR-2 or FR-0 (compact) on the basis of their 1 GHz radio morphology, as discussed in §3. As with the NVSS-6dFGS sample of

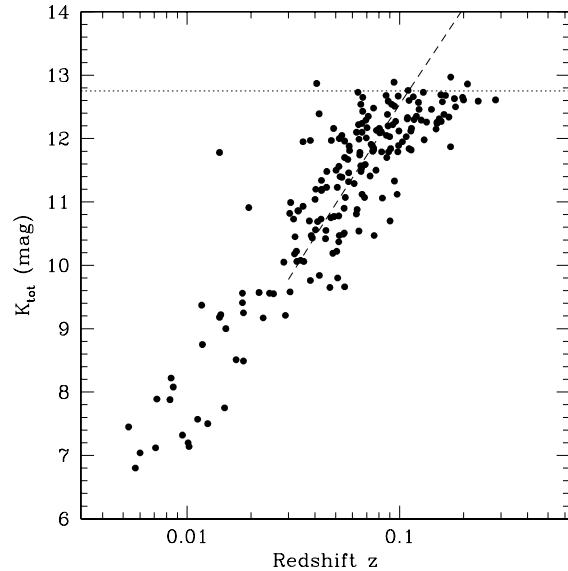


Figure 7. Plot of K-band apparent magnitude versus redshift for galaxies in the 6dFGS-AT20G sample. The horizontal dotted line shows the K=12.75 magnitude limit of the 6dFGS, and the dashed line shows an extension of the radio-galaxy K– z relation derived by Willott et al. (2003) over the redshift range $0.05 < z < 2$.

Mauch et al. (2007), almost all the AT20G-6dFGS galaxies are optically luminous (M_K brighter than -24 mag.), but there is no obvious correlation between radio and optical luminosity for galaxies above this K-band luminosity threshold.

There is a clear tendency for FR-2 radio galaxies to have a higher radio luminosity than FR-1 radio galaxies of similar stellar mass, implying that the relation found by Ledlow & Owen (1996; see their Figure 1), in which the FR-1/FR-2 division is a strong function of optical luminosity, also holds at 20 GHz. Interestingly, the compact (FR-0) sources cover the full range in 20 GHz radio power spanned by the FR-1 and FR-2 objects, and a few are also found in low-luminosity (M_K fainter than -24 mag.) galaxies. The radio galaxy Pictor A (AT20G J051949-454643) is a notable outlier in this plot, having a total 20 GHz radio power of $1.8 \times 10^{25} \text{ W Hz}^{-1}$ despite being one of the least optically-luminous galaxies in the AT20G-6dFGS sample (with $M_K = -23.9$ mag).

5.3 High-excitation and low-excitation radio galaxies

Recently, several authors (e.g. Hardcastle et al. 2007, Best & Heckman 2012 and references therein) have proposed a fundamental dichotomy between ‘high-excitation radio galaxies’ (HERGs), in which the AGN is fuelled in a radiatively efficient way by a classic accretion disk, and ‘low-excitation radio galaxies’ (LERGs) in which the accretion rate is significantly lower and radiatively inefficient. Best & Heckman (2012) derive accretion rates of one and ten per cent of the Eddington rate for HERGs, in contrast to a typical accretion rate below one per cent Eddington for the LERGs in their sample.

Observationally, HERGs are characterised by strong optical emission lines with line ratios characteristic of highly-excited gas (e.g. Kewley et al. 2006), while LERGs generally show weak or no optical emission lines. Ideally we would use a well-determined quantity such as emission-line luminosity to classify the AT20G-

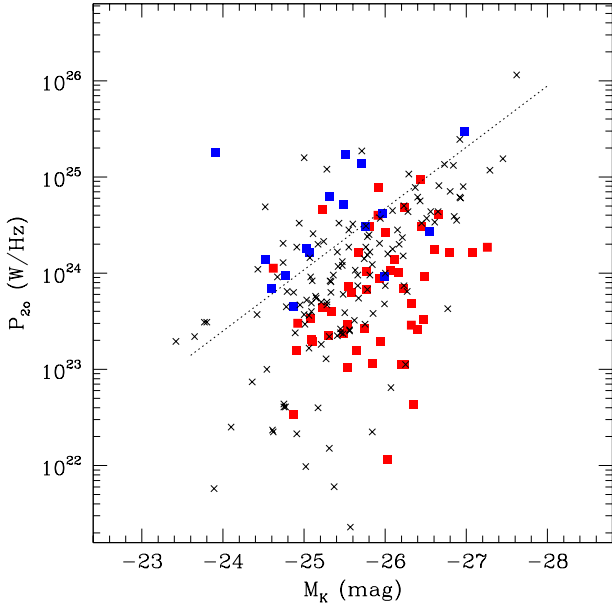


Figure 8. Distribution of the AT20G-6dFGS galaxy sample in (infrared) K-band absolute magnitude and 20 GHz radio power. FR-1 radio galaxies are shown as filled red squares, FR-2 radio galaxies as filled blue squares and compact (FR-0) sources as black crosses. The dashed line corresponds to the 1.4 GHz FR-1/FR-2 dividing line from Ledlow & Owen (1996), shifted to K-band and 20 GHz by assuming (i) a typical galaxy colour of $(R-K) = 3.0$ mag. and (ii) a characteristic radio spectral index $\alpha_{1}^{20} = -0.74$, as discussed in §4.2

6dFGS radio galaxies, but this is difficult since the 6dFGS spectra are not flux-calibrated. Instead, we make a qualitative separation by associating the ‘Ae’ and ‘AeB’ radio galaxies in our sample with the HERG class, and ‘Aa’ and ‘Aae’ objects with the LERG class.

There are several reasons why this appears reasonable:

(i) The 6dFGS spectra have a resolution of 5–6 Å in the blue and 10–12 Å in the red (Jones et al. 2004). Since our Ae classification requires that a galaxy show optical emission lines which are strong relative to the stellar continuum, these objects are likely to have an [OIII] equivalent width well above the value of 5 Å which Best & Heckman (2012) use as one of the distinguishing criteria for of their HERG class.

(ii) At least 25% of the Ae objects in our sample show broad Balmer emission characteristic of high-excitation Seyfert galaxies, while many of the narrow-line Ae objects also have a literature classification as Seyfert galaxies (see the notes in Appendix A).

(iii) We know that most early-type galaxies show weak optical emission lines (generally with low-excitation LINER-like spectra as described by Heckman 1980) if one looks carefully enough (e.g. Phillips et al. 1986). In some cases, these emission lines may be excited by hot post-AGB stars rather than an AGN (Bertelli et al. 1989; Cid Fernandes et al. 2011). For fibre spectroscopy these weak emission lines may be easier to recognize in lower-redshift galaxies, simply because the fibre contains less of the stellar light from the surrounding galaxy, as discussed by Mauch & Sadler (2007). As a result, we expect to see significant overlap between our Aa and Aae classes and so it seems plausible to associate all these objects with the LERG class.

If we make this separation, then 23% of the AT20G-6dFGS

radio sources are classified as high-excitation (HERG) systems and 77% as low-excitation (LERG). While LERGs are the majority population, the HERG fraction is higher than that seen in comparable radio-source samples selected at 1.4 GHz. Only $\sim 12\%$ of the radio AGN in the Mauch & Sadler (2007; MS07) are classified as Ae galaxies, and the HERG fraction in the Best & Heckman (2012; BH12) sample of radio AGN is even lower than this.

The higher HERG fraction seen in the 20 GHz sample is not simply an effect of comparing objects with different radio luminosities (the AT20G sources are typically more powerful than those selected from NVSS, because the AT20G catalogue has a 40 mJy flux density limit, compared to 2.5 mJy for NVSS). To check this, we compared the HERG fraction in several bins of 1.4 GHz (not 20 GHz) radio power for the AT20G-6dFGS, BH12 and MS07 galaxy samples. For radio powers in the range $10^{23.8}$ to $10^{25.6}$ W Hz^{-1} the HERG fraction in the AT20G-6dFGS sample was at least three to five times higher than in the corresponding BH12 and MS07 samples. In the highest-power bin ($10^{25.6}$ to $10^{26.5}$ W Hz^{-1}), which contains only a relatively small number of objects, all three samples showed a high HERG fraction of around 40–50%.

5.4 Optical morphology of the host galaxies

Most of the powerful radio-loud AGN in the local universe are hosted by massive elliptical galaxies (e.g. Lilly & Prestage 1987; Owen & Laing 1989; Veron-Cetty & Veron 2001), though some exceptions are known (e.g. Ledlow et al. 2001; Hota et al. 2011), and we also know that nearby spiral galaxies can host compact radio-loud AGN (e.g. Norris et al. 1988; Sadler et al. 1995).

Some of the galaxies in the AT20G-6dFGS sample are at low enough redshift ($z < 0.025$) that a reliable classification of their optical morphology is available from the RC3 (de Vaucouleurs et al. 1991) and/or ESO-Uppsala (Lauberts 1982) galaxy catalogues. We have therefore used these classifications, where available, to look at the host galaxy properties of the AT20G-6dFGS sample.

Of the 34 lowest-redshift ($z < 0.025$) galaxies in Table 3, twenty-four are classified as early-type (E or S0) galaxies and ten as late-type (spiral/disk) galaxies, implying that at the lowest 20 GHz luminosities probed by our sample (10^{21} to 10^{23} W Hz^{-1}) around 30% of the host galaxies are spirals.

Although the morphologically-classified subsample (34 AT20G-6dFGS galaxies with $z \leq 0.025$) is small, some general patterns can be seen. In particular, all nine FR-1 radio galaxies in this redshift range have E/S0 host galaxies but almost half the compact FR-0 sources are in spiral galaxies.

Table 7 lists the thirteen galaxies in our sample which are known to have spiral or disk-like optical morphology (this table also includes some objects with $z > 0.025$). Six of these galaxies (NGC 253, NGC 1068, NGC 4594, IRAS 13059-2407, NGC 5078 and NGC 5232) also belong to the sample of dusty ‘infrared-excess IRAS galaxies’ identified by Drake et al. (2004), and PMN J0315-1906 has been identified by Ledlow et al. (2001) as a rare example of an FR-1 radio source hosted by a spiral galaxy.

Since reliable morphological classifications are not available for the more distant galaxies in the 6dFGS-AT20G sample, the next section discusses the use of mid-infrared photometry from WISE as an alternative way of investigating host-galaxy properties.

Table 7. AT20G-6dFGS radio sources known to be associated with spiral galaxies. The galaxy classification in column 8 is taken from either the RC3 catalogue (de Vaucouleurs et al. 1991) or the ESO/Uppsala catalogue (Lauberts 1982), and the galaxy T-type in column 9 is from the RC3 catalogue.

AT20G name	Alt. name	Redshift z	Spectral class	M_K mag	$\log P_{20}$ W Hz^{-1}	α_1^{20}	Galaxy class	T-type	Notes
(a) Nearby ($z \leq 0.025$) galaxies classified as spiral in the RC3 and/or ESO/Uppsala catalogues									
J004733-251717	NGC 253	0.0008	SF	-22.74	20.93	-0.91	Sc	+5.0	Nuclear starburst
J024240-000046	NGC 1068	0.0038	Ae	-25.31	22.18	-0.86	Sb	+3.0	Seyfert 2 galaxy
J123959-113721	NGC 4594	0.0036	..	-25.57	21.36	-0.05	Sa	+1.0	
J130527-492804	NGC 4945	0.0019	..	-23.89	21.76	-0.64	Scd	+6.0	AGN (Liner)
J130841-242259	IRAS 13059-2407	0.0142	Ae	-22.11	22.41	-0.80	Sc?	...	Drake et al. (2003)
J131949-272437	NGC 5078	0.0071	Aae	-25.37	21.78	-0.59	Sa	+1.0	
J133608-082952	NGC 5232	0.0228	Aae	-25.78	23.83	+0.16	Sa	+0.0	
J145924-164136	NGC 5793	0.0117	..	-24.10	22.40	-1.00	Sb	+3.0	Seyfert 2 galaxy
J172341-650036	NGC 6328	0.0142	..	-24.74	24.11	-0.08	Sab	+1.8	AGN (Liner)
J220916-471000	NGC 7213	0.0060	..	-25.01	21.99	+0.01	Sa	+1.0	Seyfert 1 galaxy
(b) More distant ($z > 0.025$) galaxies noted in the literature as spirals									
J001605-234352	ESO 473-G07	0.0640	Ae	-24.79	23.81	-0.53	S...	+5.0	
J031552-190644	PMN J0315-1906	0.0671	Ae?	-24.62	24.05	+0.03	S..	...	Ledlow et al. (2001)
J220113-374654	AM 2158-380	0.0334	Ae	-24.87	23.65	-0.82	S?	..	Drake et al. (2003)

5.5 Mid-infrared photometry from WISE

Near- and mid-infrared photometry (at 3.4, 4.6, 12 and 22 μm) is now available for all the AT20G-6dFGS galaxies from the WISE mission (Wright et al. 2010). The majority of galaxies in our sample (141/202) are flagged as extended 2MASS objects (`ext_flag=5`), and for these we used the elliptical aperture magnitudes as recommended by Wright et al. (2010). For the remaining galaxies, which were flagged as unresolved in the WISE catalogue, we used the profile-fit magnitudes.

We restricted our analysis to galaxies with WISE 3.6 μm magnitude fainter than 6.0, since galaxies brighter than this may be too large on the sky to allow accurate photometry with WISE. We also excluded five galaxies which had anomalous WISE colours because of contamination from a companion galaxy or bright foreground star. This left a total of 193 AT20G-6dFGS galaxies with good-quality WISE photometry.

5.6 The WISE two-colour plot

Figure 9 shows a WISE colour-colour plot for the full AT20G-6dFGS sample, based on Figure 12 of Wright et al. (2010). The errors on individual data points are typically <0.05 mag in $[3.4] - [4.6]$ colour and <0.1 mag in $[4.6] - [12]$ colour. The dotted horizontal and vertical lines are also based on the work of Wright et al. (2010), who divide elliptical and spiral galaxies at a WISE $[4.6] - [12]$ colour of +1.5 mag, and note that the most powerful optical AGN lie above a $[3.4] - [4.6]$ colour of +0.6 mag. For nearby AT20G-6dFGS galaxies with a reliable optical classification (see §4.3 above), there is excellent agreement between the optical and WISE galaxy classes. We also see that all the galaxies in which we detected strong, broad Balmer emission lines (class AeB) lie close to the line followed by blazars and radio-loud QSOs (Massaro et al. 2012).

The WISE two-colour plot is becoming widely used for galaxy population studies, and its interpretation has recently been discussed by several authors. The $[3.4] - [4.6]$ micron colour can be used to separate normal galaxies from AGN with a strongly-radiating accretion disk (Assef et al. 2010; Yan et al. 2013), while the $[4.6] - [12]$ micron colour separates dusty star-forming galaxies

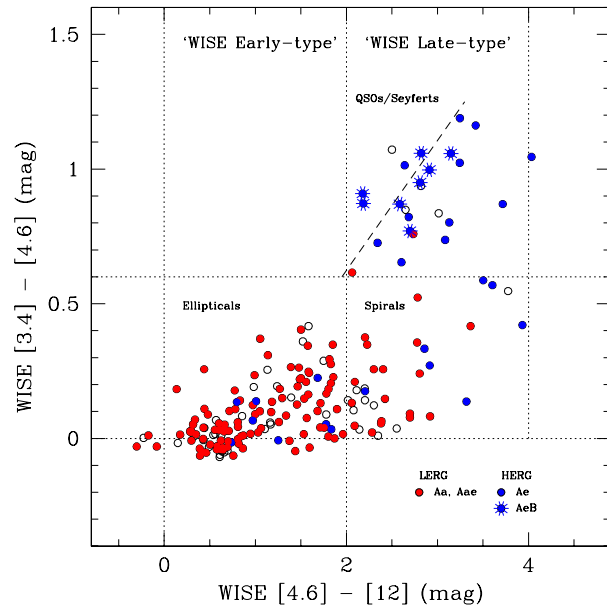


Figure 9. WISE colour-colour plot for the AT20G galaxies, which are colour-coded according to their optical spectral classification as outlined in Table 2 and §2.3. Aa and Aae galaxies (LERGs) are shown by red filled circles and Ae galaxies (HERGs) by blue filled circles. Galaxies with broad emission lines (class AeB) are shown by blue stars, and galaxies with no spectral classification (see §2.3) by black open circles. Dotted lines show the regions in which different galaxy populations are expected to lie, as discussed in §5.6 of the text, and the diagonal dashed line shows the WISE blazar sequence from Massaro et al. (2012).

(or galaxies in which the dust is heated by radiation from an AGN) from early-type galaxies with little or no warm dust. Donoso et al. (2012) have shown that the $[4.6] - [12]$ colour reflects a galaxy's specific star-formation rate (SSFR), i.e. the current star-formation rate divided by the total stellar mass.

If we follow Wright et al. (2010) and set the dividing line between WISE 'ellipticals' and 'spirals' at a colour of $[4.6] - [12] =$

1.5 mag., we find that almost half of our AT20G-6dFGS galaxies (93/193, or 48%) fall into the ‘spiral’ category. If we set a more stringent cutoff for WISE ‘spirals’ at $[4.6] - [12] \geq 2.0$ mag. (which roughly corresponds to the main locus of star-forming galaxies in Figure 8 of Donoso et al. 2012), we find a spiral fraction of 31% (60/193) for the AT20G-6dFGS sample. This is similar to the spiral fraction of $\sim 30\%$ derived from optical classification of the closest galaxies in our sample (see §4.4), so we adopt $[4.6] - [12] = 2.0$ mag. as a reasonable dividing line between host galaxies which lie in the ‘WISE elliptical’ region and those which correspond to ‘WISE spirals’. Since ‘elliptical’ and ‘spiral’ are morphological descriptions, while the WISE two-colour plot is based on the mid-infrared spectral-energy distribution, in the remainder of this paper we refer to the two classes of host galaxy as ‘WISE early-type’ ($[4.6] - [12] < 2.0$ mag) and ‘WISE late-type’ ($[4.6] - [12] \geq 2.0$ mag) galaxies respectively.

5.6.1 WISE early-type galaxies

As discussed above, around 70% of the AT20G-6dFGS galaxies have WISE colours which are typical of normal elliptical and S0 galaxies. Of the 25 ‘WISE early-type’ galaxies with an RC3 or ESO morphological type, 22 are classified as E or S0 galaxies and three as early-type (Sa) spirals, showing that there is generally good agreement between the WISE classification and the optical morphology where both are available.

5.6.2 WISE late-type galaxies

The remaining 30% of AT20G-6dFGS galaxies fall into the ‘WISE late-type’ class. Nine of them also have an RC3 or ESO morphological type – seven are classified as spirals (ranging from Sa to Scd) and two as S0 galaxies, again implying that the WISE classification is generally consistent with the observed optical morphology.

We note, however, that the ‘WISE late-type’ galaxies in our sample may be a heterogeneous class, since they are selected because they contain significant quantities of (warm or hot) dust. They include genuine spiral galaxies like those listed in Table 7, as well as elliptical and S0 galaxies with dust lanes (e.g. NGC 612 = AT20GJ013357-362935; see Ekers et al. 1978) and composite objects like the ‘radio-excess IRAS galaxies’ identified by Drake et al. (2004).

5.6.3 Host galaxies of HERGs and LERGs

Table 8 relates the WISE classification (derived from Figure 9) to the HERG/LENG spectral class for the AT20G-6dFGS galaxies. We find that almost all the WISE ‘early-type’ galaxies (92%) have low-excitation (LENG) optical spectra, while the WISE ‘late-type’ galaxies have a mix of HERG and LENG spectra.

This result is in broad agreement with earlier studies of radio galaxies selected at 1.4 GHz. Hardcastle et al. (2013) found that HERGs are typically about four times as luminous as LERGs in the far-infrared 250 μm band, and interpret this as showing that HERGs are more likely to be located in star-forming galaxies. Best & Heckman (2012) found that HERGs in their local sample typically had lower stellar masses and younger stellar populations than LERGs, again consistent with a picture in which HERGs are commonly found in star-forming galaxies.

Table 8. Distribution of spectral classifications for the AT20G-6dFGS galaxies, split by WISE colours.

WISE [4.6] - [12] μm colour	Spectral class HERG LERG	Median M_K (mag)	HERG fraction		
				HERG	LENG
< 2.0 mag	‘Early-type’	8	100	-25.67 ± 0.08	7%
≥ 2.0 mag	‘Late-type’	26	20	-25.41 ± 0.16	57%

5.7 Comparison with the 1.4 GHz-selected NVSS-6dFGS radio galaxy sample

Finally, we compare the spectroscopic properties of the current (20 GHz-selected) 6dFGS-AT20G galaxy sample with the 1.4 GHz-selected 6dFGS-NVSS sample compiled by Mauch & Sadler (2007). This is a useful comparison, since both samples were selected from the 6dFGS galaxy catalogue and so differ only in their radio flux limit and the frequency at which they were selected.

Table 10 compares the spectroscopic properties of the two samples. The AT20G survey has a significantly brighter flux-density limit (40 mJy at 20 GHz) than the NVSS (2.5 mJy at 1.4 GHz), so a comparison with a brighter NVSS sub-sample ($S \geq 100$ mJy at 1.4 GHz) is also included.

One striking difference between the 6dFGS-NVSS and 6dFGS samples is the fraction of galaxies which show optical emission lines (class Aae, Ae or AeB), which is 20–25% for radio AGN selected at 1.4 GHz, but more than twice as high (50%) for galaxies selected at 20 GHz.

This is not a redshift-based selection effect, since the AT20G–6dFGS galaxies consistently show a higher emission-line fraction than NVSS–6dFGS galaxies at the same redshift. Instead, it arises from two effects: (i) a significantly higher HERG fraction in the AT20G-6dFGS sample as a whole (23% HERGs, compared to 10–13% for the NVSS-6dFGS sample, see Table 10), and (ii) a correlation between the 1–20 GHz radio spectral index of a galaxy and the probability that it will show weak optical emission lines. We find that a radio-loud AGN selected at 1.4 GHz from the 6dFGS sample is typically three times more likely to be detected in the AT20G survey if it has an emission-line (Aae or Ae) spectrum.

Figure 10 shows that while galaxies with strong emission lines (class Ae) are seen across the full range of radio spectral index, the fraction of radio galaxies with weak optical emission lines (class Aae) increases rapidly as we move from steep-spectrum to flat-spectrum sources. Further work is needed to understand what produces this correlation. There are several possibilities. The sources may be small enough to be affected by free-free absorption in the innermost regions of the nucleus, giving rise to an observed radio spectrum which peaks at frequencies above 5 GHz, as appears to be the case in the nearby galaxy NGC 1052 (Kameno et al. 2001; Vermeulen et al. 2003). Alternatively, young radio sources may be preferentially triggered in galaxies where sufficient gas is present in the nucleus to fuel them.

Whatever the physics involved, it appears that the AT20G sample contains a distinct class of compact, flat-spectrum radio sources which lie in galaxies with (generally weak) emission-line AGN. Because of their flat or peaked radio spectra, such objects are more likely to be seen in samples selected at higher radio frequencies and so they have not been studied in a systematic way in the past.

Table 9. General radio properties of the AT20G-6dFGS sample, split by (low-frequency) radio morphology and 1-20 GHz spectral index, and excluding the nearby starburst galaxy NGC 253. The compact (FR-0) objects are also divided into three subclasses: FR-0g (candidate GPS), FR-0c (candidate CSS) and FR-0u (unclassified compact sources), as discussed in §3.5 of the text.

Class	1 GHz radio morphology	20 GHz radio morphology /spectral index	N	Median redshift	Median M_K (mag)	Median log P_{20} (W Hz^{-1})	Spectral class		WISE class	
							LERG (Aa/Aae)	HERG (Ae/AeB)	Early	Late
FR-2	Resolved, edge-brightened	Any	16	0.0604	-25.39 ± 0.25	24.45 ± 0.17	36%	64%	7%	93%
FR-1	Resolved, not edge-brightened	Any	49	0.0535	-25.92 ± 0.11	23.68 ± 0.11	98%	2%	93%	7%
FR-0 (all)	Unresolved (LAS ≤ 30 arcsec)	Any	136	0.0653	-25.49 ± 0.09	23.97 ± 0.09	75%	25%	67%	33%
FR-0g	Unresolved	Compactness param. > 0.85 , and $\alpha_1^{20} \geq 0$	34	0.0662	-25.39 ± 0.19	24.18 ± 0.15	75%	25%	64%	36%
FR-0c	Unresolved	$\alpha_1^{20} \leq -0.5$	49	0.0684	-25.48 ± 0.16	24.07 ± 0.15	67%	33%	67%	33%
FR-0u	Unresolved	(not in FR-0g or 0c class)	53	0.0517	-25.55 ± 0.13	23.76 ± 0.15	84%	16%	69%	31%
All flat-spectrum sources ($\alpha_1^{20} > -0.5$)			97	0.0576	-25.49 ± 0.10	23.91 ± 0.10	81%	19%	68%	32%
All steep-spectrum sources ($\alpha_1^{20} \leq -0.5$)			104	0.0596	-25.73 ± 0.10	24.02 ± 0.10	74%	26%	69%	31%
All AT20G-6dFGS AGN			201	0.0581	-25.58 ± 0.07	23.97 ± 0.07	77%	23%	68%	32%

Table 10. A comparison between the 20 GHz-selected AT20G-6dFGS sample discussed in this paper and the 1.4 GHz-selected NVSS-6dFGS sample of radio AGN studied by Mauch & Sadler (2007).

	6dFGS-NVSS (1.4 GHz)		6dFGS-AT20G (20 GHz)
	Mauch & Sadler (2007)		This paper
	all radio AGN	$S_{1.4} > 100$ mJy only	all AGN
No. of galaxies	2784	271	201
Magnitude limit	$K_{\text{tot}} < 12.75$	$K_{\text{tot}} < 12.75$	$K_{\text{tot}} < 12.75$
S_{lim} (mJy)	2.5	100.0	40.0
Area (sr)	2.16	2.16	5.19
Median z	0.073	0.0798	0.0596
Median absolute magnitude M_K	-25.50	-25.69	-25.59 ± 0.07
HERG fraction (Ae, AeB) (%)	13 ± 1	10 ± 2	23 ± 3
Emission-line fraction (Aae, Ae, AeB)(%)	26 ± 1	19 ± 3	50 ± 6

6 DISCUSSION

6.1 Radio and optical properties of the AT20G-6dFGS sample

We have measured three main radio parameters for galaxies in our sample: the radio *morphology*, radio *luminosity* and *spectral index*. We also have three key optical/infrared measurements: the K-band ($2.2 \mu\text{m}$) *absolute magnitude*, which is a proxy for galaxy stellar mass, the WISE *mid-infrared colours*, which can reveal the presence of dust heated by star formation, or a radiatively-efficient AGN, and the *spectral class* (Aa, Aae or Ae), which is thought to reflect the efficiency of gas accretion onto the central black hole.

Four of these parameters (radio luminosity, radio morphology, galaxy stellar mass and spectral class) have been examined in previous large studies of radio-source populations, using galaxy samples selected at frequencies of 1.4 GHz or below. In terms of the interplay of these four properties, our results (which we discuss briefly below) are in broad agreement with earlier work.

The other parameters (radio spectral index and WISE mid-infrared colours) are less well-studied. The WISE data (Wright et al. 2010) are relatively new, but are rapidly coming into wide use

for studies of galaxy evolution. Earlier studies of local radio-source populations have generally not had any radio spectral-index information which allowed them to distinguish between steep-spectrum and flat-spectrum sources, though a flux-limited multi-frequency catalogue of northern radio sources extending up to 5 GHz has been published by Kimball & Ivezić (2008).

Table 9 summarizes the overall properties of the AT20G-6dFGS galaxies as a function of Fanaroff-Riley class (FR 0, 1 and 2) and radio spectral index. We can draw several conclusions from this:

6.1.1 Radio morphology:

Only one-third of the AT20G-6dFGS sources (32%) are associated with classical FR-1 and FR-2 radio galaxies – the other two-thirds appear to be relatively compact sources even at low radio frequencies (0.8-1 GHz).

The host galaxies of FR-2 radio sources are typically less massive than the hosts of FR-1 galaxies (as measured by their infrared K-band luminosity), and the FR-2 galaxies also have a much higher fraction of HERG (Ae/AeB) spectra, in broad agreement with the

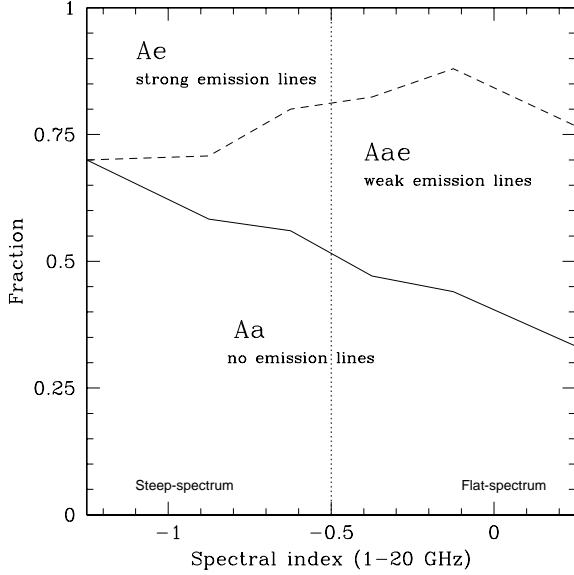


Figure 10. Fraction of AT20G-6dFGS galaxies showing optical emission lines in the 6dFGS spectrum, plotted against the 1-20 GHz radio spectral index.

results of Best & Heckman (2012) and earlier studies (e.g. Hardcastle et al. 2004).

The compact (FR-0) radio galaxies have typical properties which are intermediate between the FR-1 and FR-2 systems in both stellar mass and spectral class. The FR-0 class contains a mix of HERG and LERG systems, and seems likely to be a composite class which includes the early stages of both FR-1 and FR-2 radio galaxies, as well as some sources in which the core is brightened by relativistic beaming. We discuss this question further in §6.2 and §6.3.

Baum et al. (1998) found that GPS radio sources tend to have lower emission-line luminosities than CSS sources. The fraction of galaxies with strong optical emission lines is slightly higher for the candidate CSS (FR-0c) sources ($33 \pm 8\%$) than in the GPS (FR-0g) sources ($25 \pm 8\%$), but the difference is not statistically significant in this relatively small sample.

6.1.2 Radio luminosity

By selecting our sample from the AT20G catalogue, which has a cutoff flux density of 40 mJy, we are by definition selecting the more luminous radio galaxies in the local universe. The median 20 GHz radio luminosity of the AT20G-6dFGS galaxies is just below $10^{24} \text{ W Hz}^{-1}$, i.e. close to the dividing line between classical FR-1 and FR-2 radio galaxies.

The FR-2 radio galaxies have a significantly higher median radio luminosity at 20 GHz (by almost an order of magnitude) than the FR-1 objects, even though the FR-1 sources generally lie in more massive galaxies. Our data support the finding of Ledlow and Owen (1996) that FR-2 radio sources are more powerful than FR-1 sources in galaxies of similar stellar mass. It is interesting that the ‘Ledlow-Owen’ line derived for the total radio power at 1.4 GHz also these objects reasonably well at 20 GHz, with the majority of FR-2 sources (69%) lying above the line and the majority of FR-1 sources (92%) below.

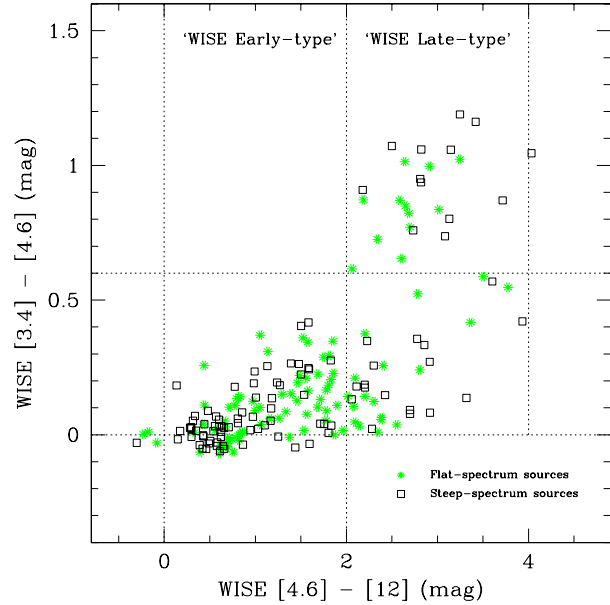


Figure 11. WISE colour-colour plot for the AT20G-6dFGS galaxies with flat (green stars) and steep (black open squares) 1–20 GHz radio spectral index.

6.1.3 Radio spectral index:

As discussed in §3.4, roughly half of the AT20G-6dFGS galaxies have flat-spectrum radio sources and (as shown in Figure 2) there is a close relationship between radio morphology and spectral index, with flat-spectrum sources being more compact than steep-spectrum ones.

Figure 11 shows a WISE two-colour plot similar to Figure 9, but with now with separate symbols for steep-spectrum ($\alpha_{1}^{20} \leq -0.5$) and flat-spectrum ($\alpha_{1}^{20} > -0.5$) radio sources. We see a roughly equal mix of flat-spectrum and steep-spectrum radio sources in both the ‘WISE early-type’ and ‘WISE late-type’ galaxies, showing that the distribution of radio spectral index does not depend on the host-galaxy type.

Table 9 also shows that the flat-spectrum and steep-spectrum radio sources in our sample are found in galaxies of similar median stellar mass. Both findings are consistent with a picture in which the flat-spectrum and steep-spectrum sources in the AT20G-6dFGS sample correspond to different stages of radio-galaxy evolution, rather than physically-distinct radio-source populations.

6.2 Relativistic beaming

De Zotti et al. (2010) note that radio surveys at frequencies of 5 GHz and above are dominated by flat-spectrum sources (at least at higher flux densities), and that most of these flat-spectrum sources are likely to be brightened by relativistic beaming because they are observed along a line of sight which is very close to the jet axis. These beamed sources generally show rapid variability at radio wavelengths, and fall into two classes: Flat-spectrum radio quasars (FSRQs), which show strong optical emission lines with broad Balmer wings, and BL Lac objects (BLLs), in which the optical emission lines are weak or absent. In unified models for AGN (Urry & Padovani 1995; Jackson & Wall 1999), BLLs and FSRQs

are assumed to be the beamed counterparts of FR-1 and FR-2 radio galaxies respectively.

Most tests of the unified model have been carried out for populations of very luminous (radio power $> 10^{25} \text{ W Hz}^{-1}$) radio sources (e.g. Padovani & Urry 1992; Cara & Lister 2008), and the extent to which the much larger population of low-luminosity, flat-spectrum radio AGN is beamed remains unclear. The radio sources in the AT20G-6dFGS sample have typical radio luminosities of 10^{23} to $10^{25} \text{ W Hz}^{-1}$ at 20 GHz.

Marcha et al. (2005) compared the emission-line luminosities of a sample of core-dominated sources (with core powers in the range 10^{21} to $10^{25} \text{ W Hz}^{-1}$ at 5 GHz) and a matched sample of FR-1 radio galaxies with similar redshift and 1.4 GHz flux density. They found that the core-dominated objects had significantly stronger optical emission lines than the matched FR-1 sample, contradicting the predictions of a simple unified model. These authors concluded that while a more sophisticated version of the unified model could fit their data, their results were equally consistent with a model in which relativistic beaming has little or no effect on the observed flux density of most low-luminosity flat-spectrum sources. Ekers et al. (1983) carried out a six-year program to monitor the 5 GHz flux densities of a sample of low-luminosity compact radio sources, and also concluded that their results did not support simple relativistic beaming models.

The AT20G-6dFGS galaxies in this paper are selected from within a sample of normal, nearby galaxies. If all the compact flat-spectrum sources in this sample are brightened at 20 GHz by relativistic beaming, then the effects at optical and mid-IR wavelengths must generally be quite subtle since only about 10% of these sources lie near the WISE ‘blazar line’ (Massaro et al. 2012) in Figure 9 and most have mid-IR colours characteristic of normal galaxies rather than beamed AGN.

A detailed test of beaming models for the AT20G-6dFGS sample would require high-quality radio imaging of these sources at VLBI resolution, and so is outside the scope of the present paper. We can however make some simple tests to estimate the fraction of AT20G-6dFGS sources which may have their observed 20 GHz radio luminosity affected by relativistic beaming. In the absence of detailed VLBI images of the galaxies in our sample, we consider (i) objects which are already identified in the literature as blazars, (ii) tests for radio variability, as used by Bonaldi et al. (2013) to distinguish between genuine High-Frequency Peakers and candidate blazars, and (iii) the evidence for a non-thermal contribution to the optical spectrum, as used by Marcha & Caccianiga (2013) to identify low-luminosity BL Lacs.

6.2.1 Individual AT20G-6dFGS galaxies identified as beamed radio sources (blazars)

Four of the galaxies in our sample (AT20G J024554-445939; J052223-072513; J130715-760245 and J180957-455241) have compact (FR-0), flat-spectrum radio emission and show broad emission lines in their optical spectra. All four can be regarded as flat-spectrum radio quasars (FSRQs), in which the high-frequency radio emission is probably beamed.

A further three galaxies (AT20G J090802-095937; J151741-242220 and J231905-420648) are classified as radio-selected BL Lacs in the literature. One of these, J151741-242220 (AP Lib; Carini et al. 1991) is a compact flat-spectrum source and a well-studied blazar which shows strong variability at both optical and radio wavelengths. The other two objects (J090802-095937, which is in the BL Lac sample studied by Nieppola et al. 2006, and J231905-

420648, identified as a radio-selected BL Lac object by Roberts et al. 1998) are both associated with FR-1 radio galaxies in clusters, rather than flat-spectrum FR-0 sources. Whether these last two objects are beamed is therefore somewhat unclear.

If we assume that all seven of these objects are blazars, we can estimate the *minimum* fraction of beamed radio sources in the local AT20G-6dFGS sample – this is roughly 3.5% (7/201) for the sample as a whole, and 6% (5/83) for the sub-sample of compact flat-spectrum (FR-0g and FR-0u) sources.

Since the classification of low-luminosity BL Lac objects in the literature is inhomogeneous and likely to be incomplete (particularly in the southern hemisphere; Massaro et al. 2009), we address the question of beaming by using two indicators which can be applied in a fairly uniform way to at least a subset of our sample. These tests are described in the next two subsections, after which we derive the likely *maximum* beaming fraction in the AT20G-6dFGS sample.

6.2.2 Radio-frequency variability of the compact, flat-spectrum (FR-0g and FR-0u) AT20G-6dFGS sources

Relativistically-beamed radio sources are expected to be strongly variable at GHz radio frequencies on timescales of months to years (e.g. Hovatta et al. 2007; Massardi et al. 2011b; Chen et al. 2013). In contrast, genuinely young GPS and CSS are not expected to be beamed, and typically vary in flux density by less than 10% on timescales of a year or so (O’Dea 1998).

Bonaldi et al. (2013) used measurements of radio variability to discriminate between candidate High Frequency Peakers (HFPs; i.e. very young radio galaxies) and candidate blazars. Over a 2–4 year timescale, they found a median variability index of 13.1% at 5 GHz and 15.0% at 9 GHz for their sample of flat-spectrum sources, 95% of which were blazars.

We are not able to measure the variability of the AT20G-6dFGS sources at 20 GHz, since at this frequency we only have data at a single epoch. We can, however, use 5 and 8 GHz flux measurements from the ATPMN survey (McConnell et al. 2012) to estimate the variability at these frequencies. Since the ATPMN survey was carried out with a different ATCA configuration which had significantly higher spatial resolution than the 5 and 8 GHz observations carried out for the AT20G survey, we can only make this test for compact, flat spectrum sources which are unresolved in both surveys.

The ATPMN observations were taken between 1992 November and 1994 March, and the AT20G observations between 2004 November and 2007 May. Thus the time interval between each pair of observations is between 10 and 15 years. We defined our 5 and 8 GHz variability sample as follows:

(i) We only included galaxies in the area of sky covered by the ATPMN survey, i.e. south of declination -37° .

(ii) We restricted our analysis to compact (FR-0) sources with flat radio spectra from 1–20 GHz (i.e. $\alpha_1^{20} > -0.5$), to avoid introducing false ‘variability’ in sources where extended 5/8 GHz structures included in the AT20G flux density measurement were partly resolved out by the smaller ATPMN beam.

This left a final sample of 26 flat-spectrum FR-0 galaxies, and for each of these objects we calculated a debiased variability index (as described by Sadler et al. 2006 and Massardi et al. 2011b) at both 5 and 8 GHz.

For the compact, flat-spectrum AT20G-6dFGS galaxies which

were also observed in the ATPMN survey, we find a median variability index of $< 6.4\%$ at 5 GHz and 6.5% at 8 GHz, over a time interval of 10–15 years. Only 35% of sources (9/26) varied by more than 10% at 5 GHz over this time interval, and 38% (10/26) varied by more than 10% at 8 GHz. Only three sources (J024326-561242, J121044-435437 and J194524-552049) varied by more than 20% at either 5 or 8 GHz over this 10–15 year interval.

In practice, the fraction of sources with observed flux density variations of $> 10\%$ is likely to be an upper limit to the blazar fraction in our sample. There are two reasons for this. Firstly, the time interval over which we measure variability (10–15 years) is much longer than the 1–2 year interval for which O’Dea (1998) characterises the variability of young GPS and CSS and CSS radio galaxies, so it is plausible than even non-beamed compact sources could vary by up to 15–20% over this longer interval. Secondly, the mean flux ratio $< S_{\text{AT20G}}/S_{\text{ATPMN}} >$ is $1.15 \pm .05$ at 5 GHz and $1.21 \pm .05$ at 8 GHz, implying that even though we have restricted our analysis to compact flat-spectrum sources, the AT20G flux measurements include some extended emission which is not seen in the higher-resolution ATPMN images. If so, the presence of this extended emission at one of our two epochs will produce a spurious rise in the measured variability level.

Since we find that around two-thirds of the flat-spectrum FR-0 sources in our sample show a long-term variability in flux density of less than 10% at 5–8 GHz, consistent with the behaviour expected for young radio galaxies rather than beamed radio sources, we estimate that the fraction of beamed sources in the combined FR-0g and FR-0u subsample is no higher than 35–40%.

A more detailed variability study of the AT20G-6dFGS sources, using a smaller time interval and better-matched array configuration, would allow more stringent limits to be placed on the likely beamed fraction.

6.2.3 Tests for a non-thermal contribution to the optical spectrum

Since the variability sample discussed above is relatively small, we make a second test using the 6dFGS optical spectra. Marcha & Caccianiga (2013) note that it can be difficult to recognise the presence of low-luminosity BL Lac nuclei concealed within optically bright galaxies, and used the contrast across the Ca H+K break at 4000 \AA to identify these weak beamed AGN. Their selection criteria required that enough non-thermal flux from the AGN was present, in addition to the starlight of the host galaxy, to reduce the contrast across the 4000 \AA break from the value of $\sim 50\%$ seen in a normal early-type galaxy to $\leq 40\%$.

We applied the same test to the 6dFGS spectra of the FR-0 and FR-1 galaxies in our sample, including both flat-spectrum (FR-0g, FR-0u) and steep-spectrum (FR-0c, FR-1) sources. The FR-2 sources were excluded from this test, since only a few of them have a suitable 6dFGS spectrum available.

Table 11 summarizes the results of these measurements. If we assume that all the galaxies with a low-contrast ($\leq 40\%$) H+K break are low-luminosity BL Lacs (Marcha & Caccianiga 2013), and that all the galaxies which show broad optical emission lines also contain beamed sources (Hardcastle et al. 1999), then the fraction of AT20G-6dFGS sources which are beamed is around 35% for flat-spectrum sources and 11% for steep-spectrum sources.

In practice, it is likely that not all the galaxies with a ‘low-contrast’ break are BL Lacs, since the presence of a young or intermediate-age stellar population will also reduce the size of the break and we have already shown (§5.6.2) that around 30% of the

Table 11. Measurements of the Ca H+K break for the AT20G-6dFGS galaxies with weak or no optical emission lines (class Aa or Aae). Galaxies with strong narrow (Ae) or broad (AeB) emission lines are also included for comparison.

Spectral type	Flat-spectrum	Steep-spectrum	
	FR-0u, 0g	FR-0c	FR-1
Aa/Aae, contrast $> 40\%$ (normal galaxy)	31	18	25
Aa/Aae, contrast $\leq 40\%$ (BLL candidate)	14	1	3
Ae	6	7	–
AeB	5	2	–
Total	56	32	28

Maximum beamed fraction:			
Galaxies with Aa/Aae spectra	31% (14/45)	5% (1/19)	
All galaxies	32% (18/56)	9% (3/32)	11% (3/28)

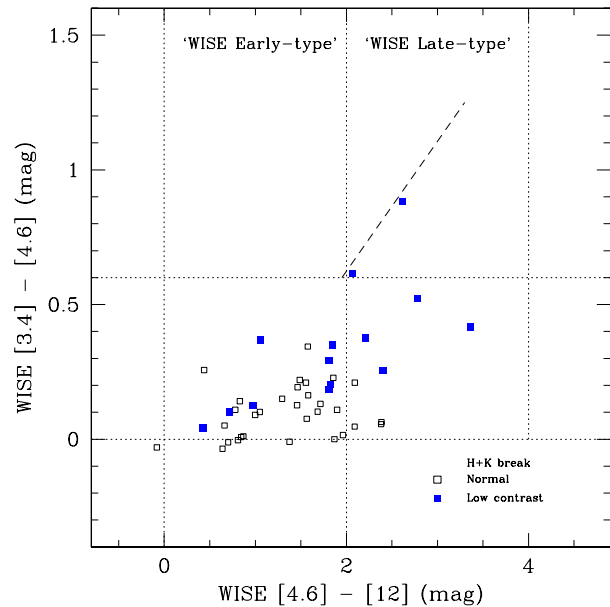


Figure 12. WISE colour-colour plot for flat-spectrum FR-0 sources with weak or no optical emission lines (type Aa or Aae spectra). Open squares show galaxies with a ‘normal’ 4000 \AA break, and filled squares galaxies with a low-contrast break which may indicate the presence of a low-luminosity BL Lac nucleus. The diagonal dashed line shows the location of the ‘WISE Blazar Strip’ defined by Massaro et al. (2012).

AT20G-6dFGS radio sources lie in galaxies with ongoing star formation. As with the variability tests described in the §6.2.2, the H+K break measurements therefore provide an upper limit to the fraction of AT20G-6dFGS galaxies in which the observed radio emission is strongly affected by beaming.

Figure 12 shows a WISE two-colour plot for the compact flat-spectrum sources for which we were able to measure the contrast across the H+K break. Filled squares show the galaxies with a low-contrast break, which could potentially host a low-luminosity BL Lac nucleus.

As can be seen from Figure 12 the WISE $[3.4] - [4.6] \mu\text{m}$ colours of the ‘low-contrast’ galaxies are significantly offset from

those of the galaxies with a ‘normal’ H+K break. Two of the ‘low-contrast’ galaxies, J091300-210320 and J151741-242220, have $[3.4] - [4.6] > 0.6$ and lie close to the WISE blazar line of Masaro et al. (2012). The remaining 12 ‘low-contrast’ galaxies have a mean $[3.4] - [4.6]$ colour of 0.27 ± 0.04 mag., compared to a mean of 0.10 ± 0.02 mag for the 31 galaxies with a normal H+K break. This shift in WISE $[3.4] - [4.6]$ colour is consistent with what might be expected if the ‘low-contrast’ galaxies host a weak (beamed) BL Lac nucleus.

6.2.4 How many of the flat-spectrum AT20G-6dFGS sources are affected by relativistic beaming?

The variability analysis in §6.2.2 and the optical H+K break measurements presented in §6.2.3 both imply that no more than 30–35% of the flat-spectrum sources in the AT20G-6dFGS sample are affected by relativistic beaming. We showed in §6.2.1 that the minimum beamed fraction is around 6%, so the overall fraction of relativistically-beamed sources within the flat-spectrum population is within the range 6–35%. More detailed VLBI and variability studies are needed to refine this further. Based on the evidence available so far, however, we conclude that at least two-thirds of the flat-spectrum sources in the AT20G-6dFGS sample are likely to be genuinely compact radio galaxies rather than low-power BL Lac objects.

6.3 WISE colours and radio morphology

Figure 13 shows a WISE colour-colour plot similar to that in Figures 9 and 11, but now split by radio morphology into the FR-0, FR-1 and FR-2 classes defined in Table 9.

This plot shows a remarkable split in the mid-infrared colours of FR-1 and FR2 hosts, at $[4.6] - [12] \sim 2.0$ mag. For the 59 FR-1 and FR-2 galaxies with reliable WISE photometry available:

- 93% (41/44) of the FR-1 hosts have $[4.6] - [12] < 2.0$ mag,
- 93% (14/15) of the FR-2 hosts have $[4.6] - [12] \geq 2.0$ mag.

In other words, there is a near-complete dichotomy between the host galaxies of our FR-1 and FR-2 radio sources, with FR-1 sources being found almost exclusively in WISE ‘early-type’ galaxies and FR-2 sources in WISE ‘late-type’ galaxies.

This provides strong evidence that the host galaxies of FR-1 and FR-2 radio sources are drawn from different galaxy populations. This is further supported by our earlier finding (§6.1.1 and Table 9) that the host galaxies of FR-1 radio sources are typically more massive than the FR-2 hosts.

6.4 An overall picture of the local radio-source population

We now attempt to interpret the results presented so far in terms of an overall picture of the local radio-source population at 20 GHz.

We first assume that the distinction between high-excitation radio galaxies (HERGs), which have a radiatively-efficient accretion disk surrounding the black hole, and low-excitation galaxies (LERGs), in which accretion is radiatively inefficient, is an important one.

Figure 14 provides some support for this. As noted by Stern et al. (2012), the WISE $[3.4] - [4.6]$ μm colour allows us to distinguish the power-law spectrum of a radiatively-efficient AGN from the blackbody stellar spectrum of a normal galaxy (which peaks near

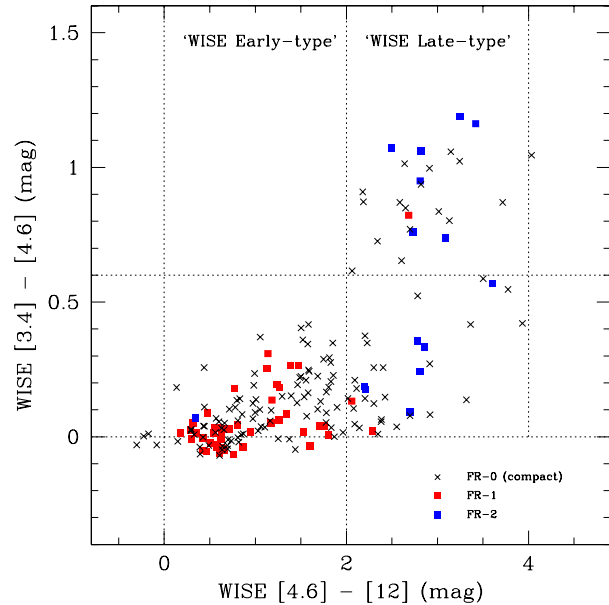


Figure 13. WISE colour-colour plot for FR-1 (red squares), FR-2 (blue squares) and compact (FR-0, black crosses) radio galaxies in the 20 GHz AT20G-6dFGS sample.

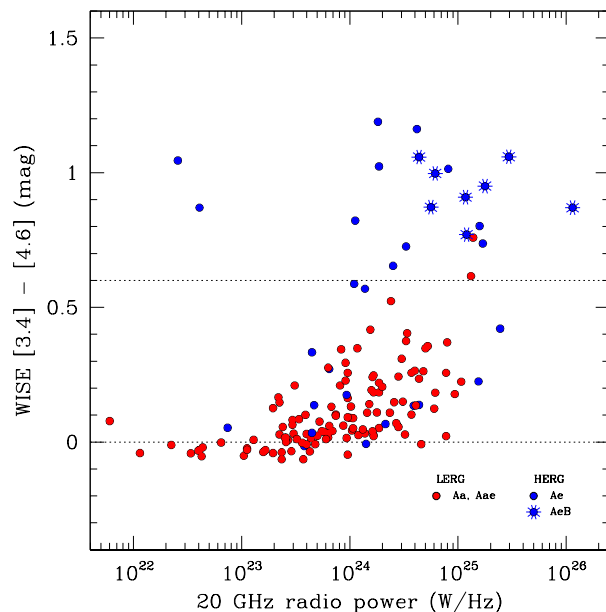


Figure 14. WISE $[3.4] - [4.6]$ μm colour, plotted against 20 GHz radio power, for HERG (blue points) and LERG (red points) objects in the AT20G-6dFGS sample. The horizontal line at $[3.4] - [4.6] = 0.6$ mag. is the canonical dividing line between normal galaxies and radiatively-efficient AGN (Wright et al. 2010).

Table 12. Summary of the radio and optical properties of low-excitation (LERG) and high-excitation (HERG) radio sources in the AT20G-6dFGS galaxy sample

Class	N	Host galaxies	Radio spectral index α_1^{20}
Low-excitation populations			
FR-0, LERG	78	WISE early-type and late-type	67% flat, 33% steep
FR-1, LERG	40	Mainly WISE early-type	Steep
FR-2, LERG	5	Mainly WISE late-type	Steep
High-excitation populations			
FR-0, HERG	26	Mainly WISE late-type	50% flat, 50% steep
FR-2, HERG	9	WISE late-type	Steep

$\sim 1.6 \mu\text{m}$) in a way which is largely immune from the effects of dust extinction. Almost all the LERGs in our sample lie below the line at $[3.4] - [4.6] = 0.6 \text{ mag.}$ which separates normal galaxies from radiatively-efficient AGN (Wright et al. 2010), while most of the HERGs lie above this line. The clear separation of the blue and red points in Figure 14 implies that the spectroscopic classification discussed in §2.3 has allowed us to separate the two classes in a reliable way.

Figure 14 also shows that for low-excitation objects with 20 GHz radio powers above about $10^{23} \text{ W Hz}^{-1}$, the median WISE $[3.4] - [4.6] \mu\text{m}$ colour moves to higher values as the 20 GHz radio power increases. Since there is no correlation between M_K and $[3.4] - [4.6]$ colour for the AT20G-6dFGS galaxies, this implies that we may be seeing the weak signature of a radiative AGN in the more powerful LERGs in our sample.

We can now split our sample into low-excitation and high-excitation populations, as summarized in Table 12.

The *low-excitation systems* (LERGs) in Table 12 span the full range of radio morphologies (FR-0, FR-1 and FR-2). The compact (FR-0) sources are seen across a wide range of host galaxy morphology, spanning both WISE ‘early-type’ and WISE ‘late-type’ galaxies. However, the radio sources which show extended radio emission at 1 GHz (which we assume are the longer-lived counterparts of some of the FR-0 objects) are generally seen as FR-1 radio galaxies if their host is a ‘WISE early-type’ galaxy and (low-excitation) FR-2 radio galaxies if their host is a ‘WISE late-type’ galaxy.

This strongly suggests that some factor related to the host-galaxy morphology or large-scale environment, rather than the accretion rate alone, determines whether a young radio source undergoing radiatively-inefficient accretion evolves into an extended FR-1 radio galaxy or an FR-2 system.

The *high-excitation systems* (HERGs) in Table 12 are a minority population in the AT20G-6dFGS sample, and their interpretation appears more straightforward. Here we see only compact FR-0 and extended FR-2 systems, suggesting that compact radio sources with radiatively-efficient accretion disks are likely to evolve into FR-2 radio galaxies rather than FR-1 systems.

6.5 Two radio-galaxy populations?

The concept of a dual radio-source population in which the two populations undergo different cosmic evolution is a long-standing one, and is essential to explain the observed radio source counts (Longair 1966). Several alternative models have been proposed for

these two populations, as discussed in a recent review by De Zotti et al. (2010).

Dunlop & Peacock (1990) developed a model in which radio luminosity was the key parameter, with luminous radio sources undergoing rapid cosmic evolution while sources below some critical radio luminosity evolve more slowly or not at all. Wall (1980) identified the two populations with FR-1 and FR-2 radio galaxies, a model which was later extended by Jackson & Wall (1999) to include flat-spectrum sources as the beamed counterparts of the steep-spectrum FR-1 and FR-2 sources. Willott et al. (2001) used emission-line strength rather than the FR-1/2 classification to define the two populations. All these models were developed at a time when the local radio-source population was still poorly studied and the local radio luminosity function poorly determined, making it difficult to carry out a detailed comparison with the data. De Zotti et al. (2010) note that the possible dichotomies between evolutionary properties of low- versus high-luminosity and of flat- versus steep-spectrum AGN-powered radio sources remain an unresolved question.

More recently, and using a much larger data set, Best & Heckman (2012) have proposed a picture in which HERGs and LERGs constitute the two radio-source populations, with the observed redshift evolution of the radio luminosity function being driven at least partly by changes in the relative contribution of these two populations. In this picture, the key discriminant is the accretion rate onto the central black hole, with HERGs typically having accretion rates of 1–10 per cent of the Eddington rate and LERGs generally accreting at a rate below one per cent Eddington. These authors find that HERGs and LERGs show different rates of cosmic evolution at a fixed radio luminosity, with HERGs evolving strongly with redshift while LERGs show weak or no evolution. They also identify LERGs with galaxies undergoing ‘radio-mode feedback’, which acts to suppress further star formation (Croton et al. 2006), and HERGs with ‘quasar-mode’ systems fuelled by the infall of cold gas, which may still have ongoing star formation.

Our results are in broad agreement with the Best & Heckman (2012) picture. We find a clear distinction between the host galaxies of FR-1 and FR-2 galaxies in our sample, with the FR-1 objects lying almost exclusively in ‘WISE early-type’ galaxies and the FR-2 objects in ‘WISE late-type’ galaxies. This implies that the host galaxy and its surrounding environment play an important role in the determining the overall properties of an individual radio galaxy, as has already been recognised by others (Heckman et al. 1986; Baum et al. 1995; Saripalli 2012; Ramos Almeida et al. 2012; Best & Heckman 2012). We also see a fairly clear distinction between the optical spectra of the two classes, with 98% of the FR-1 radio galaxies in our sample having LERG spectra while the majority (64%) of our FR-2 radio galaxies are HERGs.

As in earlier studies, however, we see a substantial population of FR-2 radio galaxies with LERG optical spectra. As Table 12 shows, the radio galaxies in our sample fall into *five* (rather than two or three) distinct sub-populations once we take into account the host-galaxy type, radio morphology and observed optical spectrum/accretion mode. If we also take into account that (as discussed in §6.2) the flat-spectrum FR-0 sources include a small subset of beamed objects, then the number of potential sub-populations is further increased.

If the Best & Heckman (2012) model is correct, then it should be possible to fit all these sub-populations into a dual-population model with one rapidly-evolving and one slowly-evolving (or non-evolving) radio-source population. To do this, we would need to know how each of the sub-populations in Table 12 evolves with

redshift. Such a test is clearly beyond the scope of the current paper, but would be interesting to carry out with a larger sample spanning a wider range in redshift.

7 SUMMARY AND FUTURE WORK

We have carried out the first detailed study of the high-frequency radio-source population in the local universe. By selecting our sample at 20 GHz, rather than at 1.4 GHz as most other recent studies have done, we select galaxies based on the recent radio emission from their central regions rather than the longer-lived extended emission from their jets and lobes (which reflects the activity of the central black hole on longer timescales of up to $10^7 - 10^8$ years).

We now summarize the main results from this study, and highlight a number of areas where follow-up work would be particularly useful. Some follow-up work is already in progress, in particular a study of associated 21 cm HI absorption in compact sources from the AT20G-6dFGS sample (Allison et al. 2012).

(i) *Compact ‘FR-0’ radio galaxies are the dominant source population in the AT20G-6dFGS galaxy sample.* These compact FR-0 sources are a heterogeneous population in terms of both host-galaxy morphology (75% in early-type galaxies, 25% in star-forming galaxies) and optical spectra (75% LERG; 25% HERG).

Their observed properties are consistent with them being a mixture of several kinds of objects. Some of the weaker flat-spectrum sources in our sample, like NGC 1052 and NGC 4594 (which have 20 GHz radio power below $10^{23} \text{ W Hz}^{-1}$), are known to be less than a few parsecs in size (e.g. Slee et al. 1994; Sadler et al. 1995) and strongly affected by absorption. These low-luminosity sources could plausibly be maintained over much of the life of the host galaxy, and need not necessarily be young. The FR-0 class is also likely to contain young Compact Steep-Spectrum (CSS) and Gigahertz-Peaked Spectrum (GPS) radio sources, as well as a minority population of beamed radio sources.

Since the FR-0 objects make up around 70-75% of the AT20G-6dFGS sources at all radio powers between about 10^{22} and $10^{26} \text{ W Hz}^{-1}$ it seems unlikely that all of them can grow into long-lived FR-1 or FR-2 radio galaxies. Instead, it seems likely that many of the FR-0 sources have short duty cycles, so that they switch on and off regularly but are never ‘on’ for long enough to drive large-scale jets and lobes (e.g. Conway 2002).

A more detailed study of these objects would be very interesting, since they are likely to contain the largest and most complete sample of candidate CSS and GPS radio sources in the local universe.

Such a study would ideally include detailed measurements of the radio spectrum over at least the range 1–20 GHz, to determine the spectral shape and peak frequency; detailed 1.4 GHz imaging to search for low surface-brightness jets and lobes which may lie below the limits of current large-area surveys; and high-resolution VLBI imaging to examine the parsec-scale source structure and look for evidence of long-term expansion or motion. While it appears that no more than 30–35% of the compact flat-spectrum sources in our sample are brightened by relativistic beaming, it would clearly be valuable to quantify this more accurately.

(ii) *We find a roughly-equal mixture of flat-spectrum and steep-spectrum radio galaxies in our sample.* The classical FR-1 and FR-2 radio galaxies in our sample have steep ($\alpha \leq -0.5$) radio spectral indices due to the extended low-frequency emission from

their jets and lobes. The compact (FR-0) sources include both flat-spectrum ($\alpha > -0.5$) and steep-spectrum sources, and we see no correlation between radio spectral index and radio luminosity or host-galaxy morphology. We therefore conclude that flat-spectrum and steep-spectrum sources in our sample are not drawn from different parent-galaxy populations, but instead are likely to represent different evolutionary stages of the overall radio-galaxy population.

(iii) *The FR-1 and FR-2 radio sources in our sample lie in different kinds of host galaxies.* Mid-infrared photometry from WISE (Wright et al. 2010; Donoso et al. 2012) shows that the host galaxies of the FR-1 and FR-2 galaxies in our sample are very different, with the FR-1 sources found almost exclusively in early-type galaxies and the FR-2 sources in late-type galaxies with dust and/or ongoing star formation. At 20 GHz, we also find that FR-2 radio sources are more powerful (typically by almost an order of magnitude in 20 GHz radio luminosity) than the FR-1 radio sources in galaxies of similar stellar mass. The dividing line seen by Ledlow & Owen (1996) at 1.4 GHz also divides the FR-1 and FR-2 populations reasonably well at 20 GHz if shifted appropriately in radio spectral index and (R-K) colour.

(iv) *Galaxies with optical emission lines are more common in our 20 GHz-selected sample than in a similar radio-galaxy sample selected at 1.4 GHz.* HERG sources with strong optical emission lines make up 23% of the AT20G-6dFGS sample, a significantly higher fraction than the 10-13% seen in the lower-frequency 6dFGS-NVSS (Mauch & Sadler 2007) sample. The HERG fraction is similar for flat-spectrum and steep-spectrum sources in the AT20G-6dFGS sample, but within the LERG population, weak optical emission-lines (class Aae) are much more common in galaxies which host flat-spectrum radio sources. The reason for the observed correlation between emission-line fraction and radio spectral index is not yet clear, and a more detailed study of the interstellar medium in these sources is needed to investigate whether the difference is mainly due to shock ionization of circumnuclear gas (Dopita et al. 1997), free-free absorption in the most compact sources (Kameno et al. 2005) or some other mechanism.

(v) *Around 30% of the AT20G-6dFGS radio galaxies are late-type, dusty or star-forming galaxies.* Although most of the radio-loud AGN in the AT20G-6dFGS sample are hosted by massive early-type galaxies, both the catalogued optical morphology (where available) and the WISE infrared colours imply that $\sim 30\%$ of the host galaxies are spirals or other dusty, late-type galaxies with some ongoing star-formation. This is very similar to the $\sim 35\%$ fraction of powerful 3CRR and 2Jy radio galaxies which were found by Dicken et al. (2012) to show ongoing star formation, based on the detection of infrared polycyclic aromatic hydrocarbon (PAH) spectral features.

Finally, we note that the increased continuum sensitivity now provided routinely by new wide-band correlators on large radio interferometers, including the Compact Array Broadband Backend correlator (CABB; Wilson et al. 2011) on the Australia Telescope Compact Array and the Wideband Interferometric Digital ARchitecture (WIDAR) correlator on the Jansky Very Large Array will make it far easier to carry out high-frequency and multi-frequency radio studies of large galaxy samples in the future. One goal of this paper is to give some idea of what these studies might discover, and how they might help to improve our understanding of the com-

plex physical processes which shape the formation and evolution of radio galaxies.

8 ACKNOWLEDGEMENTS

We thank our colleagues in the AT20G and 6dFGS survey teams, who carried out the surveys which underpin much of the work presented here. We are also grateful to Tom Jarrett for several useful discussions on the WISE infrared data. We acknowledge financial support from the Australian Research Council through the award of an ARC Australian Professorial Fellowship to EMS. This research has made use of the NASA/IPAC Extragalactic Database (NED) which is operated by the Jet Propulsion Laboratory, California Institute of Technology, under contract with the National Aeronautics and Space Administration.

REFERENCES

- Abdo A.A. et al., 2010, *ApJ*, 709, L152
- Allison, J. R., Curran, S. J., Emonts, B. H. C., Gereb, K., Mahony, E. K., Reeves, S., Sadler, E. M., Tanna, A., Whiting, M. T., Zwaan, M. A., 2012, *MNRAS* 423, 2601
- Allison, J. R., Curran, S. J., Sadler, E. M., Reeves, S. N., 2013, *MNRAS* 430, 157
- Arp, H., 1966, *ApJS*, 14, 1
- Assef, R. J. et al., 2010, *ApJ*, 713, 970
- Auremma C., Perola G. C., Ekers R. D., Fanti R., Lari C., Jaffe W.J., Ulrich M.-H., 1977, *A&A*, 57, 41
- Baldi, R. D., Capetti, A., 2009, *A&A*, 508, 603
- Bauer, F.E., Condon, J.J., Thuan, T.X., Broderick, J.J., 2000, *ApJS*, 129, 547
- Baum S.A., Heckman T., Bridle, A., van Breugel W., Miley G., 1988, *ApJS*, 68, 643
- Baum, S. A., Zirbel, E. L., O’Dea, C. P., 1995, *ApJ*, 451, 88
- Bell, M. E. et al., 2011, *MNRAS*, 411, 402
- Bertelli, G., Chiosi, C., Bertola, F., 1989, *ApJ*, 339, 889
- Bertola, F., Bettoni, D., Danziger, J., Sadler, E., Sparke, L., de Zeeuw, T., 1991, *ApJ*, 373, 369
- Best P.N., Kauffmann G., Heckman T.M., Ivezić Z., 2005a, *MNRAS*, 362, 9
- Best P.N., Kauffmann G., Heckman, T.M., Brinchmann, J., Charlot, S., Ivezić, Z., White, S.D.M., 2005b, *MNRAS*, 362, 25
- Best, P. N., Heckman, T. M., 2012, *MNRAS*, 421, 1569
- Birkinshaw, M., Davies, R. L., 1985, *ApJ*, 291, 32
- Bock, D.C.-J., Large, M.I., Sadler, E.M. 1999, *AJ*, 117, 1593
- Bonaldi, A., Bonavera, L., Massardi, M., De Zotti, G., 2013, *MNRAS*, 428, 1845
- Buchanan C.L., McGregor P.J., Bicknell G.V., Dopita M.A., 2006, *AJ*, 132, 27
- Burgess A.M., Hunstead R.W., 2006, *AJ*, 131, 100
- Burke-Spolaor, S., Ekers, R. D., Massardi, M., Murphy, T., Partridge, B., Ricci, R., Sadler, E. M., 2009, *MNRAS*, 395, 504
- Burns J.O., Feigelson E.D., Schreier E.J.; 1983, *ApJ*, 273, 128
- Cara, M., Lister, M.L., 2008, *ApJ*, 674, 111
- Carini, M.T., Miller, H.R., Noble, J.C., Sadun, A.C., 1991, *AJ*, 101, 1196
- Cappellari, M., Verolme, E. K., van der Marel, R. P., Verdoes Kleijn, G. A., Illingworth, G. D., Franx, M., Carollo, C. M., de Zeeuw, P. T., 2002, *ApJ*, 578, 787
- Carter D., Efstathiou G., Ellis R.S., Inglis I., Godwin J., 1981, *MNRAS*, 195, 15P
- Chen, X., Rachen, J. P., Lopez-Caniego, M., Dickinson, C., Pearson, T. J., Fuhrmann, L., Krichbaum, T. P., Partridge, B., 2013, *A&A*, 553, 107
- Chhetri, R., Ekers, R. D., Mahony, E. K., Jones, P. A., Massardi, M., Ricci, R., Sadler, E. M., 2012, *MNRAS*, 422, 2274
- Christlein, D., Zabludoff, A.I., 2003, *ApJ*, 591, 764
- Cid Fernandes, R., Stasinska, G., Mateus, A., Vale Asari, N., 2011, *MNRAS*, 413, 1687
- Condon J. J., 1989, *ApJ*, 338, 13
- Condon, J. J., Cotton, W. D., Greisen, E. W., Yin, Q. F., Perley, R. A., Taylor, G. B., Broderick, J. J., 1998, *AJ*, 115, 1693
- Condon J. J., Cotton W. D., Broderick J. J., 2002, *AJ*, 124, 675
- Conway, J. E., 2002, *New Astronomy Reviews*, 46, 263
- Crawford, C.S., Fabian, A.C., 1994, *MNRAS*, 266, 669
- Croton, D. et al., 2006, *MNRAS*, 365, 11
- Danziger I. J., Fosbury R. A. E., Boksenberg A., Goss W. M., Bland J., 1984, *MNRAS*, 208, 589
- De Breuck, C., van Breugel, W., Stanford, S. A., Röttgering, H., Miley, G., Stern, D., 2002, *AJ*, 123, 637
- de Vaucouleurs, G., de Vaucouleurs, A., Corwin, H. G., Jr., Buta, R. J., Paturel, G., Fouque, P., 1991, *Third Reference Catalogue of Bright Galaxies (RC3)*. Springer, New York, NY (USA),
- De Zotti G., Ricci R., Mesa D., Silva L., Mazzotta P., Toffolatti L., Gonzalez-Nuevo J., 2005, *A&A*. 431, 893
- De Zotti G., Massardi M., Negrello M., Wall J., 2010, *A&ARev*, 18, 1
- Dicken, D., Tadhunter, C., Axon, D., Morganti, R., Robinson, A., Kouwenhoven, M. B. N., Spoon, H., Kharb, P., Inskip, K. J., Holt, J., Ramos Almeida, C., Nesvadba, N. P. H., 2012, *ApJ*, 745, 172
- di Serego-Alighieri, S., Danziger, I. J., Morganti, R., Tadhunter, C. N., 1994, *MNRAS*, 269, 998
- Donoso, E. et al., 2012, *ApJ*, 748, 80
- Dopita, M.A., Koratkar, A.P., Allen, M.G., Tsvetanov, Z.I., Ford, H.C., Bicknell, G.V., Sutherland, R.S., 1997, *ApJ*, 490, 202
- Drake, C. L., McGregor, P. J., Dopita, M. A., van Breugel, W. J. M., 2003, *AJ*, 126, 2237
- Drake, C. L., McGregor, P. J., Dopita, M. A., 2004, *AJ*, 128, 955
- Dunlop, J. S., Peacock, J. A., 1990, *MNRAS*, 247, 19
- Ekers, R. D., 1969, *Aust. J. Phys. Suppl.*, 6, 3
- Ekers, R. D., Fanti, R., Miley, G. K., 1983, *A&A*, 120, 297
- Ekers, R. D., Goss, W. M., Kotanyi, C. G., Skellern, D. J., 1978, *A&A*, 69, L21
- Eracleous M., Halpern J.P., 1994, *ApJS*, 90, 1
- Fanaroff, B.L., Riley, J.M., 1974, *MNRAS*, 167, 31
- Fanti, R., Fanti, C., Schilizzi, R.T., Spencer, R.E., Nan R., Parma, P., van Breugel, W.J.M., Venturi, T., 1990, *A&A*, 231, 333
- Franx, M., Illingworth, G. D., 1988, *ApJ*, 327, L55
- Gardner F.F., Whiteoak J.B., Norris R.P., Diamond P.J., 1992, *MNRAS*, 258, 296
- Ghisellini, G., 2011, *American Institute of Physics Conference Series*, 1381, 180
- Gregorini, L., de Ruiter, H. R., Parma, P., Sadler, E. M., Vettolani, G., Ekers, R. D., 1994, *A&AS*, 106, 1
- Gregory, P. C., Vavasour, J. D., Scott, W. K., Condon, J. J., 1994, *ApJS*, 90, 173
- Grimberg B. I., Sadler E. M., Simkin S. M., 1999, *ApJ*, 521, 121
- Hagiwara Y., Kohno K., Kawabe R., Nakai N., 1997, *PASJ*, 49, 171
- Hancock, P. J., 2009, *Astronomische Nachrichten*, 330, 180
- Hancock, P. J., Sadler, E. M., Mahony, E. K., Ricci, R., 2010, *MNRAS*, 408, 1187
- Hardcastle, M. J., Alexander, P., Pooley, G. G., Riley, J. M., 1998, *MNRAS*, 296, 445
- Hardcastle, M. J., Alexander, P., Pooley, G. G., Riley, J. M., 1999, *MNRAS*, 304, 135
- Hardcastle, M. J., 2004, *A&A*, 414, 927
- Hardcastle, M. J., Evans, D. A., Croston, J. H., 2007, *MNRAS*, 376, 1849
- Hardcastle, M. J. et al., 2013, *MNRAS*, 429, 2407
- Heckman, T. M., 1980, *A&A*, 87, 152
- Heckman, T. M., Smith, E. P., Baum, S. A., van Breugel, W. J. M., Miley, G.K., Illingworth, G. D., Bothun, G. D., Balick, B., 1986, *ApJ*, 311, 526
- Hota, A. et al., 2011, *MNRAS*, 417, L36
- Hovatta, T., Tornikoski, M., Lainela, M., Lehto, H. J., Valtaoja, E., Tornainen, I., Aller, M. F., Aller, H. D., 2007, *A&A*, 469, 899

- Ishwara-Chandra, C. H., Saikia, D. J., 1999, MNRAS, 309, 100
- Jackson, C.A., Wall, J.V., 1999, MNRAS, 304, 160
- Jackson, C. A., Wall, J. V., Shaver, P. A., Kellermann, K. I., Hook, I. M., Hawkins, M. R. S., 2002, A&A, 386, 97
- Jarrett, T.H. et al., 2000, AJ, 120, 298
- Johnston H. M., Hunstead R. W., Cotter G., Sadler E. M., 2005, MNRAS, 356, 515
- Jones, D.H. et al., 2004, MNRAS, 355, 747
- Jones, D.H. et al., 2009, MNRAS, 399, 683
- Jones, P. A., McAdam, W. B., 1992, ApJS, 80, 137
- Kameno, S., Sawada-Satoh, S., Inoue, M., Shen, Z.-Q., Wajima, K., 2001, PASJ, 53, 169
- Keel, W. C., White, R. E., Owen, F. N., Ledlow, M. J., 2006, AJ, 132, 2233
- Kewley, L. J., Groves, B., Kauffmann, G., Heckman, T., 2006, MNRAS, 372, 961
- Killeen, N.E.B., Bicknell, G.V., Ekers, R.D., 1986, ApJ, 302, 306
- Kimball, A. E., Ivezić, Z., 2008, AJ, 136, 684
- Kollgaard, R. I., Feigelson, E. D., Laurent-Muehleisen, S. A., Spinrad, H., Dey, A., Brinkmann, W., ApJ, 449, 61
- Large, M. I., Mills, B. Y., Little, A. G., Crawford, D. F., Sutton, J. M., 1981, MNRAS, 194, 693
- Lauberts, A., 1982, ESO/Uppsala survey of the ESO(B) atlas. European Southern Observatory, Garching
- Ledlow M.J., Owen F.N., 1996, AJ, 112, 9
- Ledlow M.J., Owen F.N., Keel W.C., 1998, ApJ, 495, 227
- Ledlow M.J., Owen F.N., Yun M.S., Hill J.M., 2001, ApJ, 552, 120
- Lenc, E., Tingay, S.J., 2006, AJ, 132, 1333
- Lilly, S. J., Longair, M. S., 1984, MNRAS, 211, 833
- Lilly, S. J., Prestage, R. M., 1987, MNRAS, 225, 531
- Longair, M.S. 1966, MNRAS, 133, 421
- Machacek, M. E., O'Sullivan, E., Randall, S. W., Jones, C., Forman, W. R., 2010, ApJ, 711, 1316
- Mahony, E. K. et al., 2011, MNRAS, 417, 2651
- Marcha, M.J.M., Browne, I.W.A., Jethava, N., Anton, S., 2005, MNRAS 361, 469
- Marcha, M.J.M., Caccianiga, A. 2013, MNRAS, 430, 2464
- Marshall, H. L. et al., 2005, ApJS, 156, 13
- Massardi, M. et al., 2008, MNRAS, 384, 775
- Massardi, M. et al., 2011a, MNRAS, 412, 318
- Massardi, M. et al., 2011b, MNRAS, 415, 1597
- Massaro, E., Giommi, P., Leto, C., Marchegiani, P., Maselli, A., Perri, M., Piranomonte, S., Sclavi, S., 2009, A&A, 495, 691
- Massaro, F., D'Abrusco, R., Tosti, G., Ajello, M., Gasparrini, D., Grindlay, J.E., Smith, H.A., 2012, ApJ 750, 138
- Mauch T., Murphy T., Buttery H.J., Curran J., Hunstead R.W., Piestrzynski B., Robertson J.G., Sadler E.M., 2003, MNRAS, 342, 1117
- Mauch T., Sadler E.M., 2007, MNRAS 375, 931
- McAdam, W. B., White, G. L., Bunton, J. D., 1988, MNRAS, 235, 425
- McConnell, D., Sadler, E. M., Murphy, T., Ekers, R.D., 2012, MNRAS, 422, 1527
- Morganti R., Killeen N.E.B., Tadhunter C.N., 1993, MNRAS 263, 1023
- Morganti R., Oosterloo T., Tadhunter C. N., Aiudi R., Jones P., Villar-Martin M., 1999, A&AS, 140, 355
- Morganti, R., Holt, J., Tadhunter, C., Ramos Almeida, C., Dicken, D., Inskip, K., Oosterloo, T., Tzioumis, T., 2011, A&A, 535, 97
- Morganti, R., Frieswijk, W., Oonk, R. J. B., Oosterloo, T., Tadhunter, C., 2013, A&A, 552, L4
- Murphy, T. et al., 2010, MNRAS, 402, 2403
- Nieppola, E., Tornikoski, M., Valtaoja, E., 2006, A&A 445, 441
- Norris, R. P., Allen, D. A., Roche, P. F., 1988, MNRAS, 234, 773
- O'Dea, C.P., 1998, PASP, 110, 493
- O'Dea, C.P., Owen, F.N., 1985, AJ, 90, 954
- Oosterloo, T. A., Morganti, R., Sadler, E. M., van der Hulst, T., Serra, P., 2007, A&A, 465, 787
- Owen, F. N., Laing, R. A., 1989, MNRAS, 238, 357
- Owen, F. N., Ledlow, M. J., 1997, ApJS, 108, 41
- Padovani, P., Urry, C.M., 1992, ApJ, 387, 449
- Perley R.A., Roeser H.-J., Meisenheimer K., 1997, A&A. 328, 12
- Phillips, M. M., Jenkins, C. R., Dopita, M. A., Sadler, E. M., Binette, L., 1986, AJ, 91, 1062
- Pihlström Y. M., Conway J. E., Booth R. S., Diamond P. J., Koribalski B. S., 2000, A&A, 357, 7
- Raimann, D., Storch-Bergmann, T., Quintana, H., Hunstead, R., Wisotzki, L., 2005, MNRAS, 364, 1239
- Ramos Almeida, C. et al., 2012, MNRAS, 419, 687
- Ricci R. et al., 2004a, MNRAS, 354, 305
- Ricci R., Prandoni I., Gruppioni C., Sault R.J., De Zotti G., 2004b, A&A, 415, 549
- Ricci, R., Prandoni, I., Gruppioni, C., Sault, R. J., de Zotti, G., 2006, A&A, 445, 465
- Roberts, M.D. et al., 1998, A&A, 337, 25
- Sadler E.M., Slee, O.B., Reynolds, J.E., Roy, A.L., 1995, MNRAS, 276, 1373
- Sadler, E. M., McIntyre, V. J., Jackson, C. A., Cannon, R. D., 1999, PASA, 16, 247
- Sadler E.M. et al. 2002, MNRAS, 329, 227
- Sadler, E. M. et al., 2006, MNRAS, 371, 898
- Saripalli, L., 2012, AJ, 144, 85
- Serra, P., Oosterloo, T. A., 2010, MNRAS, 401, L29
- Schmidt, M. 1968, ApJ, 151, 393
- Slee, O. B., Sadler, E. M., Reynolds, J. E., Ekers, R. D., 1994, MNRAS, 269, 928
- Smith, R.M., Bicknell, G.V., 1986, ApJ, 308, 36
- Snellen, I.A.G. et al. 2000, MNRAS, 319, 445
- Simpson C., Clements D.L., Rawlings S., Ward M., 1993, MNRAS, 262, 889
- Stanghellini, C., O'Dea, C. P., Baum, S. A., Dallacasa, D., Fanti, R., Fanti, C., 1997, A&A, 325, 943
- Stern, D. et al., 2012, ApJ, 753, 30
- Subrahmanyan R., Saripalli L., Hunstead R.W., 1996, MNRAS, 279, 257
- Tadhunter C. N., Morganti R., di Serego-Alighieri S., Fosbury R. A. E., Danziger I. J., 1993, MNRAS, 263, 999
- Taylor, G. B., Sanders, J. S., Fabian, A. C., Allen, S. W., 2006, MNRAS, 365, 705
- Tingay S.J., 1997, A&A, 327, 550
- Tingay, S. J., Edwards, P. G., Tzioumis, A. K., 2003, MNRAS, 346, 327
- Tingay S.J., 2004, AJ, 127, 10
- Tzioumis, A. et al., 2002, A&A 392, 841
- Ulvestad J.S., Antonucci R.J., 1997, ApJ, 488, 621
- Urry, C.M., Padovani, P., 1995, PASP, 107, 803
- Vermeulen, R. C., Ros, E., Kellermann, K. I., Cohen, M. H., Zensus, J. A., van Langevelde, H. J., 2003, PASA, 20, 65
- Veron-Cetty, M. P., Veron, P., 1988, A&A, 204, 28
- Veron-Cetty, M. P., Veron, P., 2001, A&A, 375, 791
- Veron-Cetty, M.-P., Woltjer, L., Ekers, R. D., Staveley-Smith, L., 1995, A&A, 297, L79
- Wall, J. V., 1980, Royal Soc. Phil. Trans. A, 296, 367
- Willott, C.J., Rawlings, S., Jarvis, M.J., Blundell, K.M., MNRAS, 2003, 339, 173
- Wilman, R.J. et al., 2008, MNRAS, 388, 1355
- Wilson, W. E. et al., 2011, MNRAS, 416, 832
- Wright, E. L. et al., 2010, AJ, 140, 1868
- Yan, L. et al., 2013, AJ, 145, 55
- Zirbel, E.L., Baum, S.A., 1995, A&A, 448, 521

APPENDIX A: NOTES ON INDIVIDUAL SOURCES

J000311-544516 (PKS 0000-550)

The radio source is resolved into a 1 arcmin double at 20 GHz (see Figure A1), and the catalogued AT20G position corresponds to the southern hotspot. No core is seen in the 20 GHz image, though a faint core is visible at 5 and 8 GHz. The source is only slightly resolved in the lower-frequency SUMSS image, with a largest angular size of 50 arcsec.

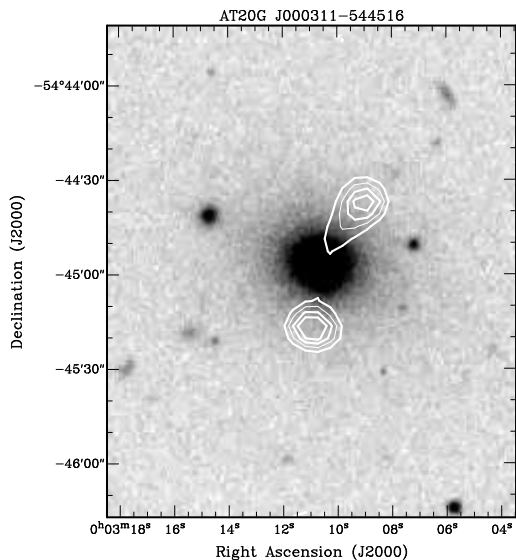


Figure A1. The resolved AT20G source J000311-544516 (PKS 0000-550). The greyscale is an optical B(J) image from Supercosmos and the white contours (at levels of 10, 15, 20 and 25 mJy/beam) show 20 GHz emission from the AT20G followup image. The rms noise in the 20 GHz AT20G snapshot image was 3.6 mJy/beam.

J000413-525458 (PKS 0001-531)

This resolved 20 GHz source is the core of a wide (~ 6 arcmin) triple source at low frequency, and the 843 MHz flux density listed in Table 3 is the sum of three SUMSS components. The AT20G images show a single source with an extension to the north-west in the direction of the northern low-frequency radio lobe. We tentatively classify this as an FR-1 radio galaxy based on the SUMSS image.

J001605-234352 (PKS 0013-240, ESO 473-G07)

This AT20G source is associated with the nucleus of a spiral galaxy. Slee et al. (1994) detected a parsec-scale radio core with an 8.4 GHz flux density of 60 mJy, suggesting that most of the observed 20 GHz emission comes from a central AGN. Allison et al. (2012) detected the 21cm HI line in absorption against the central continuum source.

J002736-540907

The optical spectrum shows only weak absorption lines, suggesting this is a possible BL Lac object.

J002901-011341 (PKS 0026-014)

The 2dFGRS spectrum of this galaxy (TGS 819Z353) shows weak optical emission lines on a strong stellar continuum (spectral type Aae).

J003704-010907 (3C 15, PKS 0034-01)

The AT20G source is the core of a well-studied FR-2 radio galaxy in the 2 Jy sample of Morganti et al. (1993). The fractional linear polarization of 3.7% measured at 20 GHz is close to the NVSS value of 4.1% at 1.4 GHz.

J004613-420700 and **J004622-420842** (PKS 0043-42)

A well-studied FR-2 radio galaxy roughly ~ 3 arcmin in angular size. The hotspots are detected as two separate AT20G sources at 20 GHz and are strongly polarized, with fractional linear polarizations of 7.4% and 17.9% for the northern and southern hotspots respectively. The galaxy nucleus is undetected at 20 GHz, implying

a core flux density below 10-15 mJy. There is no 6dFGS spectrum, but Morganti et al. (1999) note that an optical spectrum shows only weak, low-ionization emission lines and a stellar continuum typical of early-type galaxies. They remark that this is an example of a powerful FR-2 radio galaxy with significantly weaker emission lines than expected from the radio power-emission line luminosity correlation. We adopt the redshift of $z = 0.116$ published by di Serego Alighieri et al. (1994).

J004733-251717 (NGC 253)

A well-studied nearby spiral galaxy in the Sculptor group. The galaxy hosts a nuclear starburst as well as more extended star formation (Ulvestad & Antonucci 1997), and has been detected as a gamma-ray source by the Fermi satellite (Abdo et al. 2010). The radio source is extended in the AT20G image, and the listed AT20G flux density is a lower limit to the total value. The flux density measured by WMAP at 23 GHz is 1.3 Jy. NGC 253 is the closest galaxy (and lowest-luminosity 20 GHz source) detected in the AT20G survey. Since no VLBI core component is detected (Sadler et al. 1995; Tingay 2004), the observed 20 GHz emission probably arises from a compact nuclear starburst rather than an AGN.

J005734-012328 (PKS 0055-01)

The AT20G source corresponds to the core of an FR-1 radio galaxy which belongs to the 2 Jy sample of Morganti et al. (1993).

J012600-012041 (NGC 547)

The AT20G point source is associated with NGC 547, which lies in the cluster Abell 194 and has a close companion galaxy NGC 545. The low-frequency emission is ~ 10 arcmin in extent and is resolved into several components in NVSS. The 1.4 GHz flux density listed in Table 3 is from Condon, Cotton & Broderick (2002). Although this source is listed as a FR-2 radio galaxy in the 2 Jy sample of Morganti et al. (1993), based on the original classification by O’Dea & Owen (1985), more recent radio images suggest it should be reclassified as an FR-1 (Jackson et al. 2002).

J013357-362935 (NGC 612)

This is a well-studied FR-2 radio galaxy in the 2 Jy sample of Morganti et al. (1993). Ekers et al. (1978) noted that the host galaxy has a well-defined disk, and this was the first-known example of a powerful radio galaxy in disk galaxy. The 20 GHz radio emission extends over at least 6 arcmin, as shown in the mosaic image made by Burke-Spolaor et al. (2009). The 20 GHz flux density listed in Table 3 is also from Burke-Spolaor et al. (2009), and is a lower limit to the total value since the source is larger than the field imaged by these authors.

J021645-474908 (ESO 198-G01, PKS 0214-48)

This is a resolved triple source at 20 GHz, with a total extent of ~ 1.5 arcmin. The catalogued AT20G position corresponds to the core. This object is classified as an FR-1 radio galaxy in the MS4 sample of Burgess & Hunstead (2006).

J023137-204021 (PKS 0229-208)

This AT20G source is the core of the radio galaxy PKS 0229-208, which is an extended source (around 3 arcmin in extent) at low frequencies. The NVSS flux density listed in Table 3 is for the central component (as also listed by Mauch & Sadler 2007), and the extended emission at 1.4 GHz is split into at least six overlapping components in the NVSS catalogue. We tentatively classify this as an FR-1 radio galaxy on the basis of the NVSS image.

J024104-081520 (NGC 1052)

This is a nearby and well-studied elliptical galaxy with a double-sided VLBI radio jet (Kameno et al. 2001). Tingay et al. (2003) identify NGC 1052 as a GPS radio source.

J024240-000046 (NGC 1068, PKS 0240-00)

NGC 1068 is a nearby spiral galaxy with a well-studied active nucleus. The central radio source is resolved at 20 GHz.

J031552-190644 (PMN J0315-1906)

This galaxy has been studied in detail by Ledlow et al. (1998; 2001), who identify it as a rare example of an FR-1 radio source in a spiral host galaxy. Their 1.4 GHz VLA image shows a faint jet extending south-west from the nucleus, and they also detect HI in absorption against the bright radio core. Only the core component is seen in the AT20G image. Keel et al. (2006) present HST and Chandra images of the host galaxy, noting that it has a very luminous bulge. The WISE infrared colours ($[3.4] - [4.6] = 0.82$ mag; $[4.6] - [12] = 2.68$ mag) imply that this is a late-type galaxy which probably hosts a radiatively-efficient accretion disk.

J034630-342246 (PKS 0344-34) This AT20G source is the core of a radio galaxy in the MS4 catalogue of Burgess & Hunstead (2006). The source has extended low-frequency emission, and is a 5 arcmin double in the 843 MHz SUMSS image. We classify this as an FR-2 radio galaxy on the basis of the low-frequency NVSS and SUMSS images. Raimann et al. (2005) note that the optical spectrum of this galaxy shows strong, narrow emission lines (class Ae).

J035145-274311 (PKS 0349-27)

The listed AT20G source is the northern hotspot of an FR-2 radio galaxy (Morganti et al. 1993), and has a fractional polarization of 24.8% at 20 GHz. The core and southern hotspot were not detected in the AT20G survey. The galaxy has an extended optical emission-line region with a disturbed velocity structure which may result from a recent collision or merger (Danziger et al. 1984, Grimberg et al. 1999).

J035257-683117 (PKS 0352-686)

This source is core-dominated, and only slightly resolved in the 20 GHz image. It is unresolved in the lower-frequency SUMSS image.

J042908-534940 (IC 2082, PKS 0427-53)

The AT20G source is the core of a head-tail or wide-angle tail FR-1 radio galaxy (Ekers 1969; McAdam et al. 1988) associated with a dumbbell galaxy (Carter et al. 1981) at the centre of a cluster. This galaxy is also in the 2 Jy (Morganti et al. 1993) and MS4 (Burgess et al. 2006) radio samples, and Raimann et al. (2005) note that its optical spectrum shows weak optical emission lines (class Aae).

J043022-613201 (PKS 0429-61)

The AT20G source is centred on the 6dFGS galaxy, but is significantly offset from the extended lower-frequency emission seen in the SUMSS image. The galaxy is classified as FR-1 by Burgess & Hunstead (2006).

J045523-203409 (NGC 1692) This is a compact (~ 30 arcsec) double at 20 GHz, with the emission probably arising from a pair of hotspots rather than a core. Tadhunter et al. (1993) note that no optical emission lines are detected in this galaxy and the continuum appears typical of early-type galaxies.

J050453-101451 (Arp 187, PKS 0502-10)

The radio source is associated with a disturbed or interacting galaxy listed in the Arp (1966) Atlas of Peculiar Galaxies. Although the 20 GHz emission is flagged as extended in the AT20G catalogue, it is unresolved by NVSS at 1.4 GHz.

J051949-454643, **J051926-454554** and **J052006-454745** (Pictor A, PKS 0518-45)

A well-studied FR-2 radio galaxy, imaged in detail at the VLA by Perley, Roeser & Meisenheimer (1997). Three separately-catalogued AT20G sources correspond to the core and two hotspots. The 20 GHz flux density listed in Table 3 is from Burke-Spolaor et al. (2009). The optical spectrum (Eracleous & Halpern 1994) shows strong, broad emission lines.

J054754-195805 (PKS 0545-199)

The AT20G source is resolved at 20 GHz, and the 1.4 GHz emission is also extended. Zirbel & Baum (1995) identify this as an FR-1 radio galaxy.

J055049-314428 (ESO 424-G27, PKS 0548-317)

This is a compact ($\sim 30''$ separation) double in the AT20G image. The catalogued AT20G position corresponds to one of two hotspots, rather than the core, and both hotspots lie just beyond the optical galaxy. The lower-frequency NVSS source is only slightly extended, with an angular size of about 20 arcsec in the NVSS catalogue.

J062143-524132 (PKS 0620-52)

This source is core-dominated but slightly resolved at 20 GHz. The low-frequency emission seen in the SUMSS image is characteristic of a wide-angle tail (WAT) source, and the galaxy is classified as an FR-1 by Morganti et al. (1993).

J062620-534151 (ESO 161-IG07, PKS 0625-53)

This AT20G source is a resolved double at 20 GHz, and is classified as an FR-1 radio galaxy in the 2 Jy (Morganti et al. 1993) and MS4 (Burgess et al. 2006) samples. The optical ID is a dumbbell galaxy at the centre of a cluster (Lilly & Prestage 1987; Gregorini et al. 1994). The catalogued AT20G position is offset by about 15 arcsec from the optical galaxy, and probably corresponds to the southern hotspot of a compact double, rather than the core.

J062648-543214 (PKS 0625-545)

This is a resolved triple source at 20 GHz, about 1.5 arcmin in extent. The AT20G catalogue position corresponds to the northern hotspot, but the core is also detected at 20 GHz.

J062706-352916 (PKS 0625-35)

This is the central galaxy of the cluster Abell 3392, and is classified as an FR-1 radio galaxy by Morganti et al. (1993).

J063631-202857 and **J063633-204239** (PKS 0634-20)

These two AT20G sources correspond to hotspots of a very extended (~ 15 arcmin in angular size) FR-2 radio galaxy. No core component is detected in the AT20G survey. The host galaxy is well-studied at both optical and radio wavelengths, and a detailed 1.4 GHz image was made at the VLA by Baum et al. (1988). This object is classified by Ishwara-Chandra & Saikia (1999) as a Giant Radio Galaxy, with the overall projected size of the radio emission exceeding 1 Mpc.

J065153-602158 (PKS 0651-60)

The catalogued AT20G position appears to correspond to the northern hotspot of a ~ 1 arcmin double at 20 GHz. A second, fainter 20 GHz source is seen at the position of the optical galaxy. The lower-frequency SUMSS emission extends over several arcmin, and we tentatively classify this as an FR-1 radio galaxy based on the low-frequency morphology.

J065359-415144 (PKS 0652-417)

The 6dFGS DR3 catalogue lists the redshift of this galaxy as $z=0.00$, based on (foreground) Galactic nebular emission lines. We have remeasured the correct redshift as $z=0.0908$, based on the position of the Ca H and K absorption lines in the 6dFGS spectrum. We tentatively classify this as an FR-1 radio galaxy on the basis of the 843 MHz SUMSS image, which shows extended jet-like emission.

J070240-284149 (NGC 2325)

This is a nearby and well-studied elliptical galaxy with a dust lane (Veron-Cetty & Veron 1988).

J070459-490459 (ESO 207-G19)

The SUMSS image shows extended low-frequency emission, from which we classify this as an FR-1 radio galaxy.

J070914-360121 (PKS 0707-35)

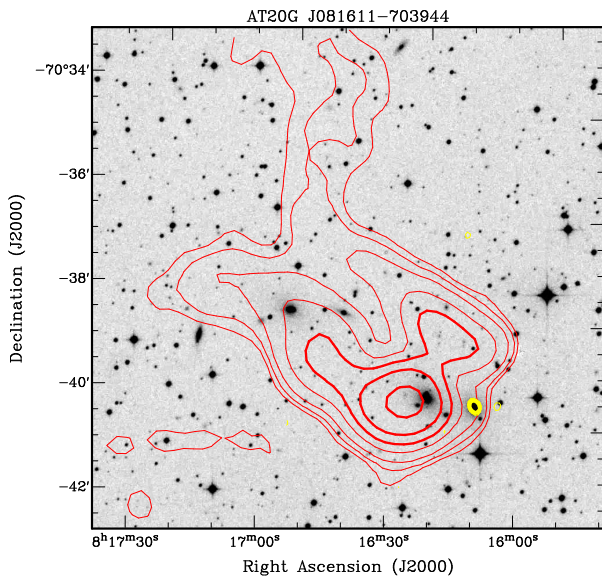


Figure A2. The AT20G radio source J081611-703944, with yellow contours marking 20 GHz emission from the AT20G image and red contours marking the low-frequency emission from the 843 MHz SUMSS image.

The AT20G source is the core of a radio galaxy which has an extended ‘double-double’ structure at low frequencies. The low-frequency emission has an FR-2 morphology extending over about 8 arcmin on the sky. The source has been studied in detail by Subrahmanyan et al. (1996), and is in the Ishwara-Chandra & Saikia (1999) sample of giant radio sources with a projected size larger than 1 Mpc.

J080537-005819 (PKS 0803-00, 3C 193)

The 20 GHz emission extends over about 20-30 arcsec. The 1.4 GHz VLA image made by Owen & Ledlow (1997) shows that this is a wide-angle tail (WAT) galaxy in the cluster Abell 623. We classify this as an FR-1 radio galaxy based on the 1.4 GHz image.

J080852-102832 (PKS 0806-10, 3C195)

The catalogued AT20G source is the southern hotspot of an FR-2 radio galaxy about 2.5 arcmin in extent (Morganti et al. 1993). The core and northern hotspot were not detected in the AT20G survey. This galaxy is in the ‘radio-excess IRAS galaxy’ sample of Buchanan et al. (2006), who note that the optical spectrum shows strong, narrow emission lines.

J081611-703944 (ESO 060-IG02, PKS 0816-705)

The AT20G source is centred on the 6dFGS galaxy g0816118-703945 at $z=0.0333$, but is significantly offset from the centroid of the low-frequency emission (see Figure A2).

J084452-100059 (PMN J0844-1001) This galaxy has extended low-frequency emission in the 1.4 GHz NVSS image, and we tentatively classify it as an FR-1 radio galaxy.

J090802-095937 (PMN J0908-1000)

This galaxy is listed as a BL Lac object by Nieppola et al. (2006), and was also detected as a ROSAT X-ray source (Bauer et al. 2000). The galaxy lies in an Abell cluster, and the NVSS image shows extended, complex low-frequency emission. O’Dea & Owen (1985) classify this as a narrow-angle tail radio source based on a higher-resolution 1.4 GHz VLA image. We have classified it as an FR-1

radio galaxy based on the extended low-frequency emission seen in the NVSS image.

J090825-093332 (PMN J0908-0933)

The 6dFGS spectrum looks almost featureless and is classified as poor-quality. The listed redshift is taken from Christlein & Zabludoff (2003). We tentatively classify this as an FR-1 radio galaxy based on the morphology of the low-frequency emission seen in the NVSS image.

J091300-210320 (MRC 0910-208)

The 6dFGS spectrum shows weak absorption lines, and the galaxy is classified as a possible BL Lac object by Massaro et al. (2009).

J091805-120532 (PKS 0915-11, 3C 218, Hydra A)

This is a well-studied FR-1 radio galaxy in the Hydra cluster, and belongs to the 2-Jy sample of Morganti et al. (1993). The AT20G source is a compact double, probably corresponding to two inner hotspots rather than a core and jet.

J094110-120451 (MRC 0938-118)

The AT20G image shows a resolved triple source, about 2 arcmin in extent. The catalogued AT20G position corresponds to the northern hotspot, but the core is also detected. This source is a resolved double in the 1.4 GHz NVSS image, and the 1.4 GHz flux density listed in Table 3 is the sum of the two NVSS components. We tentatively classify this as an FR-2 radio galaxy on the basis of the NVSS morphology.

J094409-015116 (PMN J0944-0151)

Buchanan et al. (2006) include this object in their sample of ‘radio-excess IRAS galaxies’. Their optical spectrum shows strong, narrow emission lines superimposed on a stellar continuum with Balmer absorption features typical of post-starburst systems.

J105533-283134 (PKS 1053-282)

This source appears to have a complex, diffuse structure at 20 GHz, which is poorly imaged by the AT20G snapshot observation. The source is less than 30 arcsec in extent in the 1.4 GHz NVSS image. Slee et al. (1994) detected a parsec-scale radio core with an inverted radio spectrum at 2–8 GHz.

J110957-373220 (NGC 3557)

This is a well-studied nearby elliptical galaxy which hosts a FR-1 radio source (Birkinshaw & Davies 1985).

J112119-001316 (PKS 1118+000)

The low-frequency NVSS emission is extended and offset from the AT20G emission, and the higher-resolution FIRST image shows that this is a wide-angle tail (WAT) radio galaxy with a bright core and complex extended structure at 1.4 GHz.

J113305-040046 (PKS 1130-037)

This AT20G source is the core of a radio galaxy which is extended at low frequencies and spans almost 10 arcmin on the sky in the NVSS image. We tentatively classify this as an FR-1 radio galaxy based on the 1.4 GHz NVSS image.

J122343-423532 (PKS 1221-42)

The redshift of $z=0.0266$ listed in the 6dFGS catalogue is incorrect and the correct redshift is $z=0.1706$ (Simpson et al. 1993). The host galaxy and its stellar population have been studied in detail by Johnston et al. (2005), who note that this is a young compact steep-spectrum (CSS) radio source with double lobes located well within the optical galaxy.

J123959-113721 (NGC 4594)

This is a well-studied nearby spiral (the ‘Sombrero Galaxy’). Sadler et al. (1995) found that at 8.4 GHz, the central radio source was smaller than 0.03 arcsec (i.e. < 3 parsec) in angular size.

J124849-411840 (NGC 4696 = PKS 1245-41)

This is the central galaxy of the Centaurus cluster, recently studied

in detail by Taylor et al. (2006). The radio emission is resolved at 20 GHz, but not in the lower-frequency SUMSS image.

J125438-123255 (NGC 4783 = PKS 1251-12, 3C 278)

This is an extended AT20G source associated with an FR-1 radio galaxy (Morganti et al. 1993). The optical ID is one of a close pair of elliptical galaxies, NGC 4782 and 4783. Baum et al. (1988) identify NGC 4782 as the optical ID, but both the AT20G catalogue position and the core position measured by Ricci et al. (2006) are closer to NGC 4783, so we tentatively identify this galaxy as the optical counterpart of the AT20G source.

J130100-322628 (ESO 443-G24 = PKS 1258-321)

This object has extended emission at 1.4 GHz in the NVSS image, and is classified as a low-power FR-1 radio galaxy by Marshall et al. (2005).

J130527-492804 (NGC 4945)

This is a nearby, well-studied spiral galaxy with an active nucleus.

J130841-242259 (IRAS 13059-2407)

This edge-on disk galaxy (tentatively classified as an Sc spiral in the NASA Extragalactic Database) has the lowest infrared K-band luminosity of the 202 galaxies in our AT20G-6dFGS sample. It is also classified as a ‘radio-excess IRAS galaxy’ by Drake et al. (2003). Allison et al. (2012; 2013) recently detected associated 21 cm HI absorption against the central radio source.

J131124-442240 (PKS 1308-441)

The 843 MHz SUMSS image shows low-frequency emission extending over more than 15 arcmin on the sky. Tingay (1997) notes that this is a giant radio galaxy with a morphology intermediate between FR-1 and FR-2. We tentatively classify it as FR-1 on the basis of the SUMSS image.

J131931-123925 (NGC 5077)

This elliptical galaxy has an extended disk of ionised gas along its minor axis which has been studied in detail by Bertola et al. (1991), who note that this galaxy also contains a substantial amount of neutral hydrogen (see also Serra & Oosterloo 2010).

J131949-272437 (NGC 5078)

This is a nearby spiral galaxy with a prominent dust lane.

J132112-434216 (NGC 5090)

The catalogued AT20G source is the core of an FR-1 galaxy with very extended low-frequency radio emission (Morganti et al. 1993). NGC 5090 has a close (probably interacting) spiral companion, NGC 5091 (Smith & Bicknell 1986).

J132527-430108 (NGC 5128, Centaurus A)

The AT20G source is the core of the well-studied nearby radio galaxy NGC 5128. The radio luminosity used in this paper was calculated using the total 20 GHz flux density of 28.350 Jy listed in the AT20G catalogue (Murphy et al. 2010). Israel et al. (2008) measured a higher flux density of 112 ± 13 Jy at 23 GHz using WMAP images which include the emission from the outer radio lobes.

J133639-335756 (IC 4296)

The catalogued AT20G source is the core of a well-studied FR-1 radio galaxy which has very extended emission at low frequencies (Killeen et al. 1986). The listed 1.4 GHz flux density is the sum of four NVSS components, and the 843 MHz flux density is from Jones & McAdam (1992).

J134624-375816 (ESO 325-G16, PKS 1343-377)

This AT20G source has complex, highly extended low-frequency emission, and appears to be the core of a head-tail radio galaxy in the cluster Abell 3570.

J141949-192825 (PKS 1417-19) The 20 GHz emission is centred on the 6dFGS galaxy, while the lower-frequency NVSS source has a centroid significantly offset from the optical position.

J145509-365508 (PKS 1452-367)

The galaxy has extended low-frequency emission on scales of 3–4 arcmin in the SUMSS and NVSS images, and we tentatively classify it as an FR-1 radio galaxy based on the low-frequency morphology.

J145924-16413 (NGC 5793)

This AT20G source is the core of a spiral galaxy. Gardner et al. (1992) detected a VLBI core less than 0.03 arcsec in size, with HI seen in absorption against the core. Hagiwara et al. (1997) detected an H₂O megamaser in NGC 5793. The HI absorption system has been studied in detail with the VLBA by Pihlström, et al. (2000).

J151741-242220 (AP Lib)

This well-studied BL Lac object is the most luminous AT20G source in the local ($z < 0.1$) universe, and is known to be variable at optical as well as radio wavelengths (Carini et al. 1991).

J164416-771548 (PKS 1637-77)

The catalogued AT20G source is the core of an FR-2 radio galaxy with low-frequency radio emission extending over at least 4-5 arcmin in the SUMSS image. There is no 6dFGS spectrum, but Tadhunter et al. (1993) note that the optical spectrum shows strong emission lines.

J172019-005851 and **J172034-005824** (PKS 1717-00, 3C253)

Two hotspots of this FR-2 radio galaxy are detected as separate AT20G sources 3.6 arcmin apart. The galaxy core was not detected in the AT20G survey.

J172341-650036 (NGC 6328)

This well-studied galaxy is a strong, compact radio source at 20 GHz, and has been identified by Tingay (1997) as one of the closest GPS radio galaxies. The galaxy shows faint spiral structure in the optical and has been detected in HI by Veron-Cetty et al. (1995), who suggest that this object is the result of a recent merger involving a gas-rich spiral galaxy.

J173722-563630 and **J173742-563246** (PKS 1733-56)

FR-2 radio galaxy with the two hotspots detected as separate AT20G sources 4.7 arcmin apart. The galaxy core was not detected in the AT20G survey.

J180207-471930 (MRC 1758-473)

This galaxy has extended radio emission in the 843 MHz SUMSS image, and we tentatively classify it as an FR-1 radio galaxy.

J180712-701234 (PKS 1801-702)

This source is a compact double at 20 GHz, with the two components separated by about 20 arcsec. It appears to be unresolved in the lower-frequency SUMSS image.

J180957-455241 (PKS 1806-458)

Kollgaard et al. (1995) found that this source had a GHz-peaked spectrum with a maximum around 4 GHz, and remarked that it was much brighter than the vast majority of other GHz-peaked sources and should be studied further. More recently Massardi et al. (2011b) made multi-frequency observations at several epochs, which showed the radio spectrum peaking above 10 GHz. The high radio luminosity of this source, together with the presence of broad emission lines in the optical spectrum, suggest that (as discussed in §6.2.1 above) this is probably a blazar seen in a flaring state rather than a genuine GPS radio galaxy.

J181857-550815 (PMN J1818-5508)

This 20 GHz source is the core of a radio galaxy which is a resolved double in the 843 MHz SUMSS image. We tentatively classify this as an FR-1 radio galaxy.

J181934-634548 (PKS 1814-63)

This is a very strong compact source which is a member of the Morganti et al. (1993) 2 Jy sample and has classified as a CSS radio source by Tzioumis et al. (2002). The galaxy has been studied in detail by Morganti et al. (2011), who note that it is a rare example

of a powerful radio AGN hosted by a disk galaxy. In the optical, there is a very bright foreground star whose light contaminates the 6dFGS spectrum.

J184314-483622 (PKS 1839-48)

The AT20G source is the core of an FR-1 radio galaxy in the 2 Jy sample of Morganti et al. (1993).

J191457-255202 (PMN J1914-2552)

The NVSS image shows diffuse emission extending up to 5 arcmin to the west of the galaxy core, suggesting that this may be a head-tail radio source in a cluster.

J192817-293145 (ESO 460-G04, MRC 1925-296)

The NVSS image shows extended low-frequency emission, with a morphology suggesting that this is a wide-angle tail (WAT) radio galaxy in a cluster.

J195817-550923 (PKS 1954-55)

This source is a resolved double in the AT20G image at 20 GHz, with the components separated by about 1 arcmin. A detailed ATCA image made by Morganti et al. (1999) at 8 GHz shows a core together with complex, extended jet structures which are not well imaged by the limited uv coverage of the ATCA snapshot observations. This is one of the most highly-polarized sources in the AT20G catalogue, with a fractional linear polarisation of 43.5% at 20 GHz (Murphy et al. 2010).

J200954-482246 (NGC 6868)

This is a well-studied dust-lane elliptical galaxy in a group. A detailed X-ray study has been carried out by Machacek et al. (2010).

J203444-354857 (ESO 400-IG40)

The AT20G source is associated with the northern member of a close pair of galaxies in the cluster Abell 3695.

J204552-510627 (ESO 234-G68)

The SUMSS image shows very extended low-frequency radio emission, from which we tentatively classify this object as an FR-1 radio galaxy.

J205202-570407 (IC 5063)

This is a well-known dust-lane S0 galaxy recently studied in detail by Morganti et al. (2013).

J205306-162007 (IC 1335, PKS 2050-16)

The NVSS image shows extended low-frequency radio emission with a total angular total extent of at least 10 arcmin. We tentatively classify this object as an FR-1 radio galaxy based on the NVSS morphology.

J205603-195646 (PKS 2053-20)

This source is a compact double, about 0.5 arcmin in extent, at 20 GHz. The two components appear to be hotspots, and no core is detected. The catalogued AT20G position corresponds to the southern hotspot. The source is barely resolved in the lower-frequency NVSS image.

J205754-662919 (ESO 106-IG15)

The SUMSS image shows low-frequency radio emission extending over at least 5 arcmin on the sky, from which we tentatively classify this object as an FR-1 radio galaxy.

J212222-560014 (PMN J2122-5600)

The AT20G source is offset by more than 40 arcsec from the centroid of the extended low-frequency emission seen in the SUMSS image. This offset, together with the morphology of the low-frequency emission, suggests this is probably a head-tail radio source in a cluster. As noted in §3.4.1 of this paper, Hancock et al. (2010) find that the compact AT20G source has a radio spectrum peaking above 40 GHz, suggesting that this may be a rare example of a recently-restarted radio galaxy.

J213133-383703 (NGC 7075)

This galaxy has extended low-frequency emission in the NVSS

and SUMSS images, and is tentatively classified as an FR-1 radio galaxy on the basis of the low-frequency morphology.

J213741-143241 (PKS 2135-13)

The catalogued AT20G source is a hotspot of the well-studied FR-2 radio galaxy PKS 2135-13 (see Table 1). The core is also detected at 20 GHz, and the 6dFGS spectrum shows strong, broad optical emission lines.

J214824-571351 (PMN J2148-5714)

This source has extended, asymmetric radio emission at 843 MHz, and may be a head-tail radio source in a cluster.

J215129-552013 (PKS 2148-555)

The catalogued AT20G source is the core of an extended FR-1 radio galaxy, with low-frequency emission extending over at least 12 arcmin in the 843 MHz SUMSS image. The AT20G 20 GHz image shows extended emission to the south-west of the core, possibly originating in a jet. Raimann et al. (2005) note that the host galaxy has an absorption-line (Aa) optical spectrum.

J215706-694123 (ESO 075-G041, PKS 2153-69)

This is a very bright (37 Jy) double source in SUMSS, and is classified as an FR-2 radio galaxy by Morganti et al. (1993). As noted by Ricci et al. (2004), both the core and a fainter southern hotspot are seen in the AT20G 20 GHz image.

J220113-374654 (PKS 2158-30)

The catalogued AT20G source is a hotspot of the FR-2 radio galaxy PKS 2158-30 (see Table 1). The core is not detected in the AT20G image.

J220916-471000 (NGC 7213)

This is a bright, nearby early-type spiral galaxy which has recently been studied in detail at both radio and X-ray wavelengths by Bell et al. (2011).

J224559-173724 (PKS 2243-179)

Although not flagged as extended in the AT20G catalogue, this source appears extended or double in the 20 GHz image.

J225710-362744 (IC 1459)

This is a nearby and well-studied giant elliptical galaxy which has been identified by Tingay et al. (2003) as one of the closest GPS radio galaxies. Oosterloo et al. (2007) note that IC 1459 lies in a gas-rich galaxy group and has HI tidal tails extending over at least 200 kpc on the sky. Franx & Illingworth (1988) discovered a fast counter-rotating stellar core in IC 1459, and Cappellari et al. (2002) have studied the kinematics of this galaxy in detail.

J231905-420648 (PKS 2316-423)

This galaxy is a bright X-ray source (Crawford & Fabian 1994), and was identified as a radio-selected BL Lac object by Roberts et al. (1998). The SUMSS image shows extended low-frequency emission with a complex structure.

J231915-533159 (PKS 2316-538)

This galaxy has extended low-frequency emission in the SUMSS image, and is tentatively classified as an FR-1 radio galaxy on the basis of the low-frequency morphology.

J234205-160840 (PKS 2339-164)

The NVSS image shows complex, extended emission at low-frequency, and the NVSS morphology suggests that this is a wide-angle tail radio galaxy in a cluster.

J235156-010909 (PKS 2349-01)

The AT20G source is a resolved double roughly 15-20 arcsec in extent. The low-frequency emission is barely resolved in NVSS, but the higher-resolution FIRST image at 1.4 GHz shows a compact double with similar morphology to the AT20G image.

Table 3. 6dFGS galaxies detected as AT20G radio sources. The meanings of the columns are defined in §2.5 of the paper.

(1)	(2)	(3)	(4)	(5)	(6)	(7)	(8)	(9)	(10)	(11)	(12)	(13)	(14)	(15)	(16)	(17)
AT20G name	AT20G position (J2000)	S_{20} (mJy)	\pm	S_8 (mJy)	\pm	S_5 (mJy)	\pm	NVSS (mJy)	SUMSS (mJy)	6dFGS name	Offset (arcsec)	K_{tot} (mag)	Redshift	Q	Class	Notes
(a)6dFGS galaxies identified with AT20G point sources																
J000922-513011	00 09 22.06 -51 30 11.9	49	3	59	3	56	3	...	45.1	g0009220-513012	0.5	12.30	0.1170	4	Aa	
J000935-321637	00 09 35.67 -32 16 37.3	221	10	275	14	313	16	521.6	558.8	g0009355-321637	1.5	9.55	0.0255	4	Aae	IC 1531
J001215-384618	00 12 15.13 -38 46 18.8	80	4	105	5	103	5	65.4	52.2	g0012152-384619	0.5	11.82	0.0755	4	Aae	
J001605-234352	00 16 05.81 -23 43 52.1	68	4	-	-	-	-	275.8	...	g0016057-234352	0.9	12.22	0.0640	4	Ae	ESO 473-G07
J002301-565005	00 23 01.58 -56 50 05.2	99	5	99	5	106	5	...	208.4	g0023015-565005	0.6	10.08	0.0342	4	Aae	
J002736-540907	00 27 36.69 -54 09 07.7	43	2	-	-	-	-	...	58.3	g0027366-540908	0.8	12.46	0.1235	4	Aa	
J002901-011341	00 29 01.01 -01 13 41.7	207	9	-	-	-	-	284.8	...	g0029010-011342	0.6	11.06	0.0830	
J003033-581914	00 30 33.78 -58 19 14.7	51	3	53	3	29	2	...	35.6	g0030338-581915	0.4	12.97	0.1740	4	Aa	
J003908-222001	00 39 08.17 -22 20 01.3	49	3	-	-	-	-	113.5	...	g0039082-222001	0.6	11.99	0.0644	
J003939-130059	00 39 39.94 -13 00 59.7	68	3	-	-	-	-	47.3	...	g0039399-130060	0.8	12.03	0.1075	4	Aae	
J004048-204339	00 40 48.16 -20 43 39.1	103	7	215	11	333	17	641.2	...	g0040482-204339	0.5	12.54	0.0918	4	Ae	
J005452-043704	00 54 52.67 -04 37 04.5	49	3	-	-	-	-	177.0	...	g0054526-043703	1.4	11.59	0.0689	3	Aa	
J005620-093631	00 56 20.14 -09 36 31.1	78	4	-	-	-	-	199.2	...	g0056201-093630	1.3	11.95	0.1031	
J005734-012328	00 57 34.88 -01 23 28.0	55	2	-	-	-	-	5365.4	...	g0057349-012328	0.5	10.55	0.0450	J	Aa	
J010249-795604	01 02 49.45 -79 56 04.9	113	6	110	6	233	11	...	837.9	g0102490-795604	1.6	11.67	0.0570	
J010633-463836	01 06 33.06 -46 38 36.5	47	3	49	3	52	3	...	85.2	g0106330-463837	0.5	10.99	0.0307	ESO 243-G29
J011132-730209	01 11 32.25 -73 02 09.9	74	4	72	4	72	4	...	86.4	g0111325-730210	1.2	11.12	0.0666	4	Aa	
J012600-012041	01 26 00.61 -01 20 41.9	147	7	-	-	-	-	3730.7	...	g0126006-012043	0.7	8.49	0.0184	J	Aa	NGC 547
J012820-564939	01 28 20.38 -56 49 39.7	189	10	141	7	130	7	...	82.6	g0128205-564940	0.9	12.24	0.0666	4	Ae	
J013241-080405	01 32 41.06 -08 04 05.1	131	5	-	-	-	-	306.8	...	g0132411-080405	1.3	12.15	0.1485	
J014648-520233	01 46 48.63 -52 02 33.5	226	11	212	11	225	12	...	349.5	g0146486-520234	0.4	11.79	0.0981	4	Aa	
J015422-023454	01 54 22.79 -02 34 54.6	118	5	-	-	-	-	193.6	...	g0154228-023454	0.5	11.79	0.0823	4	Aae	
J021316-294326	02 13 16.42 -29 43 26.5	84	6	167	9	175	9	114.6	...	g0213164-294326	0.5	10.93	0.0351	4	Aae	ESO 415-G07
J023109-575505	02 31 09.32 -57 55 05.8	104	5	120	6	140	7	...	254.4	g0231093-575506	0.4	10.18	0.0320	ESO 115-G15
J023137-204021	02 31 37.01 -20 40 21.4	160	11	212	11	170	9	169.1	...	g0231370-204022	0.6	12.03	0.0898	4	Aa	
J023241-112020	02 32 41.77 -11 20 20.1	69	4	-	-	-	-	242.8	...	g0232419-112020	2.7	12.86	0.2087	3	Aa	
J023749-823252	02 37 49.54 -82 32 52.8	50	3	41	2	74	4	...	457.3	g0237503-823256	3.9	12.48	0.0754	4	Aae	
J024104-081520	02 41 04.77 -08 15 20.5	1199	59	-	-	-	-	912.5	...	g0241048-081521	0.6	7.45	0.0053	4	Ae	NGC 1052
J024326-561242	02 43 26.57 -56 12 42.3	114	6	224	11	312	16	...	181.9	g0243265-561242	0.3	12.73	0.0637	4	Ae	
J024524-110717	02 45 24.96 -11 07 17.1	167	8	-	-	-	-	141.2	...	g0245250-110717	0.2	11.89	0.0989	4	Aae	
J024554-445939	02 45 54.07 -44 59 39.5	581	29	591	30	688	34	...	1972.0	g0245541-445939	0.4	12.61	0.2829	4	AeB	
J025544-141227	02 55 44.13 -14 12 27.9	60	3	-	-	-	-	94.7	...	g0255442-141228	1.2	9.21	0.0290	IC 270
J025926-394037	02 59 26.51 -39 40 37.7	71	4	149	8	304	15	984.8	1552.0	g0259267-394038	2.2	11.53	0.0662	4	Aae	
J025955-123635	02 59 55.24 -12 36 35.1	92	5	-	-	-	-	518.1	...	g0259553-123635	0.8	12.05	0.0867	4	Aae	
J031357-395403	03 13 57.83 -39 54 03.4	78	4	129	7	236	12	597.1	917.6	g0313579-395404	1.0	12.16	0.0803	4	Aa	
J031552-190644	03 15 52.16 -19 06 44.5	108	7	121	6	99	5	100.1	...	g0315521-190644	0.7	12.65	0.0671	4	Ae?	
J031757-441416	03 17 57.66 -44 14 16.8	258	13	449	23	611	31	...	1915.0	g0317577-441417	0.6	10.47	0.0759	ESO 248-G06
J033114-524148	03 31 14.99 -52 41 48.2	55	3	59	3	56	3	...	51.0	g0331150-524148	0.1	12.10	0.0665	
J033913-173600	03 39 13.73 -17 36 00.9	97	6	120	6	130	7	170.0	...	g0339137-173601	0.5	11.57	0.0656	4	Aa	
J034630-342246	03 46 30.56 -34 22 46.1	102	4	-	-	-	-	1724.5	1789.4	g0346306-342246	0.3	12.05	0.0535	

Table 3. 6dFGS galaxies detected as AT20G radio sources.

(1)	(2)	(3)	(4)	(5)	(6)	(7)	(8)	(9)	(10)	(11)	(12)	(13)	(14)	(15)	(16)	(17)	Notes
AT20G name	AT20G position (J2000)	S_{20} (mJy)	\pm	S_8 (mJy)	\pm	S_5 (mJy)	\pm	NVSS (mJy)	SUMSS (mJy)	6dFGS name	Offset (arcsec)	K_{tot} (mag)	Redshift	Q	Class		
J035145-274311	03 51 45.09	-27 43 11.4	122	8	-	-	-	5340.2	..	g0351358-274435	>60	12.54	0.0657	4	Ae		Hotspot of PKS 0349-27
J035410-265013	03 54 10.07	-26 50 13.7	98	6	114	6	104	5	86.5	...	g0354102-265014	1.4	11.78	0.0650	4	Aa	
J040106-160640	04 01 06.75	-16 06 40.0	403	26	452	24	236	12	88.2	...	g0401066-160639	1.9	10.73	0.0317	4	Aae	
J042203-562127	04 22 03.84	-56 21 27.3	95	5	105	5	85	4	...	25.5	g0422038-562128	0.7	11.97	0.0380	4	Aa	
J043022-613201	04 30 22.00	-61 32 01.0	148	7	177	9	156	9	...	2790.	g0430220-613201	0.5	11.07	0.0555	4	Aa	
J043754-425853	04 37 54.73	-42 58 53.9	119	4	119	6	122	6	...	173.2	g0437547-425854	0.2	10.75	0.0475	4	Aae	
J051103-255450	05 11 03.77	-25 54 50.9	123	8	113	6	92	5	43.4	...	g0511038-255451	0.5	12.22	0.0929	4	Aa	
J052200-285608	05 22 00.78	-28 56 08.4	43	3	61	5	211	11	574.1	...	g0522008-285610	1.1	12.43	0.0670	3	Ae	
J052223-072513	05 22 23.21	-07 25 13.7	91	4	-	-	-	-	54.7	...	g0522232-072513	0.6	12.68	0.1645	4	AeB	
J052851-104114	05 28 51.23	-10 41 14.0	82	4	-	-	-	-	43.4	...	g0528512-104114	0.3	12.12	0.1130	4	Aa	
J053533-120222	05 35 33.28	-12 02 22.6	212	10	-	-	-	-	1356.7	...	g0535333-120223	0.5	12.27	0.1570	
J054828-331331	05 48 28.51	-33 13 31.5	53	3	38	3	32	2	6.0	...	g0548285-331331	0.4	12.87	0.0407	4	Aa	
J055712-372836	05 57 12.45	-37 28 36.3	82	4	120	6	165	8	301.8	457.5	g0557126-372837	1.2	10.42	0.0448	4	Ae	ESO 364-G18
J060554-351808	06 05 54.10	-35 18 08.3	117	5	283	14	531	27	1337.0	1799.0	g0605540-351808	0.9	12.46	0.1412	4	Aa	
J060555-392905	06 05 55.98	-39 29 05.0	79	4	101	5	110	6	108.8	84.3	g0605560-392906	0.7	11.48	0.0454	3	Aa	
J061324-421824	06 13 24.09	-42 18 24.1	95	4	156	8	243	12	...	650.2	g0613241-421824	0.2	12.76	0.1097	4	Aa	
J062706-352916	06 27 06.73	-35 29 16.0	688	29	962	48	1301	65	4632.9	4592.0	g0627067-352915	0.7	10.51	0.0549	4	Aa	
J065359-415144	06 53 59.97	-41 51 44.8	56	3	72	4	102	5	...	727.5	g0653599-415145	0.7	11.84	0.0908	4	Aa	
J070240-284149	07 02 40.37	-28 41 49.9	194	13	-	-	-	-	239.4	...	g0702404-284150	0.4	7.89	0.0072	NGC 2325
J070459-490459	07 04 59.20	-49 04 59.5	84	4	94	6	92	5	...	41.2	g0704593-490460	0.6	9.84	0.0419	ESO 207-G19
J070914-360121	07 09 14.07	-36 01 21.6	94	5	-	-	-	-	1865.4	3420.	g0709141-360122	1.8	12.60	0.1108	
J081611-703944	08 16 11.64	-70 39 44.4	62	3	-	-	-	-	...	1940.1	g0816118-703945	1.0	10.86	0.0332	4	Aa	ESO 060-IG02
J084452-100059	08 44 52.73	-10 00 59.0	46	4	-	-	-	-	311.9	...	g0844527-100059	0.8	11.18	0.0429	4	Aa	
J090802-095937	09 08 02.23	-09 59 37.5	60	4	-	-	-	-	182.3	...	g0908022-095938	0.7	11.39	0.0535	4	Aa	
J090825-093332	09 08 25.37	-09 33 32.5	46	2	-	-	-	-	264.6	...	g0908253-093334	1.6	12.58	0.1590	2	..	
J091300-210320	09 13 00.22	-21 03 20.6	135	9	170	9	198	10	328.4	...	g0913002-210321	0.3	12.65	0.1980	3	Aa	
J092338-213544	09 23 38.95	-21 35 44.9	328	22	390	20	307	20	267.7	...	g0923389-213547	2.5	12.00	0.0520	
J093626-123649	09 36 26.47	-12 36 49.0	50	3	-	-	-	-	69.8	...	g0936265-123647	1.8	11.82	0.1133	4	Aa	
J093955-241516	09 39 55.72	-24 15 16.8	40	2	39	2	32	2	30.2	...	g0939558-241517	0.5	11.48	0.0658	4	Aae	
J094409-015116	09 44 09.86	-01 51 16.3	78	5	-	-	-	-	88.5	...	g0944099-015115	1.3	12.39	0.0418	
J095513-212303	09 55 13.59	-21 23 03.3	93	6	81	4	61	3	58.3	...	g0955136-212303	0.5	12.31	0.1087	4	Ae	
J095824-265538	09 58 24.45	-26 55 38.7	142	9	152	8	187	9	313.1	...	g0958246-265536	3.6	7.88	0.0083	NGC 3078
J100040-313952	10 00 40.82	-31 39 52.2	266	12	404	20	488	24	530.2	724.2	g1000408-313952	0.7	8.08	0.0086	4	Aae	NGC 3100
J100833-042839	10 08 33.63	-04 28 39.8	44	3	-	-	-	-	250.1	...	g1008337-042840	0.8	11.23	0.0509	
J103859-422353	10 38 59.73	-42 23 53.4	85	4	191	10	339	17	...	1157.0	g1038597-422355	1.4	12.16	0.1137	4	Aa	
J110957-373220	11 09 57.70	-37 32 20.3	52	4	23	2	77	4	582.8	567.4	g1109577-373221	0.8	7.20	0.0101	4	Aa	NGC 3557
J112119-001316	11 21 19.47	-00 13 16.0	108	5	-	-	-	-	648.9	...	g1121194-001316	0.9	12.12	0.0993	
J113305-040046	11 33 05.21	-04 00 46.4	108	6	-	-	-	-	979.1	...	g1133051-040048	2.0	10.47	0.0520	4	Aa	
J114503-325824	11 45 03.50	-32 58 24.1	75	4	91	5	69	4	31.5	39.7	g1145035-325824	0.7	10.47	0.0384	4	Aae	
J114539-105350	11 45 39.02	-10 53 50.4	73	4	-	-	-	-	102.4	...	g1145389-105352	2.5	11.50	0.0774	4	Aa	

Table 3. 6dFGS galaxies detected as AT20G radio sources.

(1)	(2)	(3)	(4)	(5)	(6)	(7)	(8)	(9)	(10)	(11)	(12)	(13)	(14)	(15)	(16)	(17)
AT20G name	AT20G position (J2000)	S ₂₀ (mJy)	±	S ₈ (mJy)	±	S ₅ (mJy)	±	NVSS (mJy)	SUMSS (mJy)	6dFGS name	Offset (arcsec)	K _{tot} (mag)	Redshift	Q	Class	Notes
J121044-435437	12 10 44.67 -43 54 37.4	129	6	168	9	136	7	...	122.7	g1210448-435437	1.5	12.29	0.0693	4	Aae	
J122343-423532	12 23 43.40 -42 35 32.2	330	17	507	19	999	41	...	3105.0	g1223434-423532	0.8	12.34	0.1706	4	Ae	
J123148-321314	12 31 48.73 -32 13 14.1	106	6	184	9	176	9	165.1	137.5	g1231487-321314	0.3	12.59	0.0884	4	Aae	
J123449-243232	12 34 49.79 -24 32 32.1	73	4	104	5	58	4	29.0	...	g1234497-243233	1.4	12.63	0.1812	3	Aa?	
J123959-113721	12 39 59.32 -11 37 21.4	81	4	-	-	-	-	93.4	...	g1239594-113723	2.2	4.96	0.0036	NGC 4594
J125457-442456	12 54 57.67 -44 24 56.9	344	15	356	18	330	17	...	368.1	g1254575-442457	2.1	10.69	0.0411	4	Aae	
J125615-114635	12 56 15.96 -11 46 35.7	123	6	-	-	-	-	54.4	...	g1256160-114637	1.4	11.88	0.0579	4	Aa	
J125711-172434	12 57 11.59 -17 24 34.0	83	5	132	7	164	8	98.4	...	g1257116-172434	0.2	9.65	0.0470	4	Aa	
J130031-441442	13 00 31.06 -44 14 42.6	78	3	104	5	68	4	...	26.9	g1300310-441442	1.2	10.45	0.0322	
J130058-231215	13 00 58.52 -23 12 15.6	188	10	-	-	-	-	777.0	...	g1300589-231210	7.9	12.73	0.1294	4	Aa	
J130100-322628	13 01 00.80 -32 26 28.0	176	9	378	19	574	29	1387.0	1574.0	g1301008-322629	0.9	8.51	0.0170	ESO 443-G24
J130527-492804	13 05 27.47 -49 28 04.7	726	36	786	39	1566	78	...	5549.0	g1305273-492805	1.7	4.48	0.0019	NGC 4945
J130715-760245	13 07 15.46 -76 02 45.6	71	1	118	6	114	6	...	139.1	g1307156-760245	0.6	12.50	0.1833	4	AeB	
J130841-242259	13 08 41.92 -24 22 59.9	57	4	-	-	-	-	474.5	...	g1308420-242258	2.3	11.78	0.0142	4	Ae	
J131124-442240	13 11 24.04 -44 22 40.5	44	2	50	4	80	5	...	208.3	g1311238-442240	2.4	10.22	0.0506	4	Aae	
J131931-123925	13 19 31.42 -12 39 25.5	149	8	-	-	-	-	156.7	...	g1319317-123925	3.3	8.22	0.0084	NGC 5077
J131949-272437	13 19 49.86 -27 24 37.5	54	4	35	5	86	5	262.3	...	g1319500-272436	2.8	7.12	0.0071	4	Aae	NGC 5078
J132112-434216	13 21 12.81 -43 42 16.7	705	35	496	18	447	27	...	1325.8	g1321129-434217	0.6	7.57	0.0112	J	Aae	NGC 5090
J132340-410123	13 23 40.83 -41 01 23.4	156	8	244	12	326	16	...	208.3	g1323408-410124	0.5	12.89	0.0941	3	Aae	
J132920-264022	13 29 20.70 -26 40 22.2	101	6	118	6	118	6	102.4	...	g1329208-264022	2.0	11.50	0.0502	4	Aa	
J133608-082952	13 36 08.30 -08 29 52.3	591	29	-	-	-	-	388.8	...	g1336083-082952	0.8	9.17	0.0228	4	Aae	NGC 5232
J133639-335756	13 36 39.01 -33 57 56.3	323	14	298	22	262	34	2334.2	14900.	g1336390-335757	1.0	7.50	0.0125	J	Aae	IC 4296
J134624-375816	13 46 24.13 -37 58 16.0	71	4	55	3	68	5	697.1	1225.7	g1346240-375816	1.7	10.70	0.0376	4	Aa	ESO 325-G16
J135036-163449	13 50 36.28 -16 34 49.4	186	12	220	12	173	9	109.2	...	g1350362-163450	2.0	12.38	0.0877	4	Ae	
J135607-172433	13 56 07.02 -17 24 33.1	239	16	271	14	255	13	180.1	...	g1356070-172432	1.7	11.80	0.0747	4	Aae	
J140729-270105	14 07 29.76 -27 01 05.4	202	13	415	22	552	28	645.5	...	g1407298-270104	1.1	9.57	0.0218	IC 4374
J140912-231550	14 09 12.03 -23 15 50.1	137	9	356	19	521	26	599.4	...	g1409120-231550	0.9	12.68	0.0864	4	Aae	
J145509-365508	14 55 09.60 -36 55 08.6	198	10	205	11	241	12	1207.5	1869.0	g1455096-365508	0.9	11.33	0.0946	4	Aae	
J145924-164136	14 59 24.78 -16 41 36.5	83	5	-	-	-	-	1200.5	...	g1459248-164137	0.1	9.37	0.0117	NGC 5793
J145928-181045	14 59 28.74 -18 10 45.2	118	7	-	-	-	-	105.4	...	g1459288-181045	0.2	12.59	0.2344	3	Ae	
J151741-242220	15 17 41.76 -24 22 20.2	3449	226	3647	190	3173	158	2041.9	...	g1517418-242219	1.2	10.77	0.0490	4	Aae	AP Lib
J152433-301221	15 24 33.40 -30 12 21.8	255	13	351	18	323	16	174.3	187.0	g1524334-301221	0.4	10.91	0.0195	4	Aae	
J155821-141000	15 58 21.83 -14 10 00.0	172	9	-	-	-	-	460.6	...	g1558220-140959	2.1	11.12	0.0974	4	Ae	
J164416-771548	16 44 16.03 -77 15 48.5	399	20	238	13	245	14	...	1165.9	g1644161-771549	0.5	11.20	0.0430	J	Aae	
J165710-735544	16 57 10.08 -73 55 44.5	42	1	137	7	128	7	...	99.3	g1657105-735542	2.6	12.35	0.0712	4	Aa	
J170241-774156	17 02 41.29 -77 41 56.3	50	1	172	15	306	27	...	2912.0	g1702410-774157	1.2	12.51	0.0947	4	Aa	
J171522-652018	17 15 22.19 -65 20 18.6	53	3	86	4	97	5	...	190.5	g1715223-652018	0.8	10.77	0.0492	4	Aae	
J172341-650036	17 23 41.10 -65 00 36.3	2872	143	4603	230	5605	280	...	3699.0	g1723410-650037	0.8	9.18	0.0142	NGC 6328
J180207-471930	18 02 07.68 -47 19 30.3	114	6	119	6	123	7	...	681.1	g1802076-471932	2.0	12.57	0.1227	3	Aa	
J180228-523645	18 02 28.50 -52 36 45.9	100	5	196	10	257	13	...	686.9	g1802285-523646	0.7	11.98	0.1306	4	Ae	

Table 3. 6dFGS galaxies detected as AT20G radio sources.

(1)	(2)		(3)	(4)	(5)	(6)	(7)	(8)	(9)	(10)	(11)	(12)	(13)	(14)	(15)	(16)	(17)
AT20G name	AT20G position (J2000)		S ₂₀ (mJy)	±	S ₈ (mJy)	±	S ₅ (mJy)	±	NVSS (mJy)	SUMSS (mJy)	6dFGS name	Offset (arcsec)	K _{tot} (mag)	Redshift	Q	Class	Notes
J180957-455241	18 09 57.79	-45 52 41.2	1087	54	-	-	-	-	...	1530.0	g1809579-455241	0.6	12.01	0.0697	4	AeB	
J181857-550815	18 18 57.99	-55 08 15.0	75	4	54	4	42	5	...	185.6	g1818580-550815	0.5	11.41	0.0726	4	Aa	
J181934-634548	18 19 34.99	-63 45 48.2	1704	85	3567	178	5562	277	...	19886.0	g1819351-634548	0.2	12.10	0.0647	J	Ae	PKS 1814-63
J182125-763459	18 21 25.15	-76 34 59.6	172	9	246	12	331	17	...	704.5	g1821247-763500	1.7	9.25	0.0184	4	Aae	NGC 6557
J182507-631453	18 25 07.31	-63 14 53.7	88	4	117	6	131	7	...	141.6	g1825072-631454	0.9	9.22	0.0144	4	Aae	NGC 6614
J184038-770929	18 40 38.59	-77 09 29.1	224	11	229	12	408	20	...	1152.0	g1840386-770929	0.6	9.41	0.0182	4	Aa	ESO 045-G11
J192043-383107	19 20 43.13	-38 31 07.1	63	2	-	-	-	-	239.7	247.8	g1920430-383106	1.5	11.23	0.0453	4	Aae	
J192234-163253	19 22 34.88	-16 32 53.3	110	7	-	-	-	-	482.9	...	g1922348-163254	2.0	12.29	0.1266	4	AeB	
J192817-293145	19 28 17.05	-29 31 45.0	78	4	168	9	252	14	2108.5	...	g1928170-293144	0.8	9.56	0.0244	4	Aa	ESO 460-G04
J194524-552049	19 45 24.22	-55 20 49.2	779	39	1009	51	1059	53	...	596.3	g1945242-552049	0.4	9.00	0.0152	4	Aae	NGC 6812
J200954-482246	20 09 54.04	-48 22 46.2	113	6	135	7	143	7	...	138.8	g2009541-482246	0.5	7.32	0.0095	4	Aae	NGC 6868
J204008-711457	20 40 08.46	-71 14 57.1	53	3	65	3	88	4	...	494.2	g2040083-711460	2.8	12.38	0.1618	4	Aa	
J204552-510627	20 45 52.29	-51 06 27.7	54	3	63	3	65	3	...	620.9	g2045523-510627	0.9	10.19	0.0485	4	Aa	ESO 234-G068
J205202-570407	20 52 02.32	-57 04 07.9	130	6	230	12	453	23	...	1975.0	g2052023-570408	0.5	8.75	0.0118	4	Ae	IC 5063
J205306-162007	20 53 06.00	-16 20 07.4	56	3	-	-	-	-	116.5	...	g2053061-162008	2.1	10.73	0.0427	4	Aa	IC 1335
J205401-424238	20 54 01.79	-42 42 38.7	86	5	125	6	154	8	...	160.2	g2054018-424240	0.8	11.34	0.0429	4	Aae	
J205754-662919	20 57 54.01	-66 29 19.6	49	3	42	2	51	3	...	282.7	g2057540-662920	0.2	11.85	0.0754	4	Aa	ESO 106-IG15
J205837-575636	20 58 37.39	-57 56 36.5	97	3	203	1	333	10	...	846.2	g2058376-575636	1.6	11.40	0.0524	4	Aa	
J205846-144304	20 58 46.69	-14 43 04.7	57	3	-	-	-	-	146.6	...	g2058468-144305	1.1	12.13	0.0778	4	Aa	
J210353-093341	21 03 53.28	-09 33 41.2	103	5	-	-	-	-	145.7	...	g2103533-093342	0.2	12.20	0.0882	4	Aa	
J210602-712218	21 06 02.92	-71 22 17.9	246	13	447	22	619	31	...	1206.0	g2106029-712218	0.2	11.88	0.0745	4	Aa	
J212222-560014	21 22 22.81	-56 00 14.6	58	3	34	2	28	2	...	100.9	g2122229-560014	1.0	11.56	0.0518	4	Aae	
J213133-383703	21 31 33.09	-38 37 03.9	46	2	47	2	66	3	979.2	1145.8	g2131330-383705	1.5	9.56	0.0182	4	Aa	NGC 7075
J214824-571351	21 48 24.09	-57 13 51.5	48	3	51	3	67	4	...	447.1	g2148243-571352	1.3	12.09	0.0806	
J220156-332103	22 01 56.41	-33 21 03.3	71	2	139	6	224	11	1291.4	2111.0	g2201564-332103	0.4	12.31	0.1537	4	Aa	
J220253-563543	22 02 53.31	-56 35 43.0	69	4	81	4	84	4	...	58.4	g2202533-563542	1.1	12.16	0.0489	
J220538-053531	22 05 38.59	-05 35 31.9	67	4	-	-	-	-	187.2	...	g2205386-053533	1.1	11.46	0.0576	
J220916-471000	22 09 16.25	-47 10 00.3	123	6	161	8	136	7	...	119.6	g2209162-471000	0.3	7.04	0.0060	NGC 7213
J221220-251829	22 12 20.77	-25 18 29.0	71	5	-	-	-	-	304.4	...	g2212207-251829	1.0	10.81	0.0626	4	Aa	
J223931-360912	22 39 31.26	-36 09 12.5	64	2	138	7	182	9	661.0	842.5	g2239311-360912	1.4	11.32	0.0575	4	Aa	
J224559-173724	22 45 59.13	-17 37 24.2	43	3	-	-	-	-	395.8	...	g2245590-173732	8.4	11.07	0.0684	
J225710-362744	22 57 10.49	-36 27 44.5	554	28	851	43	1082	54	1279.7	966.2	g2257106-362744	1.3	6.80	0.0057	4	Aae	IC 1459
J230136-591320	23 01 36.31	-59 13 20.5	155	8	143	7	137	7	...	61.9	g2301363-591321	0.7	12.26	0.1501	4	Ae	
J231546-230744	23 15 46.98	-23 07 44.2	73	4	77	4	54	3	13.7	...	g2315469-230744	0.5	12.17	0.0703	4	Aae	
J231905-420648	23 19 05.92	-42 06 48.9	150	6	-	-	-	-	...	911.6	g2319059-420649	0.6	10.49	0.0543	4	Aae	
J231915-533159	23 19 15.92	-53 31 59.1	75	3	113	10	177	10	...	501.8	g2319158-533159	1.4	12.27	0.0958	4	Aa	
J232519-120727	23 25 19.74	-12 07 27.1	84	4	-	-	-	-	1874.6	...	g2325197-120727	0.4	12.10	0.0822	4	Ae	
J233355-234340	23 33 55.28	-23 43 40.8	957	48	772	39	656	33	782.1	...	g2333552-234341	0.9	11.97	0.0477	
J234129-291915	23 41 29.72	-29 19 15.3	120	8	182	10	153	8	239.6	...	g2341298-291915	1.1	10.37	0.0517	
J234205-160840	23 42 05.82	-16 08 40.4	43	3	-	-	-	-	416.7	...	g2342059-160841	0.7	11.74	0.0649	4	Aa	

Table 3. 6dFGS galaxies detected as AT20G radio sources.

(1)	(2)	(3)	(4)	(5)	(6)	(7)	(8)	(9)	(10)	(11)	(12)	(13)	(14)	(15)	(16)	(17)	Notes
AT20G name	AT20G position (J2000)	S ₂₀ (mJy)	±	S ₈ (mJy)	±	S ₅ (mJy)	±	NVSS (mJy)	SUMSS (mJy)	6dFGS name	Offset (arcsec)	K _{tot} (mag)	Redshift	Q	Class		
(b) 6dFGS galaxies identified with extended or multiple AT20G sources																	
J000311-544516	00 03 11.04 -54 45 16.8	95	3	313	3	552	9	...	1549.0	g0003112-544458	18.9	10.22	0.0327	4	Aa	Resolved double	
J000413-525458	00 04 13.97 -52 54 58.7	65	3	98	4	192	6	...	934.2	g0004140-525459	0.4	10.06	0.0328		
J003704-010907	00 37 04.24 -01 09 07.2	404	17	-	-	-	-	4067.1	...	g0037041-010908	2.5	11.91	0.0734	4	Aa		
PKS 0043-42*	00 46 17.8 -42 07 52.	438	20	-	-	-	-	...	11260.	g0046178-420752	..	12.66	0.116	J	Aae	Two AT20G sources	
J004733-251717	00 47 33.08 -25 17 17.7	608	29	1411	30	2190	60	6831.0	...	g0047331-251719	1.4	3.77	0.0008	J	SF	NGC 253	
J013357-362935	01 33 57.90 -36 29 35.3	440	-	-	-	-	-	8400.	10300.	g0133577-362936	2.0	9.58	0.0305	4	Ae	NGC 612	
J021645-474908	02 16 45.07 -47 49 08.9	93	3	-	-	-	-	...	3900.	g0216451-474909	0.4	10.54	0.0643	4	Aa	ESO 198-G01	
J024240-000046	02 42 40.72 -00 00 46.7	474	17	-	-	-	-	4610.	...	g0242407-000048	1.2	5.79	0.0038	J	Ae	NGC 1068	
J035257-683117	03 52 57.46 -68 31 17.4	68	3	114	4	165	5	...	409.4	g0352575-683117	0.6	11.70	0.0870		
J042908-534940	04 29 08.24 -53 49 40.2	145	4	244	6	782	10	...	8410.	g0429082-534940	0.3	9.76	0.0380	J	Aa	IC 2082	
J045523-203409	04 55 23.42 -20 34 09.8	331	10	-	-	-	-	4563.9	...	g0455237-203416	7.5	10.06	0.0354	J	Aa	NGC 1692	
J050453-101451	05 04 53.01 -10 14 51.5	123	5	-	-	-	-	1482.4	...	g0504531-101453	1.3	11.20	0.0403	4	Ae	Arp 187	
Pictor A*	05 19 49.70 -45 46 43.7	6320	110	-	-	-	-	...	85700.	g0519497-454644	..	11.95	0.0351	J	AeB	Three AT20G sources	
J054754-195805	05 47 54.59 -19 58 05.9	42	3	93	6	163	13	863.1	...	g0547546-195805	1.1	11.96	0.0551	4	Aa		
J055049-314428	05 50 49.12 -31 44 28.9	133	3	277	6	448	11	1034.3	1540.0	g0550498-314427	9.5	11.04	0.0400	ESO 424-G27	
J062143-524132	06 21 43.41 -52 41 32.3	266	9	442	11	928	13	...	4840.3	g0621433-524133	1.4	9.80	0.0511	J	Aae		
J062620-534151	06 26 20.58 -53 41 51.4	253	4	-	-	-	-	...	11600.	g0626205-534136	15.7	9.66	0.0551	J	Aa	ESO 161-IG07	
J062648-543214	06 26 48.91 -54 32 14.0	106	3	336	5	773	13	...	5000.	g0626496-543234	21.1	10.78	0.0517	Resolved triple	
PKS 0634-20*	06 36 31.24 -20 28 57.6	238	9	1551	20	2993	40	9625.0	...	g0636323-203453	..	11.70	0.0551	4	Ae	Two AT20G sources	
J065153-602158	06 51 53.67 -60 21 58.4	44	2	36	2	102	5	...	1849.2	g0651549-602217	20.7	12.26	0.1339	3	Aa		
J080537-005819	08 05 37.69 -00 58 19.0	81	3	-	-	-	-	1329.1	...	g0805378-005818	2.0	10.70	0.0902	4	Aa		
J080852-102832	08 08 52.49 -10 28 31.9	131	5	-	-	-	-	4256.1	...	g0808536-102740	55.2	12.33	0.1090	4	Ae	Hotspot of PKS 0806-10	
J091805-120532	09 18 05.82 -12 05 32.5	1056	52	-	-	-	-	40849.9	...	g0918057-120544	11.6	10.90	0.0548	J	Aae	Resolved double, Hydra A	
J094110-120450	09 41 10.74 -12 04 50.6	44	2	-	-	-	-	728.7	...	g0941102-120536	46.7	12.24	0.1500	3	Aa	Resolved triple	
J105533-283134	10 55 33.39 -28 31 34.7	181	8	712	4	996	17	1792.1	...	g1055334-283134	0.7	11.29	0.0611	4	Aae		
J124849-411840	12 48 49.37 -41 18 40.3	278	10	819	19	1421	45	...	5674.0	g1248493-411840	1.5	7.14	0.0102	J	Aae	NGC 4696	
J125438-123255	12 54 38.55 -12 32 55.7	83	2	-	-	-	-	8200.	...	g1254361-123353	67.5	7.75	0.015	J	Aae	Resolved double, NGC 4783	
J132527-430104	13 25 27.60 -43 01 04.9	28350	-	-	-	-	-	...	342000.	g1325277-430108	3.2	3.94	0.0018	J	Aae	Centaurus A	
J141949-192825	14 19 49.80 -19 28 25.3	117	8	-	-	-	-	1973.1	...	g1419497-192826	1.2	12.35	0.1200		
PKS 1717-00*	17 20 28.15 -00 58 46.8	435	13	-	-	-	-	56980.	...	g1720282-005847	..	10.82	0.0304	J	Aae	Two AT20G sources	
PKS 1733-56*	17 37 22.24 -56 36 30.0	696	27	-	-	-	-	...	12560.	g1737358-563403	..	12.67	0.0985	4	Ae	Two AT20G sources	
J180712-701234	18 07 12.55 -70 12 34.5	62	3	59	3	98	4	...	1278.0	g1807149-701238	12.3	10.56	0.0402	4	Aae	Resolved double	
J184314-483622	18 43 14.77 -48 36 22.8	305	9	590	10	1157	9	...	5880.	g1843146-483623	1.4	11.84	0.1108	4	Aa		
J191457-255202	19 14 57.79 -25 52 02.8	147	9	275	12	322	11	612.2	...	g1914577-255201	2.1	10.88	0.0631	4	Aa		
J195817-550923	19 58 17.08 -55 09 23.3	581	12	1132	12	2063	35	...	9700.	g1958185-550930	13.6	11.81	0.0581	J	Aae	Resolved double	
J203444-354857	20 34 44.68 -35 48 57.6	104	3	-	-	-	-	1717.1	2609.0	g2034447-354902	4.3	11.79	0.0888	4	Aa	ESO 400-IG40	
J205603-195646	20 56 03.52 -19 56 46.8	159	3	-	-	-	-	2726.2	...	g2056043-195635	15.7	12.69	0.1566	4	Aa?	Resolved double	
J213741-143241	21 37 41.17 -14 32 41.9	256	7	-	-	-	-	3864.0	...	g2137452-143256	59.9	12.61	0.1999	4	AeB	Hotspot of PKS 2135-147	
J215129-552013	21 51 29.86 -55 20 13.1	88	2	93	3	154	3	...	2450.	g2151299-552013	0.7	10.43	0.0388		
J215706-694123	21 57 06.10 -69 41 23.3	3400	210	-	-	-	-	...	37300.	g2157060-694124	0.9	10.05	0.0285	J	AeB	ESO 075-G41	
J220113-374654	22 01 13.79 -37 46 54.3	174	5	460	10	536	12	1530.	2140.	g2201171-374624	49.5	10.86	0.0334	4	Ae	Hotspot of PKS 2158-380	
J235156-010909	23 51 56.29 -01 09 09.3	141	7	-	-	-	-	1608.4	...	g2351561-010913	4.5	11.87	0.1737	4	AeB		